

Alma Mater Studiorum – Università di Bologna

DOTTORATO DI RICERCA IN

Oncologia e Patologia Sperimentale

Ciclo XXVII°

Settore Concorsuale di afferenza: 06/A2

Settore Scientifico disciplinare: MED/04

**Cancer and aging: a multidisciplinary medicinal
chemistry approach on relevant biological targets
such as proteasome, sirtuins and interleukin 6**

Presentata da: Marco Daniele Parenti

Coordinatore Dottorato
Prof. Pier Luigi Lollini

Relatore
Prof. Stefano Salvioli

Esame finale anno 2015

Table of Content

Preface.....	5
List of Abbreviations	7
1. Introduction.....	9
1.1 The Drug Discovery Process	9
1.2 Molecular Modeling and rational drug design in drug discovery	9
1.2.1 Ligand based approaches	11
1.2.2 Structure based approach	12
1.3 Cancer and Aging in drug discovery	12
1.4 Selected Targets and their Involvement in Human Pathologies.....	13
2. Aim of the Thesis	15
3. Proteasome and Immunoproteasome Inhibitors.....	16
3.1 Proteasomes: mandatory terminators.....	16
3.2 Why is i-proteasome a potential therapeutic target?.....	18
3.3 I-proteasome as target for cancer therapy.....	19
3.3.1 I-proteasome in Multiple Myeloma	20
3.3.2 I-proteasome in solid tumours.....	21
3.3.3 I-proteasome as a target for immunotherapy?.....	26
3.4 I-proteasome as target for neuropathologies	26
3.4.1 Alzheimer disease.....	27
3.4.2 Multiple Sclerosis.....	28
3.4.3 Temporal Lobe Epilepsy.....	29
3.5 An overview of selective s- and i-proteasome inhibitors and enhancers.....	30
3.6 Human immunoproteasome model.....	33
3.7 Computer-aided drug design approaches	38

3.8	Hit Identification.....	39
3.9	Conclusion and perspective.....	46
3.10	Experimental Section.....	47
4.	Sirtuins in drug discovery.....	48
4.1	Sirtuins: at the crossroad of metabolism, cancer, and inflammation.....	48
4.2	Sirtuins and cancer.....	48
4.3	Sirtuin inhibitors.....	50
4.4	Sirtuins activators.....	52
5.	Development of a Sirtuins selectivity model.....	55
5.1	Sequence and structural comparison of the catalytic cores.....	57
5.2	Structural comparison of the binding sites.....	60
5.3	Structural superposition of available three-dimensional structures.....	61
5.4	Conclusions.....	70
5.5	Experimental Procedures.....	71
6.	Discovery of new SIRT3 modulators.....	73
6.1	Targeting SIRT3 with structure-based drug design techniques.....	74
6.2	Evaluation of acetylation pattern of mitochondrial proteins.....	76
6.2.1	Evaluation of acetylation pattern of a specific protein target of SIRT3.....	77
6.3	Evaluation of cell response to toxic stimulation.....	78
6.4	Conclusions.....	79
6.5	Experimental Section.....	79
7.	Discovery of new SIRT6 inhibitors.....	81
7.1	Structure-based in silico screening.....	82
7.2	Selectivity profiling.....	85
7.3	Biological characterization of the identified SIRT6 inhibitors.....	89
7.4	Conclusions.....	92

7.5	Experimental section.....	93
8.	Optimization of SIRT6 inhibitors - Quinazolinedione derivatives.....	97
8.1	Selection of analog candidates for biological testing	97
8.2	Selectivity profiling	102
8.3	Mechanism for SIRT6 inhibition by quinazolinediones	103
8.4	Biological evaluation of quinazolinedione SIRT6 inhibitors.....	104
8.5	Quinazolinedione inhibitors sensitize cancer cells to chemotherapeutics	107
8.6	Conclusions	110
8.7	Experimental section.....	111
9.	Optimization of SIRT6 inhibitors – Salicylate derivatives	116
10.	Interleukin 6 inhibitors	118
10.1	Biologic Functions of IL-6	118
10.2	IL-6 Signaling Pathway.....	119
10.3	IL-6 in aging and aging-related diseases	120
10.4	IL-6 and cancer	121
10.5	Pharmacological approaches to blockade of IL-6 signaling.....	121
10.6	Drug repurposing.....	122
10.7	Screening for IL6 – IL6 receptor interaction modulators.....	122
10.7.1	Screening of hexameric assembly IL-6/IL-6R/gp130 ligands	122
10.7.2	Screening of Protein-Protein Interface inhibitors.....	126
10.8	Conclusion and perspective	128
10.9	Experimental section	131
11.	Concluding remarks and future perspectives	132
	Acknowledgements.....	133
	References	134

Preface

Publications and Patents

This thesis is based on the following publications and manuscripts:

Publications:

1. **Parenti MD**, Bruzzone S, Nencioni A, Del Rio A. Selectivity hot-spots of sirtuin catalytic cores. *To be Submitted to Structure*
2. Sociali G, Galeno L, **Parenti MD**, Grozio A, Bauer I, Passalacqua M, Boero S, Donadini A, Millo E, Bellotti M, Sturla L, Franceschi C, Ballestrero A, Poggi A, Bruzzone S, Nencioni A, Del Rio A. Quinazolinedione SIRT6 inhibitors sensitize cancer cells to chemotherapeutics. *To be Submitted to ACS Chemical Biology*
3. **Parenti MD**, Grozio A, Bauer I, Galeno L, Damonte P, Millo E, Sociali G, Franceschi C, Ballestrero A, Bruzzone S, Del Rio A, Nencioni A. Discovery of novel and selective SIRT6 inhibitors. *J Med Chem.* 2014 Jun 12;57(11):4796-804.
4. Bellavista E, Andreoli F, **Parenti MD**, Martucci M, Santoro A, Salvioli S, Capri M, Baruzzi A, Del Rio A, Franceschi C, Mishto M. Immunoproteasome in cancer and neuropathologies: a new therapeutic target? *Curr Pharm Des.* 2013;19(4):702-18.
5. Bruzzone S, **Parenti MD**, Grozio A, Ballestrero A, Bauer I, Del Rio A, Nencioni A. Rejuvenating sirtuins: the rise of a new family of cancer drug targets. *Curr Pharm Des.* 2013;19(4):614-23.
6. Andreoli F, Barbosa AJ, **Parenti MD**, Del Rio A. Modulation of epigenetic targets for anticancer therapy: clinicopathological relevance, structural data and drug discovery perspectives. *Curr Pharm Des.* 2013;19(4):578-613.

Patents:

- WO/2014/170875. Quinazolinedione compounds with a sirtuin inhibiting activity. Applicants: University of Genoa and Alma Mater Studiorum – University of Bologna. Inventors: DEL RIO, Alberto; (IT), FRANCESCHI, Claudio; (IT), **PARENTI, Marco, Daniele**; (IT), BAUER, Inga; (IT), BRUZZONE, Santina; (IT), GROZIO, Alessia; (IT), NENCIONI, Alessio; (IT). Priority data: MI2013A000646 19.04.2013 IT.

- WO/2014/170873. Compounds with a sirtuin inhibiting activity. Applicants: University of Genoa and Alma Mater Studiorum – University of Bologna. Inventors: DEL RIO, Alberto; (IT), FRANCESCHI, Claudio; (IT), **PARENTI, Marco, Daniele**; (IT), BAUER, Inga; (IT), BRUZZONE, Santina; (IT), GROZIO, Alessia; (IT), NENCIONI, Alessio; (IT). Priority data: MI2013A000647 19.04.2013 IT.

Author's contribution

The rational design and optimization of active molecules through molecular modeling techniques was carried out by the candidate in the framework of the BioChemoInformatics Lab (Dept. of Experimental, Diagnostic and Specialty Medicine, University of Bologna) while the biological testing of compounds was conducted in collaboration with external laboratories.

Intellectual Property Issues

Chemical structures of sirtuin 3 modulators discussed in chapter 6 are considered for patenting, therefore are not disclosed.

Salicylate derivatives of sirtuin 6 inhibitors discussed in chapter 8 are currently under biological testing, and will be disclosed in a forthcoming publication.

List of Abbreviations

2-NBDG	=	2-[N-(7-nitrobenz-2-oxa-1,3-diazol-4-yl)amino]-2-deoxy-D-glucose
AD	=	Alzheimer's disease
AML	=	acute myeloid leukemia
APM	=	antigen-processing machinery
APP	=	amyloid precursor protein
C-like	=	caspase-like
CNS	=	central nervous system
CTL	=	CD8+ cytotoxic T cell
CT-like	=	chymotrypsin-like
DUBs	=	deubiquitylating enzymes
EAE	=	autoimmune encephalomyelitis
ER	=	endoplasmic reticulum
ETC	=	electron transport chain
HD	=	Huntington's disease
HMGB1	=	high-mobility group box-1
HTS	=	High throughput screening
IL	=	interleukin
IL-6	=	Interleukin 6
IL-6R	=	Interleukin 6 receptor
ILR1	=	interleukin receptor 1
i-proteasome	=	immunoproteasome
IS	=	immune system
MBP	=	myelin basic protein
MLR	=	mixed leukocyte reaction
MM	=	multiple myeloma
MS	=	multiple sclerosis
NAM	=	Nicotinamide
PBMC	=	peripheral blood mononuclear cells
PDB	=	Protein Data Bank
PHA	=	phytohemagglutinin
PHFs	=	tau-based paired helical filaments

QSAR	=	quantitative structure-activity relationships
RMSD	=	root mean square deviation
SAR	=	Structure-Activity relationship
SBDD	=	structure-based drug design
s-proteasome	=	standard proteasome
STAC	=	sirtuin activating compounds
TcR	=	T cell receptor
TLE	=	temporal lobe epilepsies
T-like	=	trypsin-like
TLR-4	=	Toll-like receptor-4
t-proteasome	=	thymus proteasome
T-reg	=	regulatory T cells
UPS	=	Ubiquitin Proteasome System

1. Introduction

1.1 The Drug Discovery Process

Drug discovery is an extremely laborious and expensive process, requires an average of 13 years of research and an investment of US\$1.8 billion to bring a single drug from the bench to a patient's bedside¹; this is not in the least surprising, when one considers the complexity of biological systems, most of which is only now beginning to be understood. Despite increase in investment in drug discovery, the output is considerably low due to high rate of drug failure in clinical trials². Consequently, in order to reduce the cost and time of a drug to reach market, new technologies were ventured. The genomics and the post-genomics eras, with the parallel advances in high-throughput experimental methods and screening techniques to analyze whole genomes and proteomes, are witnessing an explosion in the types and amount of information available, not only with respect to the genome sequences and protein structures but also with respect to gene-expression, regulation and protein–protein interactions. The availability of such information in publicly accessible databases and the advances in both computing power as well as in computational methods for data mining and modeling, have led to the emergence of several *in silico* approaches to systematically address several questions in biology, with an obvious impact on drug discovery^{3,4}. Today, drug discovery usually follows the general scheme presented in Figure 1.1. In short, the goal is to identify a compound that can modulate the effect of a molecular target that regulates a biological process related to a disease. Once a target has been identified and shown to be relevant in a disease model, high throughput screening, or its theoretical counterpart, virtual screening, is usually employed to generate a set of hit compounds. Following this, some of the promising molecules that show good physico-chemical properties are subject to further chemical exploration. The synthesized compounds in these lead series are evaluated and a structure–activity relationship (SAR) is derived, as well as the pharmacokinetic and pharmacodynamic profiles of the most promising compounds. The final phase in preclinical research is the transformation of a lead structure into a candidate drug, which is then considered for testing in clinical trials.

1.2 Molecular Modeling and rational drug design in drug discovery

Historically, serendipity and trial and error have played a major role in the discovery of drugs. The source of active substances has often been medical plants and herbs. With the advent of synthetic organic chemistry and modern pharmacology a more systematic search for new pharmaceutically

active compounds began, and these were often evaluated using animal experiments. The chemical modification of lead compounds, on a trial-and-error basis, typically led to compounds with improved potency, selectivity and bioavailability and reduced toxicity. However, this approach is costly and labor- and time-intensive and researchers in the pharmaceutical industry are constantly developing methods with a view to increase the efficiency of the drug discovery process. Two directions have evolved from these efforts. The 'random' approach involves the development of HTS assays and the testing of a large number of compounds, and combinatorial chemistry is used to satisfy the need for extensive compound libraries. The 'rational', approach relies on the knowledge of the structure of the target protein or knowledge about available potential compounds. Rational design approach involves the prediction of hypothetical ligands for the target protein from molecular modeling and the subsequent chemical synthesis and biological testing of specific compounds. Many rational design approaches have been suggested to increase the cost-effectiveness of discovery programs. Such approaches include *ligand based* approaches such as pharmacophore modeling, determination of quantitative structure-activity relationships (QSAR), which use accumulated information for ligands of previously executed discovery programs, and *receptor based* approaches such as docking, which use available information about target protein structure. One of most commonly used rational design approach is the so-called *virtual* or *in silico screening*; this methodology involves the computational filtering of a large body of molecules (e.g., those comprising a corporate database or a database of commercially available molecules) to identify those that have a high probability of activity in the biological test system of interest. Thus a virtual screening method takes as input all those molecules that might be acquired (or synthesized) and tested, and then outputs those few that should be tested. Although there are numerous methods for performing a virtual screening, they can be roughly classified into two main types: ligand-based approaches which do not utilize the structure of the biological target in screening, and structure-based approaches, which utilize the structure of the biological target, usually obtained by NMR or X-ray methods, and a variety of molecular docking algorithms and scoring functions. Hybrid approaches which combine aspects from ligand-based and structure-based methods are also frequently employed in virtual screening studies.

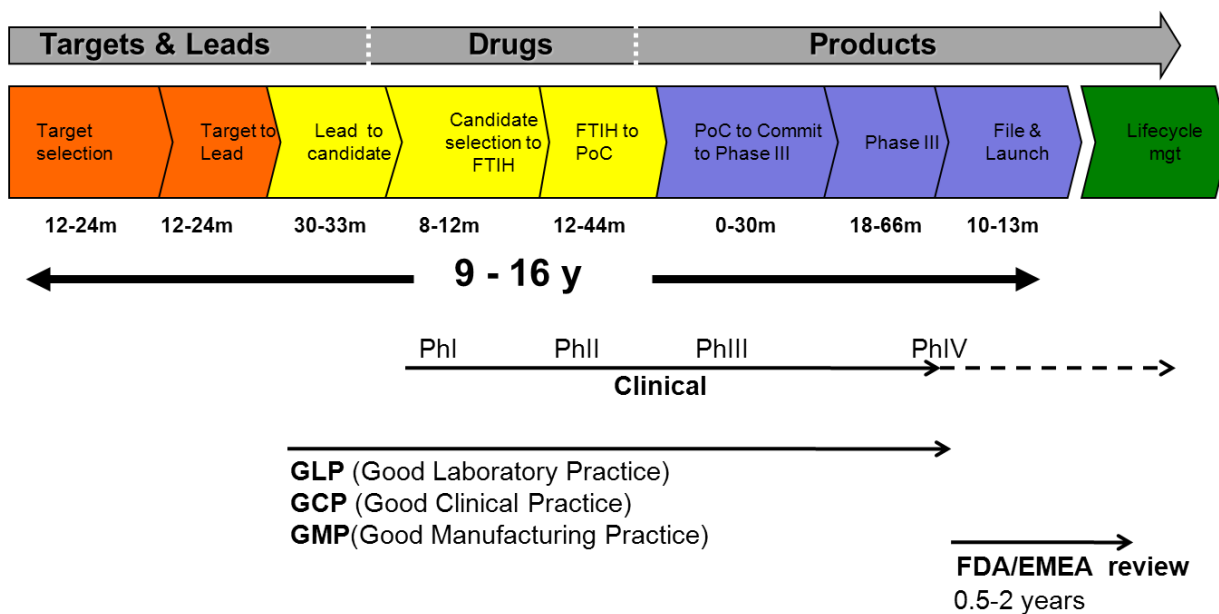


Figure 1.1 Drug Discovery Pipeline.

1.2.1 Ligand based approaches

Ligand-based approaches typically utilize knowledge of a set of compounds with known activity against the biological target. These approaches are frequently employed in the absence of structural information on the target in question. The key concept in ligand based approaches is that compounds that are structurally similar or have similar structural components to the known active compounds are more likely to have activity themselves. A variety of ligand-based screening methods have been developed, such as substructure and similarity searching, pharmacophore searching, clustering methods, and QSAR methods. Among these, the pharmacophore screening is certainly one of the most used methods.

Pharmacophore modeling allows determining the spatial arrangement of chemical features that confer drug activity toward a target receptor. Having established the chemical space occupied by active ligands, pharmacophore modeling software allows researchers to create 3D structure-activity relationships, screen databases, and generate hits without the benefit of a receptor structure. Compared to other ligand-based methods provides several advantages: i) can take into account 3D conformational variations and functional group properties such as polarity, hydrogen bond potential, aromaticity, and hydrophobicity; ii) can identify lead compounds that are structurally dissimilar to those already known, a process known as ‘scaffold-hopping’ or ‘lead-hopping’; iii) can also incorporate known structural information of the biological target’s active site, if any is known,

in the form of exclusion spheres or a molecular surface, both of which create barriers the compounds being searched are not permitted to encroach.

1.2.2 Structure based approach

In structure-based drug design (SBDD), the knowledge of the three-dimensional structure of a target is exploited to design small molecules able to tightly bind the active site and modulate the biological function in a desired way; the same tools could be used to assess the selectivity of the potential ligands towards different targets, making it easier to develop drugs with fewer side effects. This could reduce the time and resources needed to identify new interesting lead compounds. The structure-based methods, such as docking, have been successfully used to identify new hits from large libraries of chemical compounds and to predict their binding modes and affinities, and currently represent one of the primary methodologies used to discover new “hit” compounds. Molecular docking involves two main processes: pose prediction and scoring. In pose prediction a search algorithm determines an optimal conformation and orientation for a given compound in the receptor, or active site. This is followed by scoring to determine whether the pose will be accepted or rejected. Therefore, docking techniques enable both to predict the binding mode of a ligand and to roughly estimate its binding affinity for the biological target. Several scoring functions have been developed to approximate the interaction energy between proteins and related ligands, and all of these are simple linear mathematical models that estimate chemical properties (such as shape, charge distribution, hydrophobic/hydrophilic potentials and so on) of the molecules.

1.3 Cancer and Aging in drug discovery

The ultimate goal of biomedical research is to translate laboratory discoveries or clinical observations into new therapies to ameliorate disease and extend life expectancy and quality, namely the average total number of years of remaining meaningful life at a given age⁵. Ageing is a complex and multifactorial process characterized by the many forms of damage accumulation at the molecular, cellular, and tissue level that progress with advancing age, decreasing the body’s normal response and function. No single theory currently exists that can explain all of the hallmarks of ageing, suggesting that ageing is a multi-step and multi-event process⁶. At first glance, cancer and ageing have an inverse relationship because cancer cells are capable of uncontrolled growth and division, whereas ageing cells have a diminished proliferative capacity. Indeed, it has been well-established that older adults have a higher risk for cancer, as well as a higher risk of the onset of others chronic inflammation-associated diseases such as diabetes, stroke, and neurodegenerative

disease. Ageing is involved in a number of events responsible for carcinogenesis and cancer development at the molecular, cellular, and tissue levels. Actually, ageing and cancer have common origins due to internal and environmental stress and share some common hallmarks such as genomic instability, epigenetic alteration, aberrant telomeres, inflammation and immune injury, reprogrammed metabolism, and impaired degradation of intracellular biomolecules and organelles⁷.

The pharmaceutical industry is always searching for new biological targets to generate novel therapies; aging could represent a “blockbuster” market because the target patient group includes potentially every person, and humans are very willing to pay for chronic medical therapy in order to delay the aging process. Thus, there are many convincing reasons why aging and aging-related diseases should be a major focus for drug discovery⁸. At the same time, oncology has become the largest therapeutic area in the pharmaceutical industry in terms of the number of projects, clinical trials and research and development (R&D) spending⁹, but despite the enormous resources being invested in prevention and treatment, cancer remains one of the leading causes of mortality worldwide.

1.4 Selected Targets and their Involvement in Human Pathologies

Among all possible protein targets involved in aging-related diseases and cancer, we focused our attention on proteasome (and its variant immunoproteasome), sirtuins and interleukin 6. These three targets are completely unrelated and play different roles in human cells, but the modulation of its activity (activation or inhibition) using small molecules could have beneficial effects on one or more aging-related diseases and cancer.

Proteasome is the central catalytic unit of the ubiquitin proteasome system (UPS), which is used to degrade the main part of intracellular proteins. 20S standard proteasome (s-proteasome) is a cylinder-shaped complex that is composed of four stacked rings, each consisting of seven protein subunits; while associated with several regulator complexes, performs two crucial functions for cell metabolism: first of all, by degrading obsolete, misfolded or aberrant proteins proteasomes perform housekeeping function and maintain the cellular homeostasis; secondly, through the time-specific cleavage of short-life proteins, like transcription factors or transcription factor’s inhibitors, are able to switch on/off many cellular pathways. Hence, the proteasome as central core of the UPS, is a sort of mandatory terminator of proteins and its inactivation leads to cellular death by apoptosis or necrosis. The immunoproteasome (i-proteasome) originates from the substitution of some constitutive catalytic subunits stimulated by pro-inflammatory cytokines such as $\text{INF-}\gamma$ e $\text{TNF-}\alpha$,

and it is highly expressed in normal conditions only by specific cells types of the human body, such as those involved in immune-related function. Inhibiting or enhancing activity of proteasome or immunoproteasome could represent a promising strategy to counteract neurodegenerative diseases as well as cancer pathologies.

Sirtuins are a family of NAD⁺-dependent enzymes that was proposed to control organismal life span about a decade ago. While such role of sirtuins is now debated, mounting evidence involves these enzymes in numerous physiological processes and disease conditions, including metabolism, nutritional behavior, circadian rhythm, but also inflammation and cancer. In mammals, seven sirtuins have been identified (SIRT1-7), of which two are predominantly nuclear, SIRT6 and SIRT7, two are nuclear and cytosolic, SIRT1 and SIRT2, and three are mitochondrial, SIRT3-5. Sirtuin activators could slow the process of cellular senescence, and therefore could be useful in treatment of metabolic and neurodegenerative diseases, while sirtuin inhibitors could be appealing for the development of new anticancer and anti-inflammatory therapies.

Interleukin-6 (IL-6) is a pleiotropic cytokine with significant functions in the regulation of the immune system, and plays a pivotal role in host defense against pathogens and acute stress. However, increased or deregulated expression of IL-6 significantly contributes to the pathogenesis of various human diseases. The pathological roles of the IL-6 pathway in inflammation, autoimmunity, and cancer were revealed by numerous preclinical and clinical studies. Therapeutic strategies targeting the IL-6 pathway are in development for cancers, inflammatory and autoimmune diseases.

2. Aim of the Thesis

The overall aim of the work presented in this thesis was the rational design of new compounds able to modulate activity of relevant targets involved in cancer and aging-related pathologies, namely proteasome and immunoproteasome, sirtuins and interleukin 6.

The objective of the thesis was accomplished through a multidisciplinary approach that involved different steps:

Step 1: Hit identification

State-of-the-art molecular modeling techniques, mainly virtual screening methods, was applied to selected targets to identify a limited number of small molecules able to modulate their biological activity

Step 2: In Vitro Testing

Compounds identified during Step 1 were submitted to biological testing in vitro to measure biological activity and identify the structure-activity relationships (SAR) that allow understanding the minimum requirements for activation or inhibition of biological targets.

Step 3: Lead Optimization

The more promising chemical scaffolds and the SAR data coming from Step 2 were used to design specific structural modifications, obtained through chemical synthesis, by introducing and modifying functional groups able to improve biological activity and, at the same time, to affect pharmacokinetic and pharmacodynamic profiles, such as selectivity towards similar targets or bioavailability.

Step 4: Biological Profiling

Lead compound obtained from Step 3 were submitted to complete biological profiling to verify the agreement between measured activation or inhibition of each compounds and its functional activity in selected tissues.

3. Proteasome and Immunoproteasome Inhibitors

3.1 Proteasomes: mandatory terminators.

Proteasome is the central catalytic unit of the ubiquitin proteasome system (UPS), which is used to degrade the main part of intracellular proteins. 20S standard proteasome (s-proteasome) is a cylinder-shaped complex that is composed of four stacked rings, each consisting of seven protein subunits. Each of the two inner rings contain β subunits ($\beta 1 - \beta 7$), three of which ($\beta 1, \beta 2, \beta 5$) harbor the proteolytic active sites catalyzing, by their N-terminal threonine residues, a caspase-like (C-like), trypsin-like (T-like) and chymotrypsin-like (CT-like) activity, respectively. The α -subunits ($\alpha 1 - \alpha 7$), which compose the two outer rings, have other functions such as gating the central chamber (thereby enabling the entry of substrates into the inner proteolytic cavity) and the binding of regulator complexes like the PA700, PA28 and PA200^{10,11}. The association of these regulator complexes leads to formation of multiple forms of proteasomes like 26S (PA700-20S) and 30S (PA700-20S PA700), PA28-20S and PA28-20S-PA28 complexes as well as hybrid proteasomes (PA28-20S-PA700). 26S/30S proteasomes recognize target proteins by the presence of polyubiquitin chains which are then released and the target proteins are unfolded and cleaved in a ATP-dependent manner¹²⁻¹⁴. The covalent attachment of ubiquitin to acceptor lysines in a substrate is a multi-step process that begins with activation of ubiquitin by E1 enzyme, which transports ubiquitin to an ubiquitin-conjugating enzyme (E2). The latter transfers ubiquitin to substrate either by itself or in cooperation with an ubiquitin ligase (E3). Afterwards, additional ubiquitins can be added to the first, by linkage to one of its lysines, giving rise to the polyubiquitin chain. After proteasome targeting, ubiquitin is recycled by deubiquitylating enzymes (DUBs), some of which also function to oppose the action of E3s¹⁵. It is worthy to note that the binding of polyubiquitylated proteins to the 19S regulator of mammalian and yeast 26S proteasomes enhances the peptidase activities of 20S proteasome about two-fold in a process requiring ATP hydrolysis¹⁶.

UPS performs two crucial functions for cell metabolism: first of all, by degrading obsolete, misfolded or aberrant proteins proteasomes perform housekeeping function and maintain the cellular homeostasis; secondly, through the time-specific cleavage of short-life proteins, like transcription factors or transcription factor's inhibitors (e.g. UPS cleaves I κ B- α leading to the entrance of NF- κ B in the nucleus) proteasomes are able to switch on/off many cellular pathways. Hence, the proteasome as central core of the UPS, is a sort of mandatory terminator of proteins and its inactivation leads to cellular death by apoptosis or necrosis¹⁷⁻¹⁹.

Proteasome not only cleaves proteins but also can ligate two of the produced fragments, thereby generating peptides with a sequence that differs from the sequence of the original substrate. This process, also known as proteasomal splicing, has been demonstrated in vivo so far only for four MHC class I-restricted epitopes²⁰⁻²⁴, leading to the assumption that proteasomal splicing activity is a rare event, although recent results obtained in vitro suggest that it is in fact part of the normal activity of proteasomes²⁵. Because of some inherent technical difficulties and the unexpected novelty of proteasomal splicing, the biochemical models as well as the understanding of the relevance of proteasomal splicing activity were so far only partially investigated. A deeper study of this process would have also implications from the immunological point of view, taking into account that PCPS highly increases the antigenic diversity²⁶. Indeed, proteasomes are not only responsible for the degradation of the greater part of the cytoplasmic proteins but they also generate the vast majority of virus- or self-derived peptides presented by the MHC class I molecules on cell surface^{27,28}. This latter function is generally aided by the interferon- γ (IFN- γ)-induced synthesis of the PA28- α and PA28- β proteasome activator subunits as well as of the β 1i, β 2i, β 5i alternative catalytic subunits (also known as LMP2, MECL-1 and LMP7, respectively) with concomitant formation of the immunoproteasome (i-proteasome). The different catalytic subunits confer to i-proteasome differences in cleavage preferences and degradation rates, which however, vary from substrates to substrates²⁹.

Recently, it has been described a pivotal involvement of i-proteasome in cytokine-mediated inflammation in mice, because its depletion altered T cell receptor (TcR) repertoire formation, the number of CD8⁺ T cells in the spleen, T cell survival and early activation, differentiation into inflammatory effector cells, release of pro-inflammatory cytokines, such as IL-6 which plays a pivotal role also in cancer (see below), as well as response to oxidative stress³⁰⁻³³.

Although the removal of oxidized proteins by proteasomes is clearly established³⁴⁻³⁶, recent works suggest that i-proteasomes are more prone than s-proteasome at eliminating them. Indeed, blocking expression of β 1i by siRNA significantly reduces the adaptive response to mild oxidative stress in MEF cell lines³⁷ whereas β 1i $-/-$ mice exhibit higher levels of protein carbonyls in brain and liver upon aging than those of their wild-type littermates³⁸. In addition, Seifert and co-workers showed that i-proteasome is a key element for the clearance of oxidized proteins and aggresome-like induced structures upon INF- γ stimuli³⁹. These independent observations, gathered by exploiting new i-proteasome specific inhibitors as well as i-proteasome knock-out (KO) mice, opened *de facto*

a new era in the investigation of i-proteasome functions, which were so far almost merely confined to antigen presentation.

It is worth to mention that between s- and i-proteasomes a group of intermediate-type proteasomes does exist, which are characterized by different, and tissue-specific, combinations of standard and inducible catalytic subunits, and probably by different post-translational modifications, able to alter their proteolytic activity, sensitivity to inhibitors and outer surface charge⁴⁰⁻⁴². At last, but not least, the group of Tanaka described another isoform of $\beta 5$ subunit ($\beta 5t$) specific for thymus, which characterizes the so called thymus proteasome (t-proteasome), the third main isoform of proteasomes, having specific functions in the positive/negative selection of thymocyte and in CD8⁺ T cell development^{43,44}.

3.2 Why is i-proteasome a potential therapeutic target?

The research for specific modulators of the i-proteasomes activity is a very hot topic of today's biology for several reasons. The first one, and likely most relevant, is that i-proteasome is highly expressed in normal conditions only by specific cells types of the human body, such as those involved in immune-related function or few organs like the liver⁴⁵, whereas the majority of cells barely have i-proteasome. The most famous inducer of i-proteasome synthesis is IFN- γ , usually secreted by cells during inflammation, although different studies suggested also other mechanisms, such as the activation of Toll-like receptor-4 (TLR-4)^{46,47}. In pathological situation like neurodegenerative diseases, inflammatory processes induce i-proteasome synthesis in cells (e.g. in neurons) where normally i-proteasomes are absent⁴⁸⁻⁵¹. Therefore, this disease-related expression of i-proteasome becomes a potential marker of pathological processes (potentially exerting both beneficial and detrimental effects) and possibly a therapeutic target.

Studies carried out on animal models showed that the inhibition or the absence (in $\beta 5i$ KO mice, for example) of i-proteasomes could either ameliorate or worsen the course of the disease in a disease-specific manner^{31,32,52}. Although the specific enhancement of the i-proteasome activity could likely be an appealing strategy for future therapies of selected diseases, the research in this direction is dampen by the absence of effective and treatment-compatible i-proteasome enhancers. Therefore, investigations on this topic are at present carried out only with i-proteasome inhibitors. These studies highlight two issues that must be carefully considered: the specificity of the inhibitors for the i-proteasome subunits and the potential presence of compensatory mechanisms activated in i-proteasome KO mice. The first issue will be discussed in next paragraph. The latter issue, on the

contrary, has been raised by Muchamuel *et al.* by suggesting that the increased amounts of $\beta 5$ and decreased $\beta 1i$ and $\beta 2i$ subunits in $\beta 5i$ KO mice compared to wild type mice may mask the $\beta 5i$ -specific functions in complex cellular processes such as inflammatory responses³¹.

3.3 I-proteasome as target for cancer therapy.

Cancer development is a multifactorial process, which involves various genetic alterations including the activation of oncogenes, inactivation of tumour-suppressor genes, dysregulation of cell cycle progression and apoptosis, as well as modification of immunosurveillance⁵³. Because of the crucial role of proteasomes in controlling many of these biological and metabolic processes as well as the production of MHC class I-restricted epitopes responsible for CD8⁺ cytotoxic T cell (CTL) activation⁵⁴, this protease has become an attractive target for the treatment of malignancies⁵⁵⁻⁵⁸ (Table 3.1). A number of preclinical studies showed that tumour cells are often more sensitive to proteasome blockade than normal cells and different mechanisms have been hypothesized⁵⁹. For example, many types of malignant cells rapidly proliferate and might accumulate defective proteins at a much higher rate than normal cells, thereby increasing their dependency on proteasome as disposal mechanism⁵⁸. Moreover, inhibition of proteasome causes an inactivation of NF- κ B pathway, which is involved in maintaining drug or radiation resistance in cancer cells, and it might reverse or bypass some alterations of cell-cycle and apoptotic checkpoint that lead to tumourigenesis⁵⁹. In addition, while the activity of s-proteasome is generally found to be up regulated in cancer cells⁶⁰, the levels of i-proteasome seem to vary depending on tumour types. In particular, i-proteasome is induced in haematological malignancies, such as Multiple Myeloma (MM); therefore, the selective inhibition of this proteasome isoform may increase the effectiveness of proteasome blocking and alleviate side effects associated to non selective inhibitors of specific proteasome isoforms such as bortezomib, carfilzomib and NPI-0052⁶¹ (Figure 3.1 and Table 3.2). In accordance, first-generation i-proteasome inhibitors have been developed and tested in vitro and in animal model trials. Moreover, considering the involvement of proteasomes in MHC class I-restricted epitope production and the different contribution of s-proteasome, i-proteasome as well as intermediate type proteasomes to process specific antigens, the selective inhibition of these different isoforms could play a crucial role in CTL-based immunotherapy, as described below⁶².

Disease family	Disease	Type of i-proteasome modulation	Used inhibitor
Tumours	MM	Inhibition	PR-924 ⁶³
	MM	Inhibition	IPSI-001 ⁶¹
	Prostatic cancer	Inhibition	UK-101 ^{64,65}

Table 3.1. Pathologies where an i-proteasome specific inhibition as therapy has been tested. The list includes the main pathologies where an i-proteasome inhibition has been tested. MM=Multiple Myeloma.

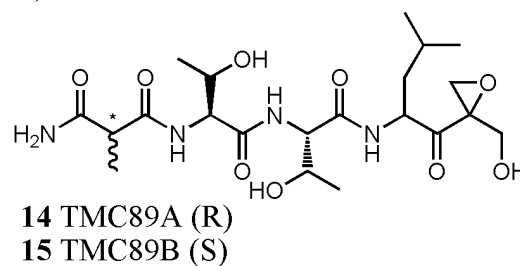
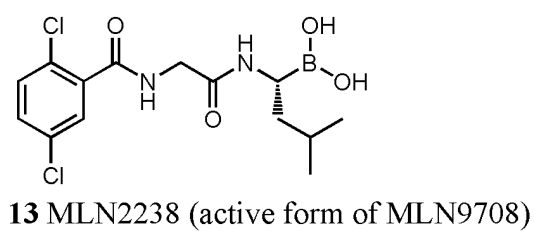
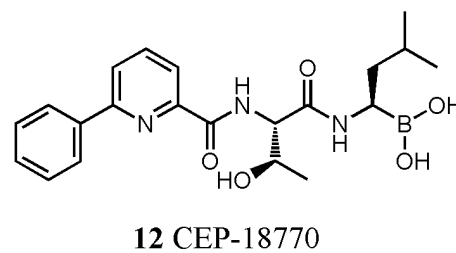
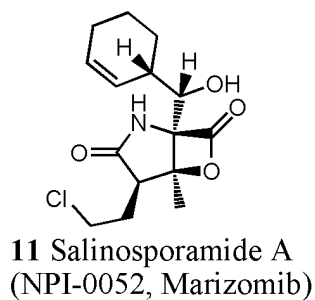
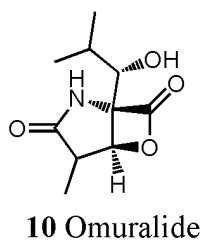
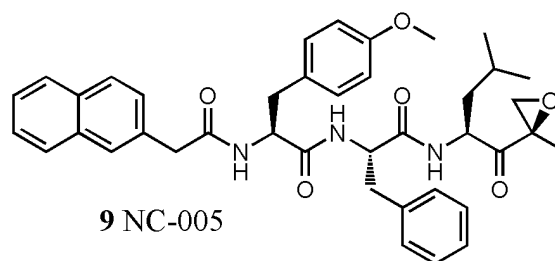
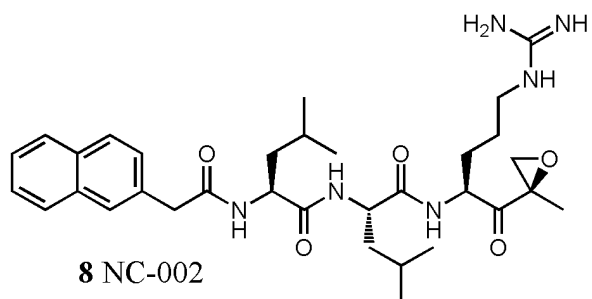
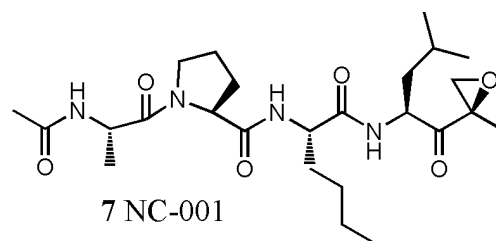
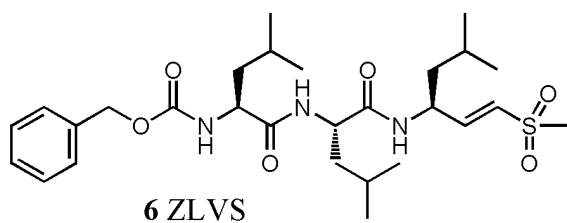
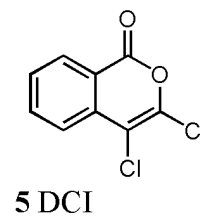
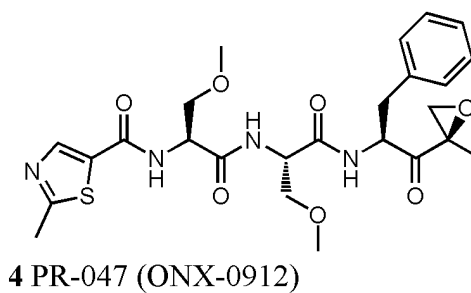
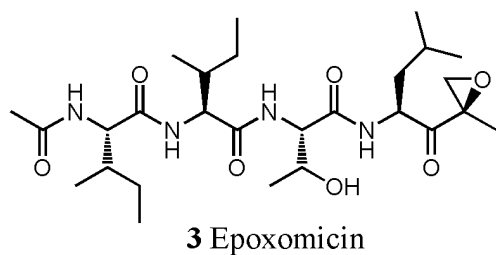
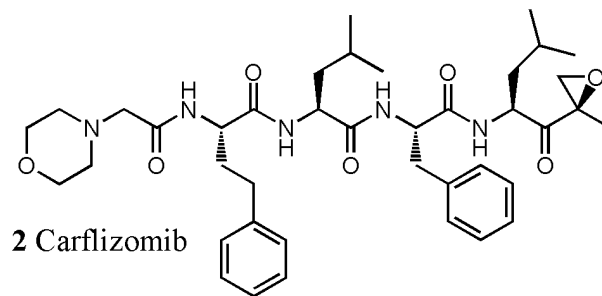
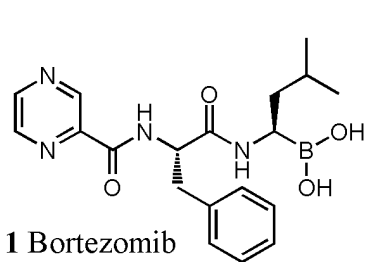
3.3.1 I-proteasome in Multiple Myeloma

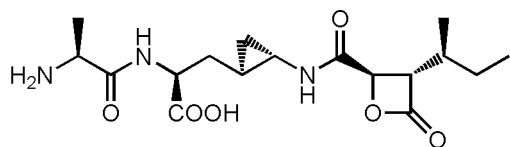
MM is a neoplastic plasma-cell disorder characterized by clonal proliferation of malignant plasma cells in the bone marrow microenvironment, accounting for approximately 1% of neoplastic diseases and 13% of haematologic cancers. Myeloma arises from an asymptomatic premalignant proliferation of monoclonal plasma cells derived from post-germinal-center B cells; multistep genetic and microenvironmental changes lead to the transformation into a malignant neoplasm. In particular, primary early chromosomal translocation occurs at the immunoglobulin switch region, while subsequent rearrangements, gene mutations and epigenetic dysregulation have been reported to affect disease progression, by altering the expression of several genes including adhesion molecules as well as responses to growth stimuli in the microenvironment. Interaction between myeloma cells and bone marrow or extracellular matrix increases tumour growth, survival and drug resistance, through the production of cytokines and growth factors such as IL-6, IL-10 and vascular endothelial growth factor among others⁶⁶. At present, the anti-myeloma therapeutic regimes are based on the different combination of immunomodulatory drugs (e.g Dexamethasone, Lenalidomide, Prednisone) and the proteasome inhibitor bortezomib, thereby leading to the disruption of several signaling pathway⁶⁷. In particular, proteasome inhibition stimulate multiple apoptotic pathways, including the induction of endoplasmic reticulum (ER) stress response, and by inhibiting the NF- κ B pathway, it down-regulates the productions of angiogenesis factors, cytokines such as IL-6 and cell adhesion molecules in the microenvironment^{58,66}. However, considering the adverse effects related to the generalized proteasome inhibition mediated by bortezomib (e.g. haematological toxicity and peripheral neuropathy) and the up-regulation of i-proteasome in primary MM patient (CD138⁺) tumour cells⁶³, a number of first-generation i-proteasome inhibitors have been tested in vitro and in animal models, showing anti-myeloma activity, mediated by several mechanisms. The selective inhibition of β 5i subunit (e.g by PR-924 or PR-957, see below) blocks

growth and triggers apoptosis in MM cell lines and MM patient's primary cells, without affecting normal peripheral blood mononuclear cells. Moreover, it allows to overcome bone marrow stromal cells mediated drug resistances, even in presence of IL-6, which is a pro-survival factor not only for MM but also for other kind of tumours, such as breast cancer⁶⁸. Additionally, it inhibits tumour growth in both human plasmacytoma xenograft and SCID-hu mouse model, by decreasing the levels of IL-6, increasing apoptosis and inhibiting angiogenesis⁶³. Noteworthy, an inhibition of the presentation of tumour epitopes that are β 5i-dependent has also been reported³¹. The same anti-proliferative activity has been showed in vitro by inhibiting the β 1i subunit (e.g by IPSI-001, see below) in lymphoid-derived tumour cells lines and MM patient-derived samples. This effect is exerted by the combined activation of the intrinsic and extrinsic apoptotic pathway and the inhibition of NF- κ B signaling. Moreover, an overcome drug resistance to doxorubicin, melphalan and bortezomib as well as an improved toxicity profile in nonhematopoietic tissues have been described⁶¹.

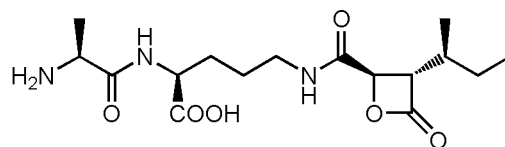
3.3.2 I-proteasome in solid tumours.

At present, no data are available on the application of i-proteasome specific inhibitors to other kind of haematological malignancies such as acute myeloid leukemia (AML) and solid tumors, although the selective inhibition of the β 1i subunit (i.e. by UK-101, see below) led to growth-inhibitory activity in prostatic cancer cells^{64,65}. In these tumours, a heterogeneous expression of the antigen-processing machinery (APM), including i-proteasome subunits, is observed and often correlates to the progression of disease and the immune response escape⁵³. Indeed, in bone marrow biopsies of AML patients multiple defects in APM expression were reported and remarkably a progressive downregulation of APM was seen from initial diagnosis to relapse⁶⁹. In renal carcinoma cells lower levels of β 1i and β 5i subunits as well as of the epitope transporters into ER (i.e. TAPs) have been found and they were more pronounced in metastatic lesions than primary tumour⁵³. The same scenario has been observed in hepatocellular carcinoma cell lines⁷⁰ and primary malignant melanoma lesions, associated with lack of spontaneous regression⁷¹ whereas mice lacking β 1i subunit develop spontaneous uterine leiomyosarcoma⁷². An up-regulation of i-proteasome and an increased CTL response against tumour antigens have been observed in vitro in hepatocarcinoma cell lines after the administration of INF- γ ⁷⁰, suggesting that in certain cases restoration rather than inhibition of i-proteasome functionality could be effective in anti-tumour induced-response, by enhancing the production of tumour-specific MHC class I-restricted epitopes.

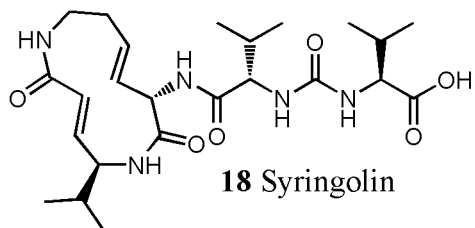




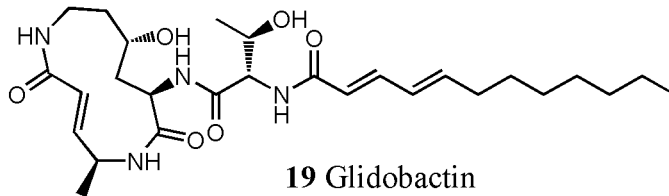
16 Belactosin A



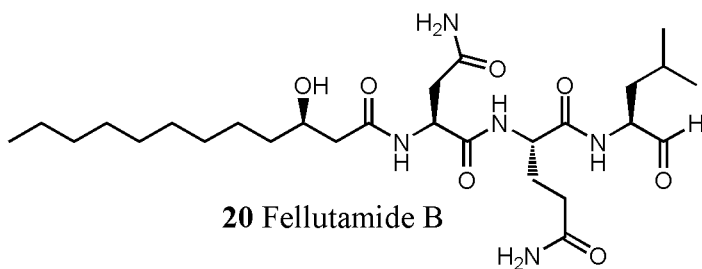
17 Belactosin C



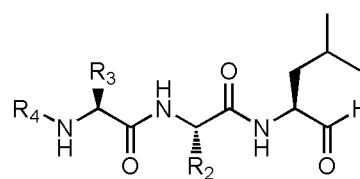
18 Syringolin



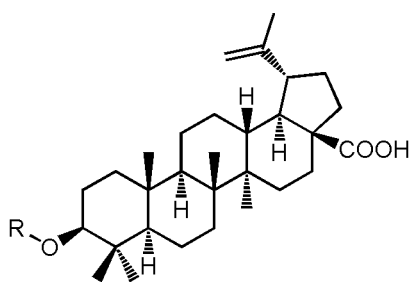
19 Glidobactin



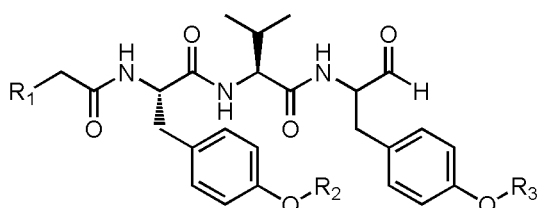
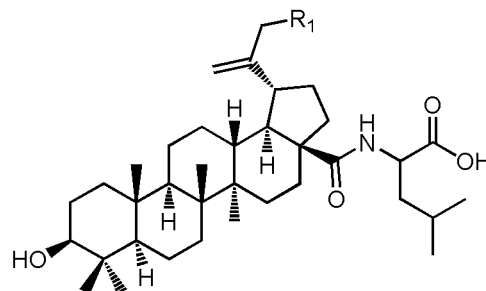
20 Fellutamide B



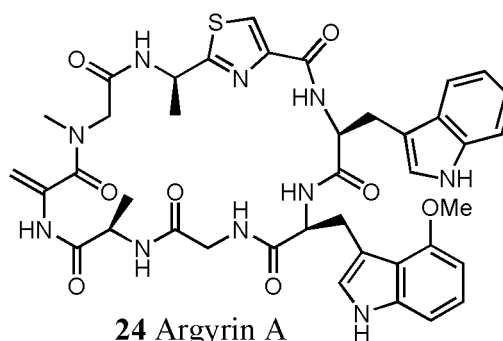
21 Peptide aldehydes



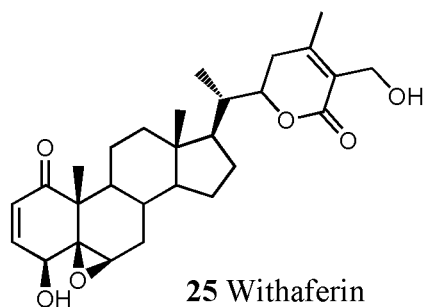
22 Betulinic acid derivatives



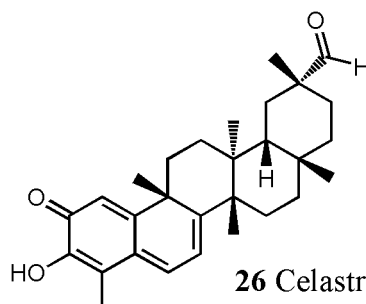
23 Tyropeptin A derivatives



24 Argyrin A



25 Withaferin



26 Celastrol

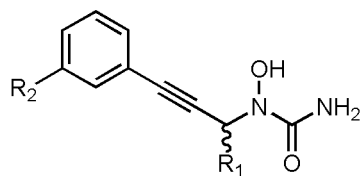
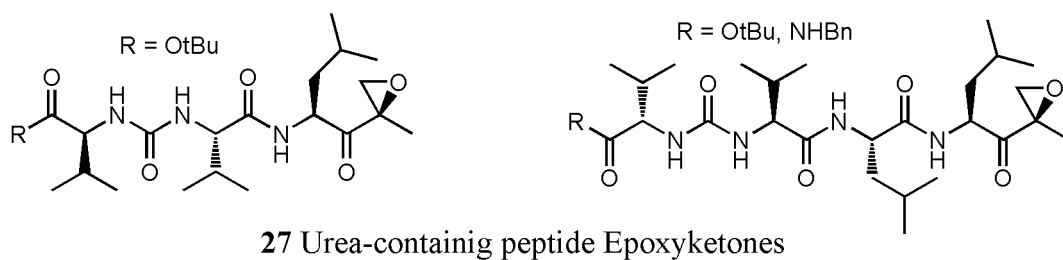


Figure 3.1. Chemical structures of promiscuous proteasome inhibitors.

Structure	Selectivity		Inhibition mechanism
	Subunit	Activity	
1	All	All	reversible
2	$\beta 5, \beta 5i$	CT-like	irreversible
3	$\beta 2, \beta 5, \beta 5i, \beta 2i$	CT-like>T-like>C-like	irreversible
4	$\beta 5, \beta 5i$	CT-like	irreversible
5	$\beta 5, \beta 1i$	CT-like	reversible
6	All	All	irreversible
7	$\beta 1, \beta 1i$	C-like	irreversible
8	$\beta 2$	T-like	irreversible
9	$\beta 5, \beta 5i$	CT-like	irreversible
10	$\beta 5$	CT-like	reversible
11	$\beta 1, \beta 2, \beta 5$	CT-like>T-like>C-like	irreversible
12	$\beta 5$	CT-like	reversible
13	$\beta 5$	CT-like>T-like, C-like	reversible
14	$\beta 2>\beta 5>\beta 1$	T-like>CT-like>C-like	irreversible
15	$\beta 2>\beta 5>\beta 1$	T-like>CT-like>C-like	irreversible
16	$\beta 5>\beta 1, \beta 2$	CT-like>C-like, T-like	irreversible
17	$\beta 5>\beta 1, \beta 2$	CT-like>C-like, T-like	irreversible
18	All	All	irreversible
19	$\beta 5$ and $\beta 2$	CT-like>T-like	irreversible
20	$\beta 5>\beta 1, \beta 2$	CT-like>C-like, T-like	reversible
21	$\beta 5$	CT-like	reversible
22	$\beta 5$	CT-like	non covalent
23	$\beta 5$	CT-like	reversible
24	$\beta 5>\beta 2, \beta 1$	CT-like> T-like, C-like	non covalent
25	$\beta 5$	CT-like	
26	$\beta 5$	CT-like	
27	$\beta 1 / \beta 5$	C-like / CT-like	irreversible
28	$\beta 5$	CT-like	non covalent

Table 3.2. Activity profiles of promiscuous inhibitors of s- and i-proteasomes. Structure enumeration of proteasome inhibitors refers to what reported in Fig. 3.1. Proteasome activities, as defined with short-fluorogenic substrate assay, are shortened as following: CT-like = chymotrypsin-like, T-like = trypsin-like, C-like = caspase-like.

3.3.3 I-proteasome as a target for immunotherapy?

The concept of using vaccination in the treatment of cancer has been tied to the history of vaccines themselves. However, the major interest in it has recently grown with the increasing understanding of the role that the immune system (IS) plays in shaping the biological behavior of cancer, including the identification of tumour antigens recognized by CTLs⁷³. As above mentioned, the MHC class I-restricted antigen presentation is generally enhanced after IFN- γ stimuli by inducing the expression of i-proteasomes, PA28- $\alpha\beta$, TAPs and MHC class I molecules²⁹. It has been proposed that i-proteasome increases the production of MHC class I-restricted epitopes because of its higher inclination for generating peptides with hydrophobic and basic C-termini, which shall have a better affinity for the APM⁷⁴. Nevertheless, the group of Van den Eynde reported some examples of MHC class I-restricted tumour (self)-epitopes that were better generated by s-proteasome than i-proteasome⁷⁵⁻⁷⁸. They speculated that s-proteasome could better generate self-epitopes in contrast to i-proteasome more efficient in viral epitope production⁷⁵. This difference between s- and i-proteasome might have fallouts on CD8⁺ T cell-mediated immune response at different levels, including thymocytes development, tolerance induction, CTL activation as well as cancer immunotherapy. Although this theory is quite appealing, we believe that the limited number of self- and viral-epitopes properly investigated so far does not allow to statistically confirm it. In addition, this theory recently evolved because the group of Van den Eynde showed also that two tumour epitopes of MAGE-A*03 and -A*10 proteins are processed exclusively by intermediate type proteasomes, which are variably expressed in tumour, dendritic cells and in normal tissues^{18,79,80}.

In summary, the results obtained in the last decade suggest that the repertoire of antigens presented by a given cell is strongly affected by its proteasome content, composition as well as the levels of their regulators, which could modify cleavage properties of protein substrates⁸¹. This observation could have strong implications on cancer immunosurveillance although further investigations are mandatory to define the role of different proteasome isoforms in immunotherapy against cancer.

3.4 I-proteasome as target for neuropathologies

Although in young healthy human central nervous system (CNS) i-proteasomes are almost absent, they have been detected in cells of different CNS areas from elderly subjects as well as from patients affected by Alzheimer (AD) or Huntington (HD) diseases^{49,51}, Multiple Sclerosis (MS) with a concomitant expression of the PA28- $\alpha\beta$ complex⁵⁰ and very recently in Temporal Lobe Epilepsies (TLE)⁴⁸ (Table 3.1). The induction of i-proteasome and PA28- $\alpha\beta$ expression in brain could have

effects on different pathways because UPS regulates in neurons, for example, the pre- and post-synaptic plasticity and the protein turnover⁸². Processes and mechanisms responsible of cerebral i-proteasome synthesis are still unknown. Neuroinflammation could be the trigger of i-proteasome expression as we hypothesized for aging, AD, MS and TLE⁴⁸⁻⁵⁰, which will be briefly here discussed as example of age-related (i.e. AD) or autoimmune (i.e. MS) neurodegenerative diseases and epilepsies (i.e. TLE). It is worthy to note that i-proteasome synthesis induction could be limited to CNS or be the result of a phenomenon started in periphery and transferred to CNS, as it might occur during the onset of MS. Accordingly, IS regulation in other organs could have implications also at CNS level, including the regulation of i-proteasome expression. For example, a cross-talk between brain and gut with implications for the IS has been proposed recently in studies on experimental autoimmune encephalomyelitis (EAE)⁸³⁻⁸⁵.

3.4.1 Alzheimer disease.

AD is a devastating neurodegenerative disorder of the CNS occurring most frequently in later stages of adulthood. AD is associated with a specific pattern of pathological changes in brain that result in neurodegeneration and progressive development of dementia. These pathological hallmarks of AD are neuronal loss accompanied by intraneuronal neurofibrillary tangles formed of tau-based paired helical filaments (PHFs) and extracellular senile plaques of β -amyloid⁸⁶. It has been reported that PHFs inhibit proteasome activity and it has been suggested that this inhibition may induce neuronal damage in AD⁸⁷. Furthermore, UPS is also involved in the control of the physiological maturation of the β -amyloid precursor protein by modulating the intracellular concentration of presenilins⁸⁸. An inhibition of proteasome activity in crude extracts from AD affected brain areas has been described, whereas an investigation carried out on 20S proteasome purified from the frontal neocortex of AD patients suggested that the observed drop of 20S proteasome activity in AD tissue could be due to the presence of inhibitory molecules more than to an intrinsic decrease of the 20S proteasome functionality^{87,89,90}.

AD occurs usually in elderly brain, where i-proteasome expression is already present in different cells types, maybe as a result of the inflamm-aging phenomenon and/or as attempt to cope with the increasing oxidative stress⁹¹. I-proteasome expression is further induced in hippocampi (but not in cerebellum) of AD patients⁴⁹ and its presence varies among different neuronal sub-types. It has been speculated that i-proteasome expression might be an attempt to tackle the accumulation of oxidised proteins and phosphorylated tau that occur during AD progression, since they are both preferentially degraded by i-proteasome^{39,92}. However, the few available information about the role

of i-proteasome in AD does not allow us to estimate if an inhibition of i-proteasome function would lead to a progression or a reduction of the neurological damage. In addition, AD clinical symptoms emerge when the neurological damage is already pronounced; therefore, we might speculate that a modulation of i-proteasome function at the early stages of the disease could have different effects (even opposite) than a modulation in the late stages of AD.

3.4.2 Multiple Sclerosis.

MS is the most common autoimmune disorder of the CNS. It is characterized by multifocal areas of demyelization (plaques), chronic inflammation and damage to oligodendrocytes and neurons. The cause of MS is still unknown and disease pathways are poorly understood. However, the association of HLA-DRB1*15 and other HLA class I (e.g. HLA-A*02 and HLA-A*03) and class II alleles, the presence of autoreactive T lymphocytes together with other inflammatory cells and cytokines in active MS lesions suggest an autoimmune pathogenesis. Accordingly, EAE, a classical mouse model for MS, can be induced by the administration of myelin antigens or CD4⁺ and CD8⁺ T lymphocytes specific for those antigens⁹³⁻⁹⁵. It has been proposed that the first bout of the disease is mediated by CD8⁺ T cells while the first relapse and MS progression are mediated by CD4⁺ T cells through different mechanisms such as antigen release and epitope spreading⁹⁶.

Although preliminary observations on white and grey matters of MS patients suggested that 20S and 26S proteasomes activity is decreased compared to controls⁹⁷, no information are so far available on proteasome activity in plaques, although an accumulation of i-proteasome has been observed⁵⁰. In CNS of subjects affected by MS, i-proteasomes are expressed in different cell types such as oligodendrocytes, astrocytes, macrophages/microglia, infiltrating lymphocytes and, weakly, in neurons as demonstrated by double IHC assays. A similar expression has been described also for the subunit α of the PA28 complex. Intriguingly, the polymorphic variant HH at the codon 60 of β 1i subunit was significantly less present in a sizeable Italian MS population (OR = 0.44) restricted to females carrying the HLA-A*02 allele⁵⁰. The Authors correlated this genetic data to the observation that a HLA-A*02-restricted epitope (MBP111-119), which activates memory T cells preferentially in blood of MS patients⁹⁸⁻¹⁰⁰, was produced in lower amount during *in vitro* digestion by 20S i-proteasome carrying the variant HH at the codon 60 of β 1i subunit. Authors speculated that a lower production and presentation of this epitope as well as other myelin epitopes bound to the HLA-A*02, could reduce the probability to disrupt the physiological tolerance (central or peripheral) of myelin-specific CTLs and/or their cytotoxicity towards oligodendrocytes, thereby restraining the MS onset⁵⁰. The i-proteasome activity and the β 1i R60H polymorphism might have

implications also at thymic level during the selection of myelin –reactive thymocytes although no exhaustive information is available to this regard.

Furthermore, the study of Seifert and colleagues suggested another i-proteasome-related mechanism that could affect the MS onset. Indeed, they showed that i-proteasome is essential for an efficient clearance of oxidised and polyubiquitylated proteins upon IFN- γ induced oxidative stress, thereby preserving protein homeostasis during inflammation. Accordingly to this observation, they reported that $\beta 5i$ ko mice showed an earlier onset and worst clinical score than wild type mice in an EAE model³⁹. Although these two studies would suggest that i-proteasomes may influence onset and progression of MS affecting both the myelin-specific CD8⁺ T cell activity and the response of different cell types to the inflammatory aggression both in periphery and in the CNS, further independent confirmations are needed before drawing a model connecting i-proteasome and MS which could have a remarkable spin-off for future therapeutic approaches to the disease.

3.4.3 Temporal Lobe Epilepsy.

Epilepsy is a neurological disorder that affects about 50 million people worldwide and is characterized by an enduring predisposition to generate seizures as well as by emotional and cognitive dysfunctions. About 30% of epileptic patients are defined pharmaco-resistant since they do not adequately respond to therapies and in these patients, affected by TLE, the surgical removal of the epileptic focus is often the only therapeutic option to achieve seizure control¹⁰¹.

The evidences available from experimental and clinical findings support a crucial role of immune and inflammatory processes in the aetiopathogenesis of epilepsy⁴⁷. Pronounced inflammatory processes have been described in human epileptogenic brain tissue from TLE and epilepsies associated with malformations of cortical development, where seizures are often refractory to anticonvulsant treatments¹⁰².

Pharmacological studies in experimental models and the use of transgenic mice with perturbed cytokine systems showed that proinflammatory cytokines (e.g. IL-1 β , TNF- α), danger signals (e.g. HMGB1), complement factors and prostaglandins significantly contribute to seizure activity and cell loss, and that inhibition of the production of these molecules or blockade of their receptors (e.g. ILR1, TLR-4), significantly reduced seizure activity¹⁰³.

Recently, i-proteasomes have been detected in cortex and hippocampus of patients affected by different TLE forms⁴⁸. By IHC staining i-proteasomes were revealed in glia and neurons of TLE hippocampi whereas controls showed positivity to $\beta 1i$ and $\beta 5i$ only in luminal endothelial cells, as

observed in other studies^{49,50}. Intriguingly, the neuronal i-proteasome expression differs between TLE forms. Furthermore, no IFN- γ was detected in TLE specimens suggesting that in this disease i-proteasome synthesis is induced by a different mechanism. A good candidate could be TLR-4, which can be triggered by LPS treatment, a well-known i-proteasome inducer. Thus, taking into account the role that TLR-4 plays in the disease, we might speculate that i-proteasome is one of the molecules induced/activated by TLR-4 pathway that mediate the effects that this receptor has during epileptogenesis. Further investigations are however mandatory to address this issue as well as to understand the role of i-proteasome in the different neuroinflammatory processes involved in epilepsy.

It is worth to note that so far no studies have exploited the availability of i-proteasome ko mice by crossing them with disease animal models (e.g. APP/PS1 model for AD) or inducing a disease-associated symptoms by drugs such as pilocarpine or kainite (as epilepsy models), respectively. We surmise that these types of studies will provide breakthrough information on the disease aetiology/progression and the involvement of i-proteasome in the pathological mechanisms.

3.5 An overview of selective s- and i-proteasome inhibitors and enhancers.

Despite the efforts made in recent years to discover selective inhibitors for either s-proteasome or i-proteasome, only six compounds showing some selectivity (two for the s-proteasome, PR-893 and PR-825, and four for the i-proteasome, PR-924, PR-957, IPSI-001 and UK-101) have been described (Table 3.2 and Figure 3.2). PR-893 (compound 1 in Fig. 3.2) is a tripeptide epoxyketone which shows a selectivity of 20 folds for $\beta 5$ over $\beta 5i$ subunits¹⁰⁴. This molecule was used by Parlati and co-workers to prove, in their pioneering study, the relationship between the selective inhibition of subunits ($\beta 5$ and $\beta 5i$) with chymotrypsin-like (CT-like) activity and the antitumour response in tumour cells of haematological origin. The same reactive portion of PR-893 can be found in PR-825 (compound 2 in Fig. 3.2), an analogue of carfilzomib (compound 2 in Fig. 3.1), which has been synthesized by Zhou et al. by varying the P2, P3 and N-Cap of bortezomib¹⁰⁵. These variations gave rise to an inhibitor of proteasomal CT-like activity, which is about 14 folds more selective towards $\beta 5$ as respect to $\beta 5i$. On the other hand, two selective inhibitors related to carfilzomib (compound 2, in Fig.3.1), namely PR-924 (comp. 3, Fig. 3.2) and PR-957 (comp. 4, Fig. 3.2), have been developed to target $\beta 5i$ subunit of the i-proteasome¹⁰⁶. As in the case of the above-mentioned s-proteasome inhibitors, these two compounds are tripeptide epoxyketones. Their structure differs

from s-proteasome selective inhibitors for the presence of three marked aromatic and hydrophobic pharmacophoric features. In particular, both PR-924 and PR-957 have two aromatic moieties in the proximity of the reactive group, i.e. epoxyketones phenylalanine instead of epoxyketone leucine of PR-893 and PR-825 as well as bulkier tryptophan (PR-924) and tyrosine (PR-957) instead of smaller side-chain amino acids for PR-893 and PR-825. Equally, the N-protecting groups are also more hydrophobic and large as respect to s-proteasome inhibitors. All these hydrophobic/aromatic features are expected to interact with specific moieties of the $\beta 5i$ binding site and, as discussed below, these may constitute the molecular reason for the i-proteasome selectivity over s-proteasome catalytic activity. In fact, PR-957 is reported to be 20- to 40- more selective for murine $\beta 5i$ over $\beta 5$ and $\beta 1i$ subunits and, at the concentration which allows minimal impact on other subunits, it inhibited the presentation of $\beta 5i$ -dependent epitopes³¹. Equally, PR-924 was shown to be 100-fold more selective for human $\beta 5i$ and less selective for CT-like activity of $\beta 5$ as compared to bortezomib and carfilzomib⁶³. The selective inhibition of i-proteasome has been obtained also with a dipeptide aldehydes compound, IPSI-001 (compound 5, Fig. 3.2) that targets the $\beta 1i$ subunit and inhibit i-proteasome C-like and CT-like activity *in vitro* in lymphoid-derived tumour cells lines and MM patient-derived samples. Similarly to PR-924 and PR-957, IPSI-001 has three hydrophobic and extended features such as the carboxybenzyl N-protecting group and the n-propyl side chain close to the reactive aldehyde. Finally, another $\beta 1i$ specific inhibitor, UK-101, (compound 6, Fig. 3.2) has been developed by Ho and co-workers, demonstrating growth-inhibitory activity in prostatic cancer cells expressing higher level of $\beta 1i$ with no effect on s-proteasome function^{64,65}. UK-101, like IPSI-001, is also a dipeptide with a tert-butyldimethylsilyl group attached at the C-terminal hydroxyl group⁶⁵. All the above-mentioned s- and i-proteasome inhibitors covalently modify the catalytic N-terminal Thr of the proteolytic β subunits thereby affecting specific activities by means of covalent reversible or irreversible inhibition mechanisms (Table 3.3). Considering the large number of promiscuous inhibitors of s- and i-proteasome, which can bind reversibly or irreversibly the catalytic Thr, such as epoxyketones, aldehydes, vinylsulfones, β -lactones, boronic acids, isocoumarins and Michael acceptors (Fig. 3.1 and Table 3.2), it should be pointed out that only epoxyketones and aldehydes have been reported as i- and s-proteasome specific inhibitors (compounds 1-6 in Fig. 3.2 and Table 3.3). In this regard, it should be noted that, while some efforts have been done to modify the reactive threonine-trap of s-proteasome inhibitors^{107,108}, no similar strategies have been yet explored to modify known specific i-proteasome scaffolds with other reactive groups. It is therefore unclear whether other Thr-traps may be conveniently used for the design of novel i-proteasome specific inhibitors. Similarly, it is interesting to note also that non-

peptide-like compound such as Salinosporamide (compound 11 in Fig. 3.1), Belactosin (compound 16-17 in Fig. 3.1) and Betulinic acid derivatives (compound 22 in Fig. 3.1) have been so far only described among promiscuous s- and i-proteasome inhibitors (Fig. 3.1). Even in this case, it is still to be ascertained whether it is possible to optimize classes of non-peptide-like compounds in order to reach some selectivity either for s- or i-proteasome. In this context, new insights on immunoproteasome structure obtained either by modelling results (see next paragraph) or new crystallographic resolutions promise to be highly relevant for the rational design of novel selective inhibitors. Although the inhibition mechanism of proteasomes has been extensively reviewed by several authors^{106,109–112}, few information about mechanisms of activation or reversible inhibition are available. For example, betulinic acid derivatives (compound 22 in Fig. 3.1) were proved to inhibit CT-like activity¹¹³ but there is no specific information about their inhibition mechanisms, as well as for Argyrin A (compound 24 in Fig. 3.1)¹¹⁴. On the other hand, Gallastegui et al. demonstrated, by resolving the crystal structure of s-proteasome in complex with the most potent hydroxyurea derivative (PDB ID: 3SHJ)¹¹⁵, that new hydroxyurea derivatives (compound 28 in Fig. 3.1) bind non-covalently the site with CT-like activity. In contrast to the development of 20S inhibitors, drug-like molecules that can activate or enhance proteasome activity are, at present, rare and not well characterized, even if they could represent an appealing strategy for specific diseases in which proteasome activity has to be increased to cure the patient. Apart the role of PA28, PA700 and PA200 regulators in proteasome activation, several type of small molecules including SDS, lipids (oleic and linoleic acids) and peptide-based compounds were shown to activate proteasome at relatively high concentrations¹¹⁶. On the contrary, oleuropein (compound 8, Fig. 3.2), *Phaeodactylum tricornutum* algae extract and betulinic acid (compound 7, Fig. 3.2) can activate proteasome at low micromolar concentration. Oleuropein is the major component isolated from the *Olea europaea*, it is able to increase in vitro all three proteolytic activities and delay replicative senescence of human embryonic fibroblast¹¹⁷. The same results have been obtained by *Phaeodactylum tricornutum* algae extract, which stimulates all three proteolytic activities of proteasome in vitro and in human keratinocytes thereby reducing the level of oxidized proteins¹¹⁸. Conversely, betulinic acid, a triterpene derived from many plant species, preferentially activates the CT-like activity of proteasome¹¹⁹, even if inhibitory effects have also been reported as above described. Finally, Chondrogianni and co-workers identified quercetin (compound 9, Fig. 3.2) and its derivative, namely quercetin caprylate (QU-CAP) as a proteasome activator with anti-oxidant properties that can influence cellular lifespan, survival and viability of HFL-1 primary human fibroblasts. Moreover, when these compounds were supplemented to already senescent fibroblasts,

a rejuvenating effect was observed¹²⁰. The mechanism of action of all these compounds is supposed to be linked to conformational changes of the channel gates regulated by the α subunits of the proteasome although further investigations are needed to characterize their enhancer properties. In addition, recent and ongoing research aim to elucidate the roles of other components of the UPS has identified several enzymes, beside the 20S catalytic core, that can be additional targets for therapeutic intervention by small-molecule modulators¹²¹. In particular, an enhancement of proteasome activity by a small-molecule inhibitor of the DUB USP14 has been reported¹²², as well as an anticancer activity of another compound which inhibits both UCHL5 and USP14 enzymes¹²³, suggesting that the deubiquitinating activity of the PA700 regulator could represent a new anticancer drug targets.

3.6 Human immunoproteasome model.

Despite the importance of i-proteasome as an emerging biological target for cancer and neuropathologies, until 2013 no crystallographic structure of the human form has been solved. A possible strategy to compensate that lack of knowledge was the generation of *in silico* human i-proteasome models, which could provide helpful hints for the development of selective i-proteasome modulators. Accordingly, we generated the human model of the whole i-proteasome by starting from the X-ray structure of the mammalian 20S proteasome (PDB id: 1IRU) and substituting of the six catalytic subunits of the inner rings with the related i-proteasome subunits (Table 3.4).

At first we checked the similarity between β subunits in the two inner rings of the proteasome structure. Root mean square deviation (RMSD) for each couple of homolog-subunits was found to be in the range 0.6-1.3 on all atoms, thereby indicating that homolog- β -subunits of the two inner rings can be considered equivalent. The raw models of β i-subunits were taken from the SwissModel repository¹²⁴ and aligned to chain H, I, L for β 1, β 2 and β 5, respectively. The same models were used also to represent the i-proteasome subunits of the other inner ring. The entire i-proteasome model was generated by substitution of the six catalytic chains and followed by several structural corrections/refinements such as hydrogen addition, water and ions removal, manual charges corrections, addition of missing side chains and optimization of hydrogen bonds. In order to analyze at the molecular level the aminoacidic differences between s- and i-proteasome we reported in Fig. 3.3 and Table 5.3 a pair-wise comparison of the β subunit catalytic pockets of the

mammalian s-proteasome crystallographic structure (PDB id: 1IRU) and the model of human i-proteasome that we derived.

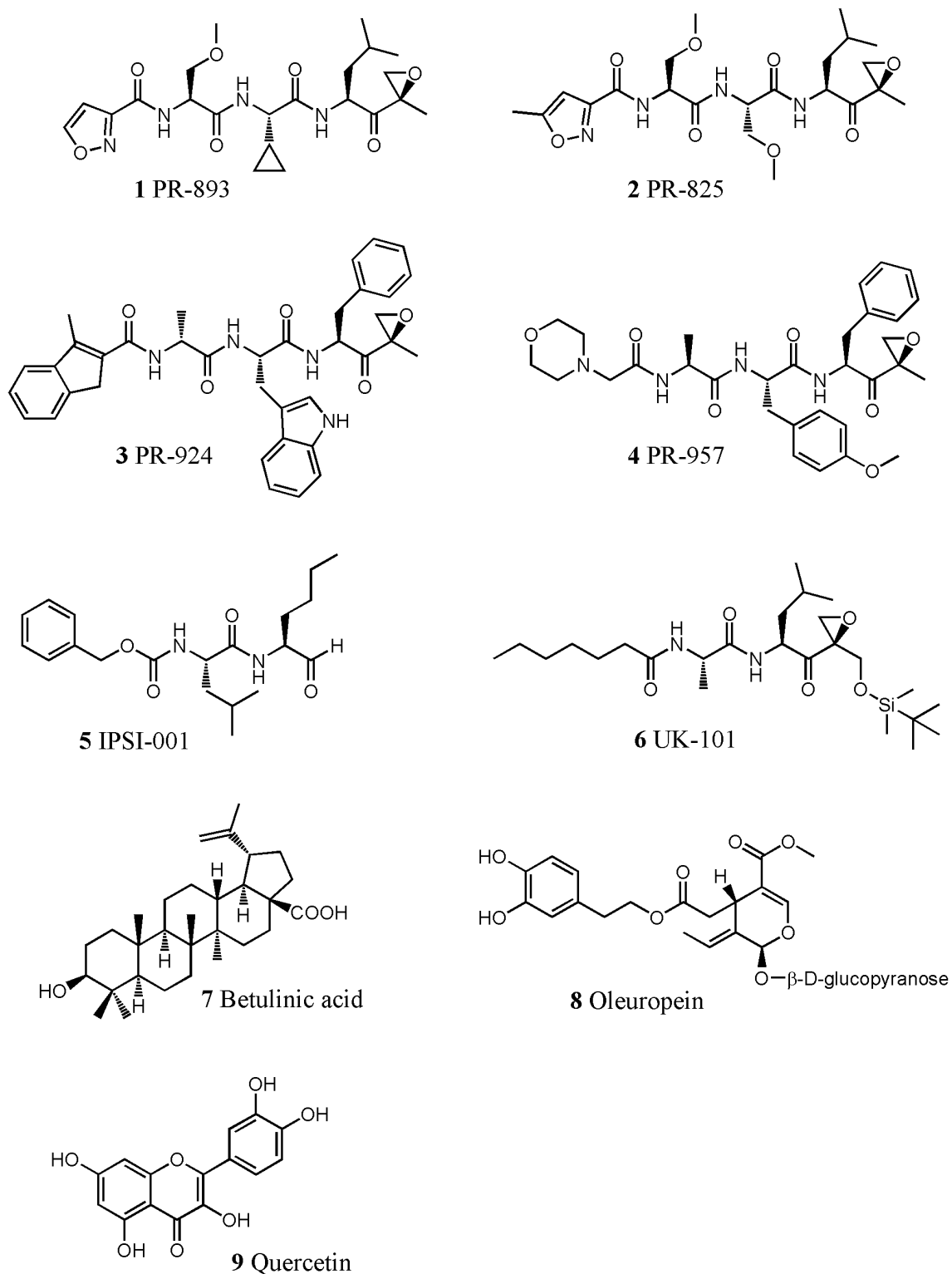


Figure 3.2. Chemical structures of selective s- and i-proteasome inhibitors and activators of proteasomes.

Compound	Selectivity		Mechanism and biological effect
	Subunit	Activity	
1	$\beta 5$	CT-like	irreversible inhibitor
2	$\beta 5$	CT-like	irreversible inhibitor
3	$\beta 5i$	CT-like	irreversible inhibitor
4	$\beta 5i$	CT-like	irreversible inhibitor
5	$\beta 1i$	CT-like > C-like > T-like BrAAP	reversible inhibitor
6	$\beta 1i$	CT-like	irreversible inhibitor
7	α^a		activator
8	α^a		activator
9	α^a		activator

Table 3.3. Activity profiles of s- and i-proteasome inhibitors as well as proteasome enhancers. Inhibition form, inhibited proteasome activities and relative references are reported. Proteasome activities, as defined with short-fluorogenic substrate assay, are shortened as following: CT-like = chymotrypsin-like, T-like = trypsin-like, C-like = caspase-like. Structure enumeration of proteasome inhibitors refers to what reported in Fig. 3.2. α^a : the mechanism of these compounds has been hypothesised to be related to conformational change perturbations of α -type subunits.

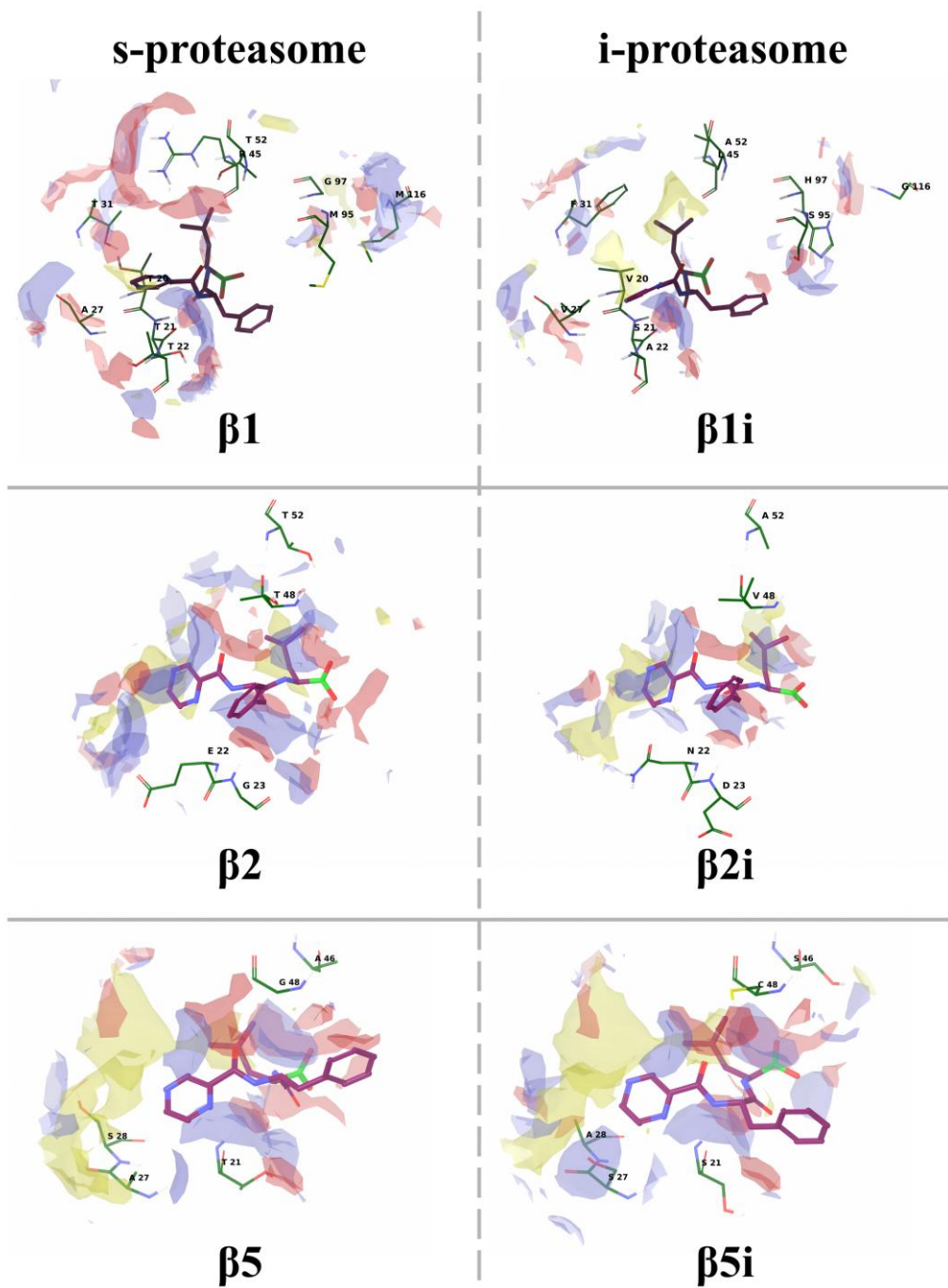


Figure 3.3. Comparison of s-proteasome and i-proteasome β -subunits in complex with bortezomib. S-proteasome subunits were taken from the crystallographic structure of the human 20S proteasome (PDB id: 1IRU) while i-proteasome subunits were derived by our model (see above). Initial binding poses of bortezomib (compound 1 in Fig. 1) were taken by the crystal structure of the yeast proteasome (PDB id: 2F16) aligned with correspondent subunits of the human proteasome (PDB id: 1IRU) and followed by ligand minimizations. Contour maps were generated with the software SiteMap [136], thereby producing hydrophobic (yellow regions), donor (blue regions) and acceptor (red regions) potentials. Contour maps represent the ideal region of the space where a corresponding ligand feature should be located in order to interact optimally with the subunits.

The catalytic binding sites of s- and i-proteasome generally show a similarity in shape and volume between $\beta 1$, $\beta 2$ and $\beta 5$ and their corresponding $\beta 1i$, $\beta 2i$ and $\beta 5i$ subunits. This simple fact might suggest that ligands with similar shape and volume properties fit equally in s- and i-proteasome homologue subunits. However, a deeper structural analysis shows that non-negligible differences between s-proteasome and i-proteasome are present in the aminoacidic composition of some of the catalytic pocket residues. In particular, we analyzed residues of the binding site that differ from s- to i-proteasome chains observing that $\beta 1$ and $\beta 1i$ subunits show the higher degree of variability since ten residues differ in the substrate binding site (Fig. 3.3 and Table 5.3). On the other hand, five residues differ from $\beta 5$ and $\beta 5i$ subunits whereas only four residues change from $\beta 2$ to $\beta 2i$ subunits. Most interesting is to analyze the differential nature and position of these changes vis-à-vis to the binding of putative s- or i-proteasome inhibitors. We did such analysis by taking advantage of the structural information available from co-crystallized structure of bortezomib with yeast s-proteasome (PDB id: 2F16). In Fig. 3.3 we graphically reported the location of the aminoacids listed in Table 5.3 and depicted binding site differences in terms of contour maps that represent the ideal region of the space where a ligand feature should be located in order to interact optimally with the single subunits. In some cases differences involve relevant changes of aminoacid properties that are likely to be important for the binding of putative selective inhibitors. For instance Arg45 of the $\beta 1$ subunit is substituted to a Leu45 in the $\beta 1i$ subunit. This change implies the existence of a noticeable hydrophobic region in the binding site of the $\beta 1i$ subunit (yellow region, Fig. 3.3) that is not present in the $\beta 1$ subunit due to the polar nature of the arginine residue. Despite such a difference occurs in the binding site of both subunits, bortezomib seems not to be influenced by this change and this might constitute one of the reasons behind the promiscuous nature of this inhibitor towards s- and i-proteasome. Another major difference involves residues of Ala27 and Ser28 of the $\beta 5$ subunit, which are inversed in the $\beta 5i$ subunit, i.e. Ser27 and Ala28. This simple inversion relocates the hydrophilicity of the serine residue thereby becoming more accessible for the putative binding of ligands. Even in this case the non-selectivity of bortezomib may be explained by the fact that its binding is not influenced by such aminoacidic switch, although selective lead compounds might be developed in light of these considerations. In contrast, $\beta 2$ and $\beta 2i$ subunits seem to be very similar in terms of aminoacidic properties. This fact is graphically reflected by similar shapes and colours of the contour maps of Fig. 3.3. Thus, from these data, it appears particularly challenging to exploit differential binding site composition of $\beta 2$ and $\beta 2i$ subunits in order to conceive selective inhibitors. This consideration may also explain why no selective s- or i-proteasome inhibitors targeting the trypsin-like (T-like) activity have been discovered so far. Finally, by comparing $\beta 1$, $\beta 2$

and $\beta 5$ subunits it is interesting to note that both in the crystal structure of the yeast proteasome (PDB id: 2F16) as well as in our i-proteasome model, bortezomib assumes a markedly different molecular conformation in $\beta 2$ and $\beta 2i$ while other subunits, i.e. $\beta 1/\beta 1i$ and $\beta 5/\beta 5i$ seem to accommodate the ligand with the same binding mode (Fig. 3.3). Huber et al.¹²⁵ published several crystal structures of the yeast 20S proteasome and of the mouse 20S s-proteasome and i-proteasome in presence or absence of the i-proteasome specific inhibitor PR-957 (compound 4 in Fig. 3.2; PDB ids: 3UN4, 3UN8, 3UNB, 3UNE, 3UNH and 3UNF). Through the analysis of the crystallographic structure the authors identified a unique catalytic feature for the i-proteasome $\beta 5i$ active site and, together with conformational changes occurring upon ligand binding, could rationalize the selectivity of PR-957 towards the $\beta 5i$ subunit. Importantly, the superposition of the above-described crystallographic subunits $\beta 1i$, $\beta 2i$ and $\beta 5i$ with those obtained by our human i-proteasome model shows a striking consistency, thereby underlining the importance to obtain structural and/or modelling data as an effective tool for the identification of potential small-molecule lead structure, as described below.

3.7 Computer-aided drug design approaches

Few approaches of computational drug design have been applied in the last years for the discovery of new lead compounds able to inhibit s-proteasome¹²⁶⁻¹²⁸. For instance, Reboud-Ravaux and colleagues carried out a multistep structure-based virtual ligand screening strategy and were able to identify several novel lead compounds inhibiting s-proteasome with micromolar range activity and reported cytotoxicity on human tumour cell lines^{127,129}. It is worth noting that no computer-aided drug design techniques have been yet reported for the discovery of selective i-proteasome inhibitors. In this context, likely, new insights on i-proteasome structure obtained by computational modelling¹²⁸, including the present work, or by means of new crystallographic evidences¹²⁵, might constitute a new way to deploy chemoinformatic techniques such as docking or pharmacophore high-throughput virtual screenings^{130,131} on large database of chemicals compounds^{132,133}. In particular, it appears that differences of aminoacids (Fig. 3.3 and Table 5.3) in the s- and i-proteasome β subunit binding sites (especially $\beta 1$ versus $\beta 1i$ and $\beta 5$ versus $\beta 5i$) might effectively constitute the molecular basis for the development of novel s- and i-proteasome specific inhibitors, keeping however into account that the design of highly-specific inhibitors may still result in challenging tasks because of the major similarities in the β subunit catalytic sites.

Proteasome subunit – gene name	Common Name	Uniprot code	Chain name (PDB id: 1IRU)	Immuno-proteasome subunit – gene name	Common Name	Uniprot code
PSMB6	β 1	P28072	H/V	PSMB9	β 1i	P28065
PSMB7	β 2	Q99436	I/W	PSMB10	β 2i	P40306
PSMB5	β 5	P28074	L/Z	PSMB8	β 5i	P28062

Table 3.4. S- and i-proteasome catalytic subunit nomenclature.

Subunits	Proximal residues (within 5Å from bortezomib pose)													
	20	21	22	23	27	28	31	45	46	48	52	95	97	116
β 1	T	T	T		A		T	R			T	M	G	M
β 1i	V	S	A		V		F	L			A	S	H	G
β 2			E	G						T	T			
β 2i			N	D						V	A			
β 5		T			A	S			A	G				
β 5i		S			S	A			S	C				

Table 3.5. Proximal amino acidic differences in the catalytic binding sites of s- and i-proteasome β -subunits.

3.8 Hit Identification

Since the growing amount literature data suggesting the pivotal role of i-proteasome in different cellular pathways, including apoptosis and inflammation, a selective modulation of i-proteasome, by inhibiting or enhancing its activity, directly with small-molecule modulators or indirectly, e.g. by regulating E3 and DUB enzymes, could represent a promising strategy to counteract these pathologies. At the time of this study, medicinal chemistry efforts identified a small number of low molecular-weight inhibitors that are able to modify 20S s- and i-proteasome functions, but only few examples of selective i-proteasome inhibitors was developed. So we started an hit identification

campaign to find new selective i-proteasome inhibitors using virtual screening methodologies. The available x-ray structure of human proteasome (PDB code 1IRU) and the generated model of i-proteasome, after a standard protein preparation procedure, were used as template to virtually screen the Asinex compound dataset, as prepared in the CoCoCo database^{132,133}, comprised of approx. 1.2M compounds. The docking grids were centered on each of the three catalytic subunits (β 1, β 2, β 5) of both standard and i-proteasome, for a total of 6 different docking runs. The results were collected and merged, to obtain a unique list of molecules (w/o duplicates) reporting the docking score versus each of the 6 receptor structures.

The first hundreds hits were visually inspected to select a reduced list of compounds to be purchased and tested. However, only a small number of molecules were present in the first 1000 molecules of the final ranked list in more than one receptor (approx. 250 molecules out of a total 6000), therefore the selectivity between the different grids was not considered as a primary selection criteria. The selection was then focused on the results obtained from the docking on β 5i subunit that showed major differences compared with its homologue subunit in standard proteasome (see above), therefore offers more chances of success in finding selective compounds. The x-ray structures of mouse i-proteasome in complex with compound PR957 (PDB code 3UNF) was used to derive specific binding features of selective inhibitor that were used as selection criteria for docking output; in particular, the final docking list of β 5i was filtered requiring for the presence of hydrogen bond interaction with SER27 (ALA in β 5c) and aromatic interactions with MET45 (present also in β 5c but in a different conformation, and responsible of PR957 selectivity as explained by Huber et al¹²⁵). In the selection process the presence of several specific interaction with other key residues in the active site was also considered (in particular THR1, GLY47, ALA49, ASP125 and SER21); non-modified peptides was discarded due to less favorable pharmacokinetic properties, and special attention was put on non-peptidic molecules. Finally, sample availability from compound providers was also verified, leading to a final list of 11 compounds that were purchased and experimentally tested (Table 6.3). Experimental test were performed in the Laboratory of Prof. Claudio Franceschi (University of Bologna). A specific assay exploiting caspase-like, trypsin-like and chymotrypsin-like activities was developed (see experimental section) and used to assess the effect of the selected compounds on i-proteasome. Among the 11 compounds tested, 2 led to a significant inhibition of i-proteasome activity, namely compound **1** and compound **6**, thus giving a remarkable hit-rate obtained with the virtual screening protocol. Nine compounds resulted inactive at the concentration used in the assay. Figure 4.3 reports the predicted binding modes of the two active molecules identified with the virtual screening.

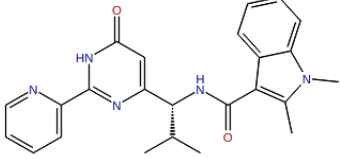
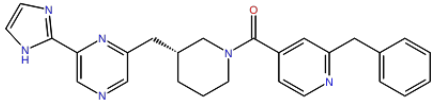
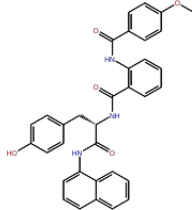
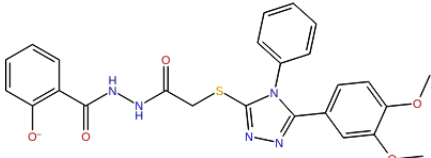
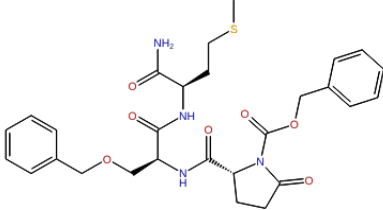
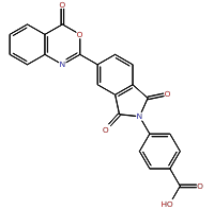
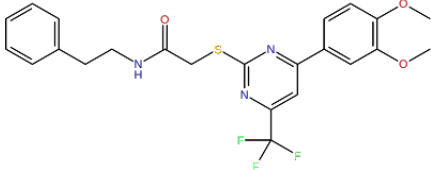
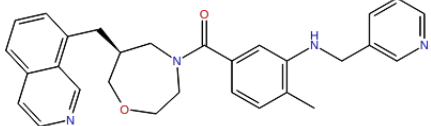
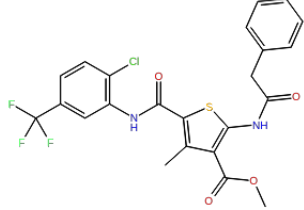
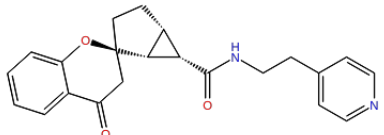
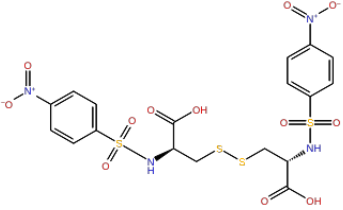
ID	Structure	ID	Structure
1		7	
2		8	
3		9	
4		10	
5		11	
6			

Table 3.6. Structures of selected compounds after the first virtual screening.

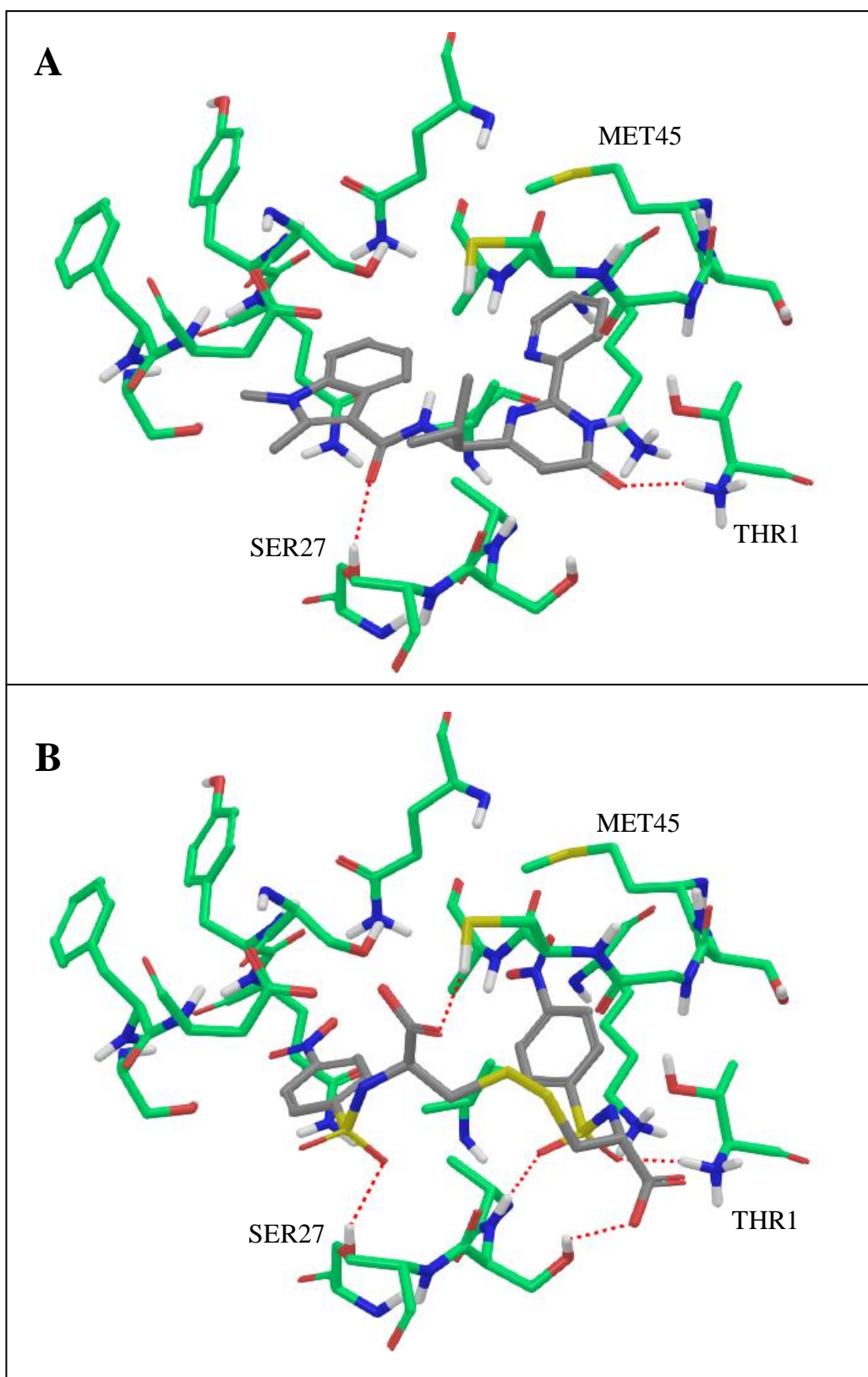


Figure 3.4. Predicted binding modes of compounds 1 (A) and 6 (B).

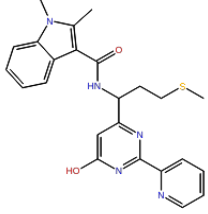
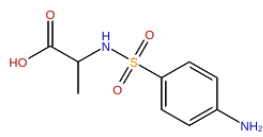
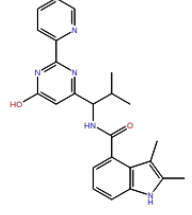
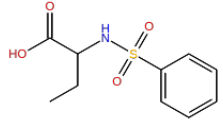
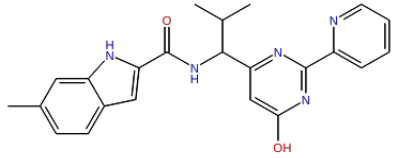
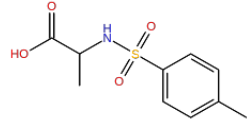
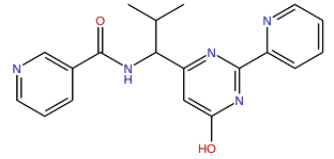
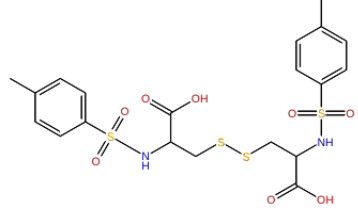
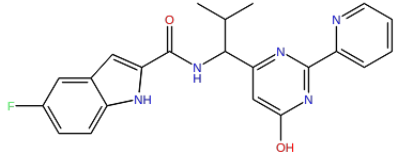
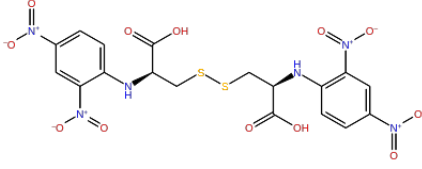
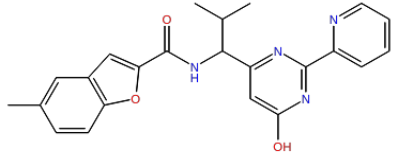
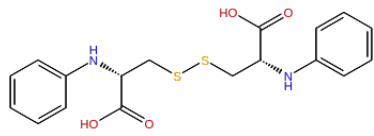
ID	Structure	ID	Structure
1a		6a	
1b		6b	
1c		6c	
1d		6d	
1e		6e	
1f		6f	

Table 3.7. Structures of selected compounds after the second virtual screening.

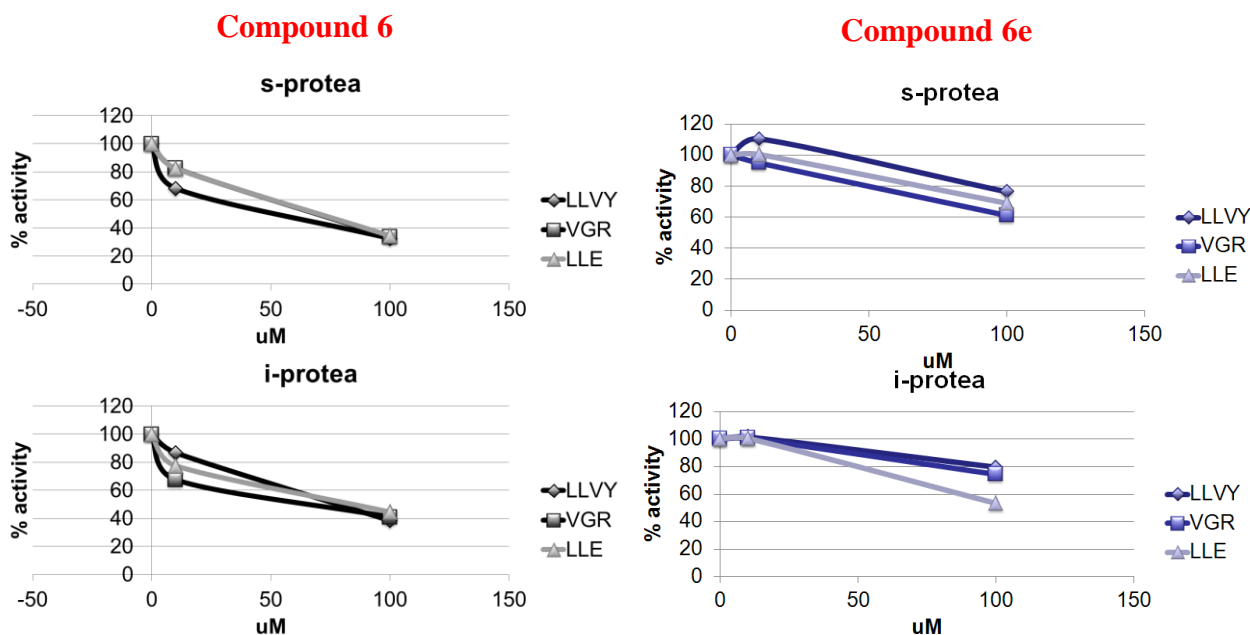


Figure 3.5. Short fluorogenic peptides in vitro assays where LLVY represents the chymotryptic-like catalytic activity, VGR the tryptic-like and the LLE the caspase-like. Compound were tested at concentration 1, 10, 100 μ M, for 60min at 37°C, with preincubation with s- and i-proteasome at room temperature.

Compound 1 is an hydroxypyrimidine derivative, while compound 6 is a symmetric tosyl-cysteine derivative; both compounds are predicted to bind the β 5i subunit close to the catalytic residue THR1, similar to the binding mode of other known inhibitors such bortezomib or PR957, even if these molecules doesn't show any reactive groups, and therefore form non-covalent reversible interactions in the active site. Both are predicted to establish hydrogen bond interactions with THR1 and SER27, and fill the putative selectivity pocket in front of MET45 with an aromatic moiety. Compound 6 is predicted to establish an extended hydrogen bond network involving also ALA20, SER21, CYS48.

To obtain a better understanding of the structure-activity relationship of this interesting hit compounds identified in first screening, and to improve its potency and selectivity, we screened the same collection of commercial compounds to identify analogues that could be easily purchased and tested. These derivatives were selected from the database using different substructure searches, considering the possible modifications on each fragment of the reference structure, and checking sample availability from compound providers. The list of selected compound is reported in Table 7.3.

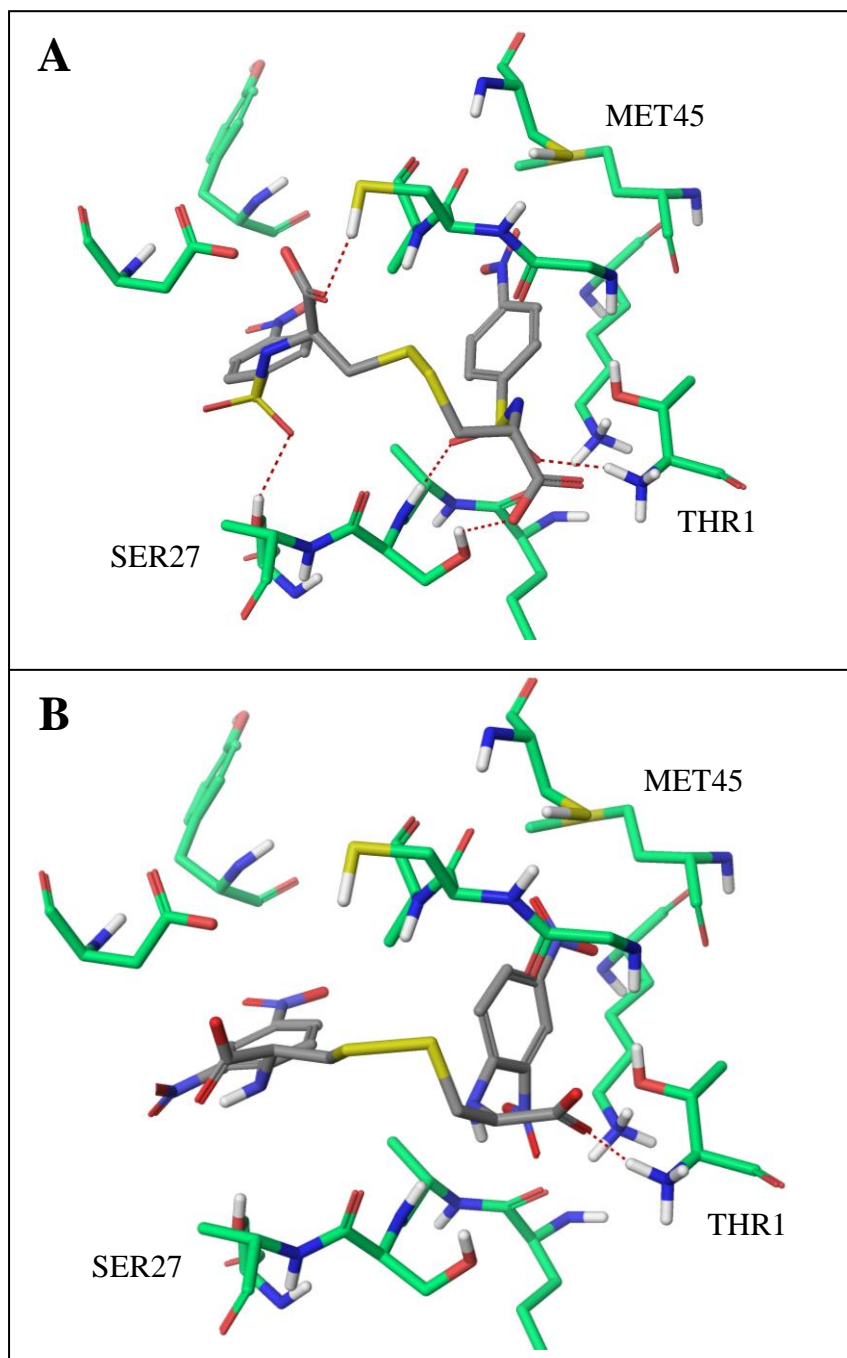


Figure 3.6. Predicted binding modes of compounds 6 (A) and 6e (B).

All derivatives were tested using the same experimental conditions of reference compounds. The derivatives of compound 1 (compounds 1a-f in Table 7.3), despite very high structural similarity with reference compound 1, showed very limited or none inhibition of both standard or i-proteasome; this results indicates the occurrence of a false positive in the first activity measurement, probably due to experimental errors or unpredictable effects of the molecule (e.g. alteration of fluorescence level unrelated to target inhibition). The derivatives of compound 6 were selected using two different criteria: modification of cystine group, to test whether the presence of only the tosyl group would be able to induce inhibition of proteasome activity (compounds 6a-c in Table 7.3), and modifications of tosyl group (compounds 6d-f in Table 7.3) while preserving the cystine moiety. Compounds 6a-c all showed no inhibition, clearly stating the need of cystine function for activity; on the contrary, compounds 6d-f all showed moderate inhibition of both standard and i-proteasome, even if slightly lower compared to reference compound 6. The activity data of most interesting compounds found during the screening are reported in Figure 5.3.

Predicted binding mode of compound 6e (Figure 6.3), the most interesting of this series, is similar to the reference compound 6. In fact, the hydrogen bond interaction with key residue THR1 is established through carboxylic group, that replaces the sulfonyl group in compound 6, and the aromatic interaction in the MET45 is maintained; an additional charge interaction is formed by an o-nitro group with LYS33, while the other one is favorably placed in a solvent-exposed area of the active site. This compound showed an interesting inhibitory activity on all catalytic functions of proteasome, but a proven also a small selectivity towards i-proteasome, in particular in the caspase-like activity; however, both selectivity and potency of the identified chemical scaffolds should be further improved.

3.9 Conclusion and perspective

We carried out virtual screening by using structural information available and searched on large database of commercial chemicals. We selected 23 compounds by visual inspection and, after purchase, we have tested them to select novel and reversible scaffolds able to inhibit s- and i-proteasome. We identified new moderately active and selective non-peptidic compounds. Their scaffolds hold promise for the development of novel improved and selective i- and –proteasome inhibitors.

3.10 Experimental Section

In silico techniques

The available X-ray structure of human proteasome (PDB code 1IRU) and the generated model of i-proteasome were used as a template for virtual screening purposes. These structures were prepared with standard preparation procedures (*protein preparation wizard*) as included in the software package Maestro¹³⁴. The docking software Glide¹³⁵ was used to perform a high-throughput virtual screening experiment. Docking grids were generated using default parameters and centred on structure of minimized PR957, the dimension of the grid was calculated on this ligand. Standard precision (SP) docking was used to perform a first round of virtual screening. The top 1500 molecules, sorted by Glide score, were further refined with the extra-precision (XP) docking. Docking results were ranked based on the Glide score and the first 1000 hits were considered for visual inspection.

Compound Sources. We screened *in silico* the Asinex subset of the CoCoCo databases. Selected molecules were purchased in milligram quantities from chemical vendor. Purity of compounds was $\geq 95\%$, as declared by the chemical vendor.

Biological assays (Laboratory of Prof. Claudio Franceschi, University of Bologna)

Proteasome activity assay. Proteasome activities were measured on 20S proteasome purified from Lymphoblastoid cell lines, according to Mishto et al.¹³⁶, as well as on commercially available 20S s- and i-proteasome (Biomol and Viva bioscience respectively) by the fluorogenic substrates Suc-LLVY-MCA, Bz-VGR-MCA and Z-LLE-MCA, specific for chymotrypsin- (CT-), trypsin- (T-), and caspase-(C-) like activities, as described elsewhere^{49,137}. Briefly, 0.1 μg of 20S proteasomes were incubated with 400 μM of Suc-LLVY, 200 μM Z-LLE-MCA and 600 μM of Bz-VGR-MCA in TEAD buffer, at 37 °C, in presence or absence of 1, 10 and 100 μM of compounds. The enzymatically released MCA was fluorometrically measured at 360 nm excitation and 460 nm emission and monitored at 0', 30', 60', 90', 120'. Proteasome activity was expressed as specific activity (nmol of free MCA/min per mg protein) and the percentage of inhibition in presence of each compound tested was calculated.

4. Sirtuins in drug discovery

4.1 Sirtuins: at the crossroad of metabolism, cancer, and inflammation

Sirtuins are enzymes that require nicotinamide adenine dinucleotide (NAD⁺) to catalyze their reactions^{138–141}. The latter include activities as mono-ADP-ribosyltransferases¹⁴² or as deacetylases. In mammals, seven sirtuins have been identified, of which two are predominantly nuclear, SIRT6 and SIRT7, two are nuclear and cytosolic, SIRT1 and SIRT2, and three are mitochondrial, SIRT3-5. Sirtuins have been ascribed roles in numerous physiological and disease conditions, including aging, metabolism, circadian clock regulation, nutritional behavior, but also cancer and inflammation^{140,143}. Due to their broad involvement in key biological functions, sirtuins are considered appealing targets for the development of pharmaceuticals.

4.2 Sirtuins and cancer

The sirtuins for which a role in cancer has been proposed include SIRT1, SIRT2, SIRT3, SIRT6 and SIRT7. In genetic mouse models, SIRT1, SIRT2, and SIRT3 were shown to act as tumor suppressors^{144–147}. In the case of SIRT1, its activity as a tumor suppressor has been ascribed to its capacity to deacetylate and consequently inhibit the RelA/p65 subunit of NF-kappaB¹⁴⁸, a transcription factor with antiapoptotic and pro-inflammatory activity. Moreover, studies show that SIRT1 also deacetylates β -catenin and thereby suppresses its ability to activate transcription and drive cell proliferation¹⁴⁹. Disruption of SIRT2, which is a tubulin deacetylase¹⁵⁰, in the mouse was found to increase the levels of mitotic regulators, such as Aurora-A and -B, aneuploidy, and mitotic cell death¹⁴⁶. SIRT2-deficient mice developed gender-specific tumorigenesis, with females developing mammary tumors and males developing hepatocellular carcinoma. Moreover, human breast cancers and hepatocellular carcinomas were reported to exhibit reduced SIRT2 levels as compared with normal tissues. SIRT3 was proposed to oppose cancer development through its role in mitochondrial metabolism, reactive oxygen species production and genome stability^{145,147}. Its deficiency was shown to favor cell transformation in response to oncogenic Ras or Myc and to lead to HIF-1 α stabilization with consequent induction of the Warburg effect. SIRT6 has also been suggested to act as a tumor suppressor since its acute overexpression in cancer cell lines of different histology was found to induce apoptosis¹⁵¹. Interestingly, this biological activity of SIRT6 appears to be linked to its mono-ADP-ribosyltransferase but not to its deacetylase activity. Finally, SIRT6

anticancer activity could also be ascribed to its capacity to negatively regulate NF- κ B and HIF-1 α ^{152,153}, the latter being a transcription factor that promotes the expression of glycolytic and pro-angiogenic genes.

The apparent consistency of this picture is complicated by evidence that these same sirtuins may actually favor certain aspects of neoplastic growth and that, at least in certain instances, their inhibition may be preferable to their activation. Numerous reports indicate that SIRT1 also has cancer-promoting functions which include deacetylation and inactivation of p53^{154,155} and of proapoptotic FOXO transcription factors¹⁵⁶, deacetylation of Ku-70 with consequent sequestration of Bax away from mitochondria¹⁵⁷, as well as inhibition of senescence and of apoptosis in c-Myc- and in PML-driven cancers^{158,159}. Accordingly, many studies attribute direct anticancer activity to SIRT1 inhibitors or show how such compounds sensitize cancer cells to anticancer agents or to oxidative stress¹⁶⁰⁻¹⁶⁶. Similar results were also reported for SIRT2. SIRT2 downregulation or chemical inhibition were found to induce anticancer effects that include p53 accumulation, cell cycle arrest and apoptosis¹⁶⁷⁻¹⁶⁹. In a recent study, the antileukemia effects of SIRT2 inhibition (with AC93253) were accompanied by Akt acetylation, de-phosphorylation, and consequent inhibition¹⁷⁰. Interestingly, evidence exists that SIRT2 inhibition could be counterproductive in certain instances, such as upon treatment with microtubules inhibitors¹⁷¹. Namely, SIRT2 downregulation appears to make cancer cells resistant to these agents by prolonging chronic mitotic arrest. Also SIRT3's role as a tumor suppressor does not seem to extend to all types of cancer. In particular, in oral squamous cell carcinomas, SIRT3 was found to be overexpressed and its downregulation had antiproliferative activity and sensitized carcinoma cells to radiation and to cisplatin¹⁷². Finally, in the case of SIRT6, studies show that this enzyme is crucial for telomere maintenance, DNA repair and genome stability^{173,174}. Thus, SIRT6 inhibitors could conceivably be used to sensitize cancer cells to chemotherapeutics or radiotherapy¹⁷⁵. Moreover, SIRT6 promotes TNF synthesis by a mechanism that appears to entail the enhancement of the efficiency with which TNF mRNA is translated^{176,177}. TNF plays a central role in some of the systemic manifestations of cancer, such as fever and cachexia, and its role in shaping the tumor microenvironment is acknowledged¹⁷⁸. SIRT6 inhibition could theoretically serve the purpose of reducing the levels of this unwanted mediator of cancer-induced inflammation and thereby interfere with invalidating systemic manifestations of disease.

Finally, a recent study suggests that SIRT7 may promote tumorigenesis by deacetylating lysine 18 of histone H3, thereby repressing genes with tumor suppressor function¹⁷⁹. SIRT7 was found to be

stabilized at target promoters by interaction with the ETS family transcription factor ELK4. According to these authors, H3K18 deacetylation by SIRT7 would be necessary to maintain essential features of cancer cells, such as anchorage-independent cell growth and loss of contact inhibition. Indeed, in line with this model, SIRT7 depletion reduced the tumorigenicity of human cancer xenografts in mice.

Overall, while it is eventually becoming clear that sirtuins play important roles in cancer pathophysiology, the final judgment as to whether a defined sirtuin should be blocked or rather activated in order to achieve a therapeutic benefit may vary depending on the type of cancer, its molecular features, stage of disease, and clinical manifestations. Either way, a crucial step in the pursuit of sirtuin-targeting approaches is the identification of compounds that could be used to specifically modulate sirtuin activity *in vivo*.

4.3 Sirtuin inhibitors

Although sirtuins emerged in the last years as therapeutic targets for small molecule-based interventions, a relatively small number of highly active molecules have been developed so far. The available inhibitors belong to several structural classes that reflect both different drug discovery strategies and the complexity of the catalytic machinery of these enzymes. The simplest approach used to identify novel active compounds was the evaluation of substrate and/or product mimetics. Among the first compounds studied were the endogenous inhibitor nicotinamide (1, Figure 4.1), which is a product of the deacetylation reaction, and its derivatives. Because of its simple chemical structure, nicotinamide is a micromolar non-competitive inhibitor of SIRT1 and SIRT2¹⁸⁰ that interact with the pocket C in the binding site. Similarly, slightly modified NAD⁺ molecules such as carbamido-NAD⁺, compete with NAD⁺ for the cofactor binding site. SIRT1 inhibition with nicotinamide was reported to have anticancer activity in B-cell chronic lymphocytic leukemia and in prostate cancer^{164,181}. However, nicotinamide and the NAD⁺ analogs have limited therapeutic potential as demonstrated by unsuccessful searches for more potent inhibitors of this class^{182,183}. Several active molecules were designed starting from substrate peptides, such as small fragments of p53 protein that were modified in order to block or reduce the catalytic activity. Thioacetyllysine derived inhibitors and other modifications of acetylated lysine residue have been demonstrated to be potent sirtuin inhibitors^{184–191}. A recent study highlighted SIRT5 preference to catalyze the hydrolysis of malonyl and succinyl group from the lysine residue rather than acetyl group, demonstrating that this preference could be used to the design of selective inhibitors¹⁹². A phenotypic screen of a small compound library led to the discovery of sirtinol (2, Fig. 4.1), a

hydroxynaphthaldehyde derivative that is active on different sirtuin isoforms¹⁹³ and has cytotoxic activity against cancer cells of different origin, including breast, lung, prostate and leukemia cells^{162,167,181,194}. A number of subsequent structure-activity relationship studies were carried out in search of derivatives of this molecule with improved activity and/or properties. Some examples are salermide (3, Fig. 4.1)¹⁹⁵, cambinol (4, Fig. 4.1)¹⁶⁰ and splitomicin (5, Fig. 4.1)¹⁹⁶. With the exception of splitomicin, which is not active on human sirtuins¹⁹⁷, also these compounds were reported to have anticancer properties^{160,167,195,198}. A series of thiobarbiturates derivatives that are similar to cambinol and inhibit SIRT1 and SIRT2 at micromolar concentrations, was identified through a structure-based virtual screening approach followed by binding energy estimation and biological testing (6, 7 and 8, Fig. 4.1)¹⁹⁹. A large high-throughput screening effort led to the discovery of a series of indole compounds as interesting inhibitors of SIRT1, including one of the most potent and selective compounds known so far, EX-527 (11, Fig. 4.1). This compound inhibits SIRT1 at nanomolar concentrations and shows remarkable selectivity over SIRT2 and SIRT3, as well as good pharmacokinetic properties²⁰⁰. It was found that EX-527 cooperates with HDAC inhibitors to induce apoptosis in leukemia cells¹⁶². However, due to its selectivity for SIRT1 and to its poor activity on other sirtuins, the anticancer activity of this inhibitor as a single agent appears to be weak¹⁶⁷.

Starting from the rationale that sirtuins and protein kinases contain an adenosine binding site, a series of known kinase inhibitors was tested against SIRT2 revealing bisindolylmaleinimides and indolinone as interesting scaffolds that are able to exert biological activity. The most interesting compounds, Ro31-8220 (9, Fig. 4.1) and GW5074 (10, Fig. 4.1) showed SIRT1/SIRT2 inhibitory properties in the low micromolar range²⁰¹.

Suramin (12, Fig. 4.1), an adenosine receptor antagonist, was discovered as a potent inhibitor of SIRT1/SIRT2 while searching for sirtuin activators²⁰². This molecule inhibits SIRT1/SIRT2 at nanomolar concentrations and appears to be selective for SIRT1. Suramin has anticancer activity and has been studied in clinical trials²⁰³. However, it is still unclear to which extent such activity is due to sirtuin inhibition or, instead, to other modes of action, such as adenosine receptor activation or ceramide accumulation²⁰⁴. The optimization of the suramine scaffold led to NF675 (13, Fig. 4.1) which is the most potent and selective molecules in this series, showing a 20-fold selectivity ratio for SIRT1 over SIRT2²⁰⁵. The binding mode of suramin was investigated by co-crystallization with human SIRT5²⁰⁶. This structure highlights that suramin binds SIRT5 by occupying the nicotinamide ribose pocket (B-pocket), the nicotinamide pocket (C-pocket) and part of the substrate-binding site.

Although this compound shows interesting potency and selectivity profile, its modest drug-likeness, especially given its high molecular weight and its anionic nature, limits the therapeutic applications.

Several other compounds with various structural cores were reported to inhibit sirtuins at micromolar concentrations, such as tenovins¹⁶¹, AGK2²⁰⁷, 1,4-dihydropyridines²⁰⁸, bisnaphthalimidopropyl derivatives²⁰⁹, AC-93253¹⁶⁹, and a series of natural products such as aristoforin²¹⁰, amurensin G²¹¹, polyphenols²¹² and tanikolide²¹³. Among these, tenovin-1 and tenovin-6 were reported to have strong anticancer activity that is associated to p53 activation¹⁶¹.

4.4 Sirtuins activators

Because sirtuins have been involved in several physiopathological conditions that include aging, metabolism and nutritional behavior²¹⁴, a major interest has been to define possible pharmacological actions that could activate sirtuin activity. The first small molecules that were reported as activators of SIRT1 were polyphenolic compounds such as resveratrol, piceatannol, butein, quercetin, and myricetin (respectively compounds 1-5 in Figure 4.2)²⁰². More potent and chemically diverse activators were subsequently reported, known as SRT1460, SRT1720 and SRT2183 (compounds 6-8 in Figure 4.2)²¹⁵, while a recent study reported allosteric modulation of SIRT1 by nonpolyphenolic compounds²¹⁶. Most of these compounds were reported to have anticancer activity^{217,218}. However, it should be noted that their mechanism of action is still unclear^{219,220} and a matter of controversy is the fact that sirtuin activation could frequently only be demonstrated with fluorescently tagged substrates²²¹⁻²²⁴. Such activation might be ascribed to other *in vivo* and *in vitro* effects that are not mediated by SIRT1. Alternatively, increased SIRT1 activity in response to these compounds may be indirect, i.e. reflect the activity of these agents on proteins that are SIRT1 interactors in the cell. Recent works by Park et al.²²⁵ and Price et al.^{226,227} investigate further the role of resveratrol. In the first study authors show that resveratrol indirectly activates Sirt1 *in vivo* due to its effect on cAMP signaling, in particular activating the cAMP-Epac1-AMPK-Sirt1 pathway; it is also speculated that other known putative Sirt1 activators such as SRT1720, SRT2183, and SRT1460, because of their similarity in metabolic effects, should act in a similar way of resveratrol. The second work establish a connection between SIRT1 and resveratrol by providing evidence that increased mitochondrial biogenesis and function, AMPK activation, and increased NAD⁺ levels in skeletal muscle are obtained when mice are treated with a moderate dose of resveratrol.

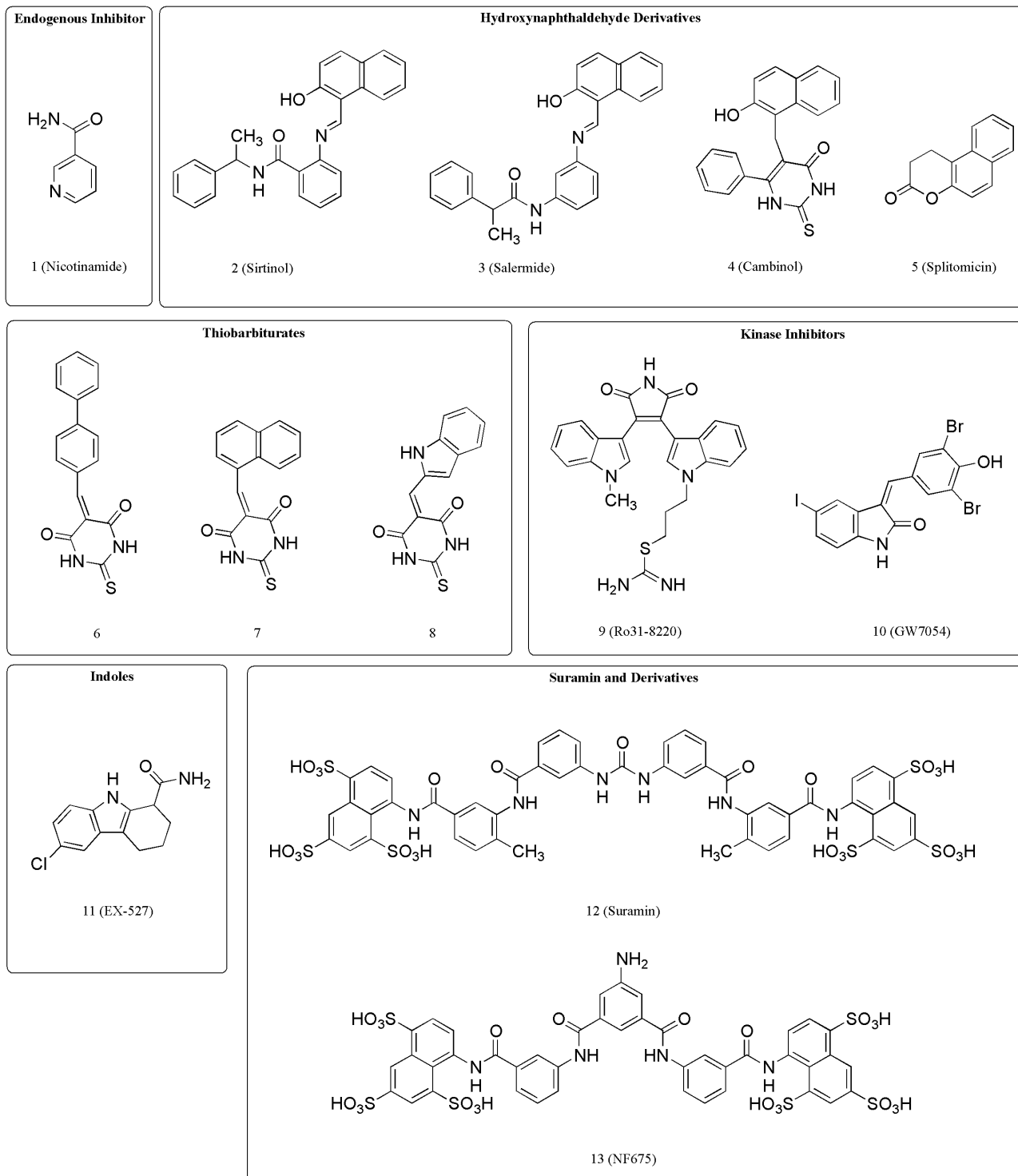
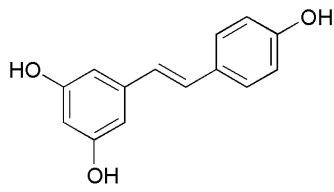
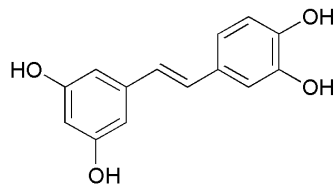


Figure 4.1. Sirtuins inhibitors.

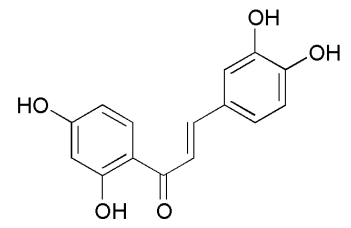
Polyphenolic Compounds



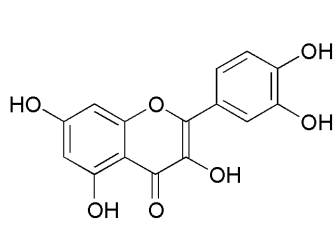
1 (Resveratrol)



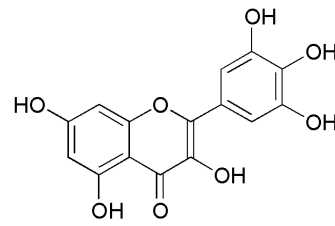
2 (Piceatannol)



3 (Butein)

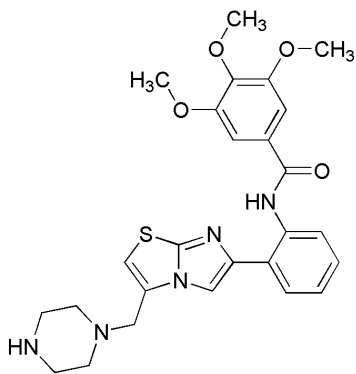


4 (Quercetin)

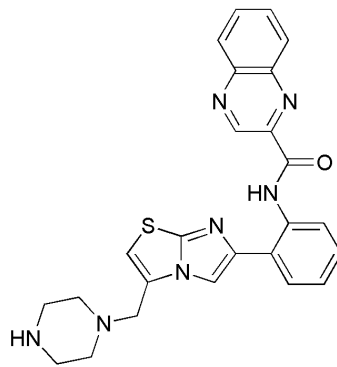


5 (Myricetin)

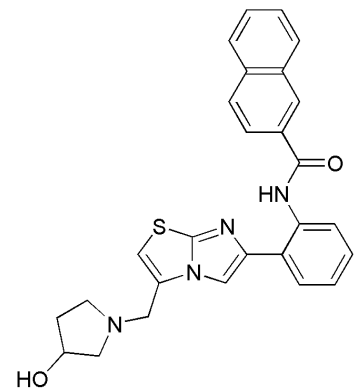
Other Activators



6 (SRT1460)



7 (SRT1720)



8 (SRT2183)

Figure 4.2. Sirtuins activators.

5. Development of a Sirtuins selectivity model

In the last decade, several three-dimensional structures of sirtuin homologs have been deposited in the Protein Data Bank, ranging from archaea to humans, providing a major understanding of structural features, catalytic mechanisms and substrate specificity of these enzymes²²⁸. Several bacterial Sir2 structures, and human SIRT1, SIRT2, SIRT3, SIRT5 and SIRT6 are available whereas, presently, no structures has been solved for human SIRT4 and SIRT7 yet²²⁹. Despite this large amount of structural information, only a relatively small number of active compounds have been identified to date, often showing limited potency and isoform selectivity²³⁰. Similarly, few three-dimensional structures of sirtuin have been solved with activators or inhibitors, reflecting the complexity of the catalytic machinery and the subtle mechanisms of pharmacological modulation of these enzymes. In particular, EX527 (1, Figure 5.1), an inhibitor that combines good potency with significant isoform selectivity was co-crystallized with SIRT1²³¹ and SIRT3²³²; SIRT3 structure is also available in complex with three potent but not selective inhibitors (2-4, Figure 5.1) identified from a large library screening²³³, with SRT1720 (5, Figure 5.1), a compound that was described as SIRT1 activator and SIRT3 inhibitor²³⁴, and also with 4'-bromo-resveratrol²³⁵ (6, Figure 5.1). SIRT5 was solved in complex with suramin (7, Figure 5.1), a potent inhibitor of SIRT1/SIRT2²³⁶, and the crystal structure of human SIRT2 was solved in complex with a macrocyclic peptide inhibitor²³⁷. Very recently, the SIRT3/SIRT5 complexes with piceatannol and resveratrol (8-9, Figure 5.1), two of the known sirtuin activating compounds (STAC²³⁸), revealed the mechanism of direct sirtuin activation²³⁹. While these three-dimensional structures highlighted the basis for inhibitor/activator binding and laid the foundations for the rational design of new and more potent compounds, additional efforts are needed to shed light on the more complex problem of isoform selectivity. The development of specific modulators able to interact with a single sirtuin isoform, or at least with a small subset, could be extremely useful to better understand the biological role of each sirtuin and, at the same time, could facilitate the identification of new therapeutic agents. In fact, the small molecules so far reported as sirtuin activators or inhibitors are often tested against a limited set of sirtuin isoforms, usually SIRT1/2/3, and their selectivity profile is usually explained by using approximate models. A previous study by Schlicker et al.²⁴⁰ described the structure-based identification of new classes of isoform specific inhibitors, showing that three-dimensional sirtuin structures in the non-inhibited state could be successfully used to highlight differences between isoforms and could help the development of new selective inhibitors. However, the selectivity determinants for the modulation of the sirtuin catalytic cores are still unclear.

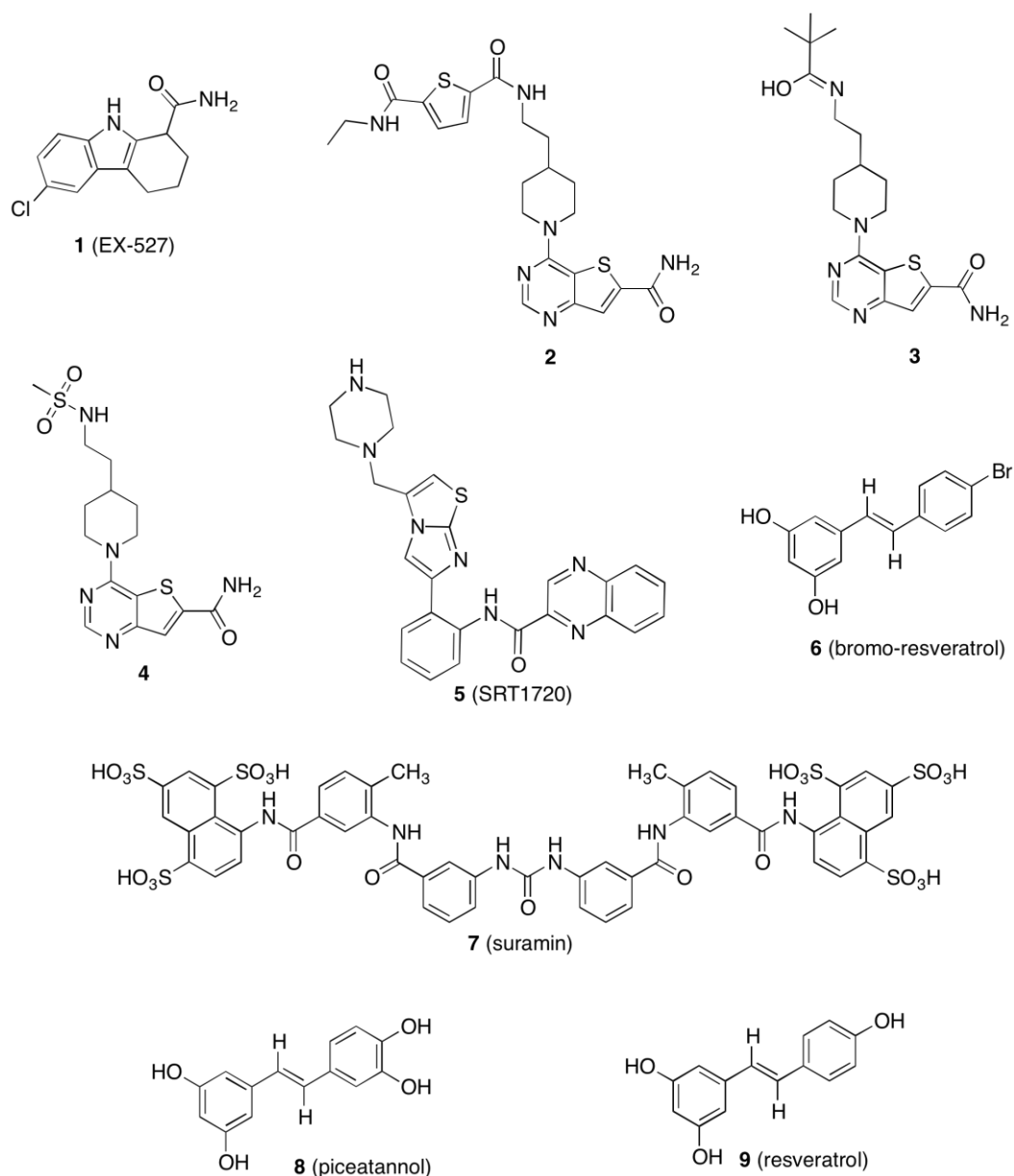


Figure 5.1. Ligands that have been solved in complex with sirtuin structures.

In this study, we aimed to gain insights into the isoform specificity of different sirtuins and to identify the functional hot-spots that could be used to guide structure-based design efforts for the identification of new selective sirtuin modulators. To this end, we developed a comprehensive selectivity model based on sequence and structure-based alignments, and characterized sirtuins through a detailed analysis of the pharmacophoric properties of the catalytic site in terms of residue differences of each family member. The model was built by including all three-dimensional structures of the human sirtuin family available in the PDB, supplemented by homology models for those isoforms that have not been solved yet. Differences in terms of key residues in the active site and the effects of conformational variations were analyzed and the results reported in simple tables

and graphs that illustrate at a glance residues that most likely are involved in selectivity and the pharmacophoric features that should be considered in the design of new selective ligands.

5.1 Sequence and structural comparison of the catalytic cores

Sirtuins contain a conserved catalytic domain of approximately 250 amino acids, responsible for NAD⁺ and substrate binding and deacetylase activity. Additionally, these proteins possess N- and C-terminal regions, variable in length and sequence, whose role in sirtuin biology is still unclear, although an effect on substrate specificity was speculated²²⁸.

The structure of the catalytic core consists of a large Rossmann-fold domain, typical of NAD⁺-binding proteins, a small zinc-binding domain, and a number of flexible loops that keep together the two domains. The binding sites of cofactor and substrate are located in a wide cleft at the interface between the large and the small domains. The sequence alignment of the catalytic core region (deacetylase domain) of the human sirtuin family (Figure 5.2) reveals a good level of sequence conservation, with the highest identity observed for residues responsible of cofactor binding and catalytic activity. A principal component analysis (PCA) of this alignment (Figure 5.3) clearly shows the presence of three different clusters: a first one including SIRT1, SIRT2 and SIRT3, a second one composed by SIRT6, SIRT7 and, slightly isolated, SIRT4, while SIRT5 completely differs from the other sirtuins. Consistently, the calculated pairwise sequence identity is the highest among the first cluster and between SIRT6 and SIRT7 (between 40% and 51%), while it is less than 30% for any other sequence pair. The large domain is characterized by a high level of structural and sequence similarity among various sirtuins; it is formed by a central β -sheet surrounded by six α -helices, except for SIRT2, which exhibits an additional long insertion of approximately 20 residues forming an additional α -helix. This domain possesses many of the specific requirements for NAD⁺-binding, such as the well known G-X-G motif²⁴¹, important for the recognition of the phosphate group, and charged residues to bind the two ribose groups. The NAD⁺ adenine base binds the C-terminal half of this domain while the nicotinamide enters the N-terminal part, as typical in inverted Rossmann-fold domains²⁴². The small domain is the most diverse region in terms of primary sequence and conformation; it is formed by two long insertion in the Rossmann-fold domain, and consist of a three-stranded antiparallel β -sheet, a variable α -helical region, and a Zn²⁺ cation coordinated by the sulphhydryl group of four strictly conserved cysteine residues. The presence of the zinc ion is required to ensure enzyme functionality²⁴³, although it does not directly participate in the catalytic mechanism of sirtuins. This domain shows the greatest variability in terms of three-

dimensional structure among human sirtuins, and its relative position to the large domain depends also on the presence of substrate and on NAD^+ conformation²⁴⁴. Several variations are found in the primary sequence of the small domain. First, SIRT6 and SIRT7 contain a deletion which results in the lack of the helix bundle found in other sirtuins. This bundle is replaced by a short loop forming few interactions with the zinc-binding module. The presence of this unique feature may provide a possible explanation for the conformation of the zinc-binding domain in these two sirtuins, which, in turn, may be responsible for the observed lower catalytic activity of SIRT6²⁴⁵. SIRT6 also shows a ten-residue insertion between the second set of cysteines, resulting in a further long loop. Secondly, the two mitochondrial sirtuins SIRT4 and SIRT5 exhibit a unique insertion in the small domain comprising a short helix and a 16 residues loop, that may be important for subcellular localization²³⁶. Finally, SIRT1 contains a 5 residues insertion adjacent to the last zinc-binding cysteine providing a distinctive small loop in this domain. The remarkable diversity in the small domain may have an important role in regulating key properties, such as substrate specificity and enzyme localization, highlighting this domain as an attractive potential binding site for selective sirtuin modulators. The cofactor binding loop, often referred to as the “flexible loop”, is the largest of the four loops linking together the large and the small domains, and it is one of the most flexible regions of the enzyme. This loop appears to be disordered in the unliganded sirtuin structures but it undergoes significant conformational changes upon binding of NAD^+ or other reaction intermediates and could adopt multiple conformations depending on the bound ligand²²⁸. When NAD^+ is bound, this loop adopts a fairly “open” conformation, and several residues mediate important interactions between the nicotinamide moiety of the cofactor and the enzyme. When the active site is not occupied by the nicotinamide moiety, as in the case of the reaction product 2'-O-acetyl-ADP-ribose (2'-OAADPr), the loops assume a more “closed” conformation, with a partial occlusion of the nicotinamide binding pocket, precluding NAD^+ to bind in a productive conformation. In human sirtuins, the conformational changes in the cofactor binding loop are observed in three-dimensional structures of SIRT3 and SIRT5 whereas in SIRT6, the cofactor binding loop is replaced by a single helix that appears to be ordered in both complexes with ADPR and 2'-N-acetyl-ADP-ribose (2'-NAADPr), indicating that the binding pocket is less flexible and that its conformation is not susceptible to changes upon binding of different ligands²⁴⁵.

```

SIRT1  EDAVKLLQ--ECKKIIVLTGAGVSVSCGIPDFRSR-DGIYARLAVDFPDLDPDQAMFDIEYFRK
SIRT2  EGVARYMQSERCRRVICLVGAGISTSAGIPDFRSPSTGLYDNLEK--YHLPYPEAIFEISYFKK
SIRT3  QDVAELIRARACQRVVVMVGAGISTSPSGIPDFRSPGSGLYSNLQQ--YDLPYPEAIFELPFFFH
SIRT4  KELQRFIT--LSKRLLVMTGAGISTESGIPDYRSEKVGLYARTDR--RPIQHGFVRSAPIRQR
SIRT5  ADFRKFFA--KAKHIVISGAGVSAESGVPTRFGA-GGYWRKWQA--QDLATPLAFAHNP--SR
SIRT6  WELARLVW--QSSSVVFHTGAGISTASGIPDFRGP-HGVWTMEER--GLAPKFDTTF-----
SIRT7  RELASAVR--NAKYLVVYTGAGISTAASIPDYRGP-NGVWVWTL LQK--GRSVSA-ADL-----

SIRT1  DPRPFFKFAKEIYPGQFQPSLCHKFIAL----SDKEGKLLRNYTQNIIDTLEQVAGIQ--RIIQC
SIRT2  HPEPFFALAKELYPGQFKPTICHYFMRL----LKDKGLLLRCYTQNIIDTLERIAGLEQEDLVEA
SIRT3  NPKPFFTLAKELYPGNYKPNVTHYFLRL----LHDKGLLLRLYTQNIIDGLERVSGIPASKLVEA
SIRT4  Y-WARNFVVGWPQ-FSSHQPNPAHWALST----WEKLGKLYWLVTONVDAHTKAGSR--RLTEL
SIRT5  V-WEFYHYRREV-MGSKEPNAGHRAIAECETRLGKQGRVVVITQNIIDELHRKAGTK--NLLLEI
SIRT6  -----ESARPTQTHMALVQ----LERVGLLRFVLSQNVDTGLHVRSGFPRDKLAEL
SIRT7  -----SEAEPTLTHMSITR----LHEQKLVQHVVSQNCDTGLHLRSGLPRTAISEL

SIRT1  HGSFATASCLII--CKY--KVDCEA-V-----RGDIFNQVV-P
SIRT2  HGTFTYSHCVSASCRH--EYPLSW-M-----KEKIFSEVT-P
SIRT3  HGTASATCTV--CQR--PFPGED-I-----RADVMADRV-P
SIRT4  HGCMDRVLCLD--CGE--QTPRGV-LQERFQV LNPTWSAEAHGLAPDGDVFLSEEQVRSFQV-P
SIRT5  HGS LFKTRCTS--CGV--VAE--N-YKS---PICPA--LSGKGA-PEP--GTQDASIPVEKL-P
SIRT6  HG NMFVEECAK--CKT--QYVRD-V-----VGTMGLKATGR
SIRT7  HGNMYIEVCTS--CVPNREYVRFDV-----TERTALHRHQTGR

SIRT1  RCP-----RCPADEPLAIMKPEIVFFGEN--L-PEQFHRAMKYDKDEVDLLLIVIGSS LKVR
SIRT2  KCE-----DC-----QSLVKPDI VFFGES--L-PARFFSCMQSDFLKV D L L L V M G T S L Q V Q
SIRT3  RCP-----VC-----TG VVKPDI VFFGEP--L-PQRFL LHV-VDFPMA D L L L I L G T S L E V E
SIRT4  TCV-----QC-----GGHLKPDV VFFGDT--V-NPDKVDFVHKRVKEA D S L L V V G S S L Q V Y
SIRT5  RCEEA-----GC-----GGLLRPHV VVFFGEN--L-DPAILEEVDRELAHC D L C L L V V G T S S V V Y
SIRT6  LCTVAKARGLRAC-----RGE LRDTI LDWEDS--L-PDRDLA LADEASRNA D L S I T L G T S L Q I R
SIRT7  TCH-----KC-----GTQLRDTI V H F G E R G T L G Q P L N W E A A T E A A S R A D T I L C L G S S L K V L

SIRT1  ---PVALIPSSI-PHEVPQI-LINREPLPHL-----HFDVELLGD CDV
SIRT2  ---PFASLISKA-PLSTPRL-LINKEKAGQSDPFLGMIMGLGGGMDFD SKKAYRDVAWLGE CDQ
SIRT3  ---PFASLTEAV-RSSVPRL-LINRD LVG PL-----AW--HPRS RDVAQLGDV VH
SIRT4  ---SGYRFILTAWEKKLP IA-ILNIGPTRSD-----DLACLKLN SRCGE
SIRT5  ---PAAMFAPQVAARGVPVA-EFNTETTPAT-----NRFRFHFG PCGT
SIRT6  ---PSGNLPLAT-KRRGRLVIVNLQPTKHD-----RHADLR IHG YVDE
SIRT7  KKY PRLWCMTKP-PSRRPKLYIVNLQWTPKD-----DWAALKLHG KCDD

SIRT1  IINELCHRLGGEYA
SIRT2  GCLALAE LLGWKKE
SIRT3  GVESLVELL GWTEE
SIRT4  LLPL-----IDPC
SIRT5  TLPEALACHENETV
SIRT6  VMTRLMKHLGLEIP
SIRT7  VMRL LMAELGLEIP

```

Figure 5.2. Sequence alignment of the deacetylase domain of human sirtuins. Residues are colored by sequence identity and boxes indicate special residues: pink for NAD⁺-binding region, cyan for zinc-binding cysteines, and grey for catalytic histidines.

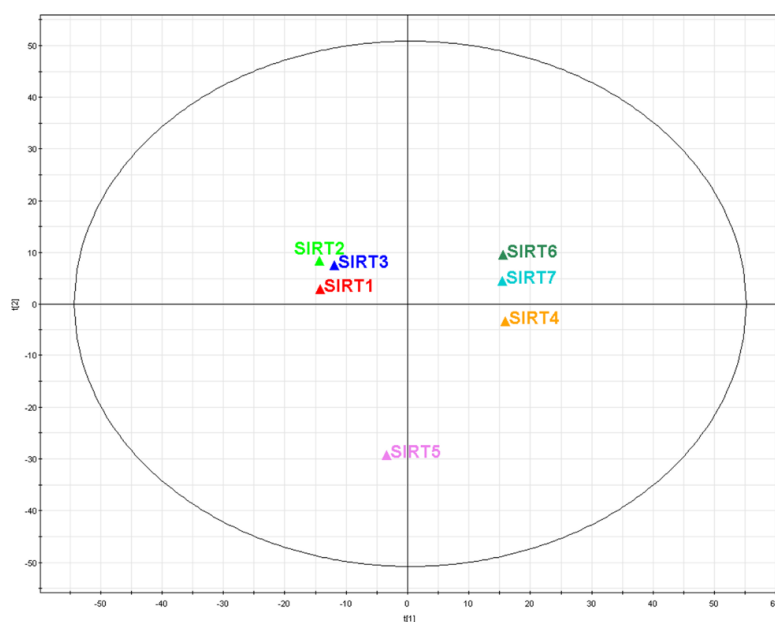


Figure 5.3. Principal component analysis of sirtuins sequence alignment. The picture reports the score plot obtained from the first two principal components ($t[1]/t[2]$).

5.2 Structural comparison of the binding sites

The NAD^+ binding site can be divided into three different pockets: an adenine binding pocket (pocket A), a nicotinamide ribose binding pocket (pocket B) and a nicotinamide moiety binding pocket (pocket C). Several cofactor interactions within these binding sites are generally conserved among different sirtuins. For instance, the adenine base establishes several van der Waals interactions including the two conserved glycines and various hydrogen bonds formed by the adenine nitrogens and polar residues such as glutamate, serine or threonine, while the hydroxyls of the adenine ribose mainly interact with a conserved asparagine residue. The phosphate group and the nicotinamide ribose moiety show a complex interaction network affected in both cases by the conformational variability of cofactor binding loop²²⁸. In particular, the nicotinamide ribose ring can adopt two slightly different conformations that may have implications in the supposed catalytic mechanism²⁴⁶. In the same way, conformational changes also occur in the pocket C, where the nicotinamide group can assume either a “non-productive” conformation, where it binds outside of the C pocket in a conformation that is not compatible with acetyl-lysine binding and the deacetylation reaction, or a “productive” conformation, in which the presence of an acetyl-lysine drives the nicotinamide moiety in the C pocket to establish interactions with invariant key residues. The substrate binding site is placed in a cleft between the large and the small domains. The backbone of the substrate peptide forms a β -strand-like interaction, known as β staple with two

loops in the enzyme, one within the Rossmann-fold domain and one that links together the two domains, while the acetyl-lysine side chain makes several interactions within an hydrophobic tunnel and an hydrogen bond between the N-atom and a backbone carbonyl of a conserved valine residue (leucine for SIRT6). The correct formation of β staple interactions and acetyl-lysine binding tunnel are induced by the binding of the substrate peptide to its pocket by means of a rigid-body rotation of the small domain relative to the large domain²⁴⁷.

5.3 Structural superposition of available three-dimensional structures

All available three-dimensional structures of human sirtuins were downloaded from Protein Data Bank and were supplemented by models obtained from the Swiss-Model database of SIRT4 and SIRT7, whose crystallographic structures are not available yet^{248–251}. With the exception of these two sirtuins, all other isoforms have between four and ten distinct three-dimensional structures solved. A total of 42 structures, in unbound form or in complex with different cofactors, substrates and/or small molecule modulators (Table 5.1) were retrieved from the PDB database. Structures were prepared and structurally aligned (see experimental section) in order to gain more insight into the differences and similarities among human sirtuins. After the structural alignment, a structure-based sequence alignment was obtained for the residues falling into a range of 4 Å from a reference ligand. This allowed a close analysis of variations in the active site residues likely to be important for binding affinity and selectivity of new ligands. This kind of structural alignment could bring at the same time the information concerning conformational variations of the same residue in a different position or mutations of the residue among different sirtuin isoforms, i.e. different kind of residues in the same position. Figure 5.4 shows the alignment of active site residues for all 42 available sirtuin structures in which all residues are aligned only considering structural superposition. Within the same sirtuin isoform, conformational variations of the catalytic core are mainly detectable in the cofactor-binding loop, while other residues remain almost unchanged. In the same way, conformational changes across different sirtuin isoforms were identified mainly in the same loop; however, assuming that every sirtuin isoform can adopt the same active site conformation depending on the bound ligand, the conformational variations appears not to be relevant in terms of ligand selectivity. Conversely, the comparison across various isoforms is mainly characterized by specific point aminoacidic differences which are relevant in terms of binding selectivity and are located on the whole structural alignment. In order to highlight the variations by specifically focusing on the catalytic core residues, a representative three-dimensional structure was selected for each sirtuin isoform and a simplified structural alignment was generated

in Figure 5.5. The representative structures were selected so as to obtain a set of three-dimensional structures with similar closed-form conformations, first considering the conformation of homology models generated for SIRT4 and SIRT7. The whole alignment was then divided in pockets A, B, C and substrate pocket, as defined above, to better depict the selectivity hot-spots.

Each residue was classified according to the estimated importance to generate ligand selectivity: conserved residues, low significance and high significance residues (Figure 5.5). Conserved residues are understandably not relevant for selectivity while some aminoacidic differences were classified as low significant for selectivity when the variation was limited to similar residues (e.g. valine/leucine) or when the side chain of the residues was directed outside the active site and therefore not prone to affect the shape and the properties of the catalytic core and the putative binding of a ligand. The nicotinamide-ribose binding pocket (Figure 5.5B) shows the higher degree of conservation and only one residue is classified as important for the selectivity, although the aminoacidic difference is limited, i.e. F to Y, and involving only two sirtuins, namely SIRT4 and SIRT7. Conversely, the structural alignments of adenine binding pocket (Figure 5.5A) and nicotinamide binding pocket (Figure 5.5C) reveal a higher degree of difference, with 5 and 8 significant residues, respectively. The substrate binding pocket is characterized by a significant conservation (Figure 5.5D) from SIRT1 to SIRT5, while SIRT6 and especially SIRT7 show differences that are the results of gaps sequence; nonetheless, four residues are predicted to have some effects on selectivity in this region.

Sirtuin	Source	Code	Ligand(s)	Notes
SIRT1	PDB	4I5I	NAD and EX-527 analog	
		4IF6	ADPR	
		4IG9	-	
		4KXQ	ADPR	
SIRT2	PDB	1J8F	-	
		3ZGO	-	
		3ZGV	ADPR	
		4L3O	Cyclic peptide S2iL5	
SIRT3	PDB	3GLT	ADPR bound to AceCS2 peptide	
		3GLS	-	
		3GLR	acetyl-lysine AceCS2 peptide	
		3GLU	AceCS2 peptide	
		4FVT	AceACS peptide and Carba-NAD	
		4HD8	Fluor-de-Lys peptide and piceatannol	
		4FZ3	Acetyl-P53 peptide coupled with MCM	
		4JSR	Inhibitor 11c	
		4JT9	Inhibitor 3	
		4JT8	Inhibitor 28	
		4BN4	ADPR	
		4BN5	SRT1720 and Carba-NAD	
		4BV3	NAD/ADPR and EX-527	
		4BVB	ADPR and EX-527	
		4BVE	Thioalkylimidate formed from thio-acetyl-lysine acs2-peptide	
		4BVF	Thioalkylimidate formed from thio-acetyl-lysine acs2-peptide	
		4BVG	alkylimidate formed from acetyl-lysine acs2-peptide	
4BVH	2-O-acetyl-ADPR and EX-527			
4C7B	Bromo-Resveratrol and Fluor-De-Lys peptide			
4C78	Bromo-Resveratrol and AceCS2 peptide			
SIRT4	SwissModel	Q9Y6E7	-	Based on Sir2 A. Fulgidus (1S7G), identity 31%
SIRT5	PDB	2B4Y	ADPR	
		2NYR	Suramin	
		3RIG	Thioacetyl peptide	
		3RIY	Succinylpeptide and NAD	
		4F4U	Succinylpeptide	
		4F56	H3K9 thiosuccinyl peptide bound with NAD	
		4G1C	Succinylpeptide and Carba-NAD	
		4HDA	Fluor-de-Lys peptide and resveratrol	
SIRT6	PDB	3K35	ADPR	
		3PKI	ADPR	
		3PKJ	2'-N-Acetyl ADPR	
		3ZG6	H3K9 myristoyl peptide and ADPR	
SIRT7	SwissModel	Q9NRC8	-	Based on Sirt6 template (3K35), identity 42%

Table 5.1. Three-dimensional structures of human sirtuins available from public domain (Protein Data Bank)

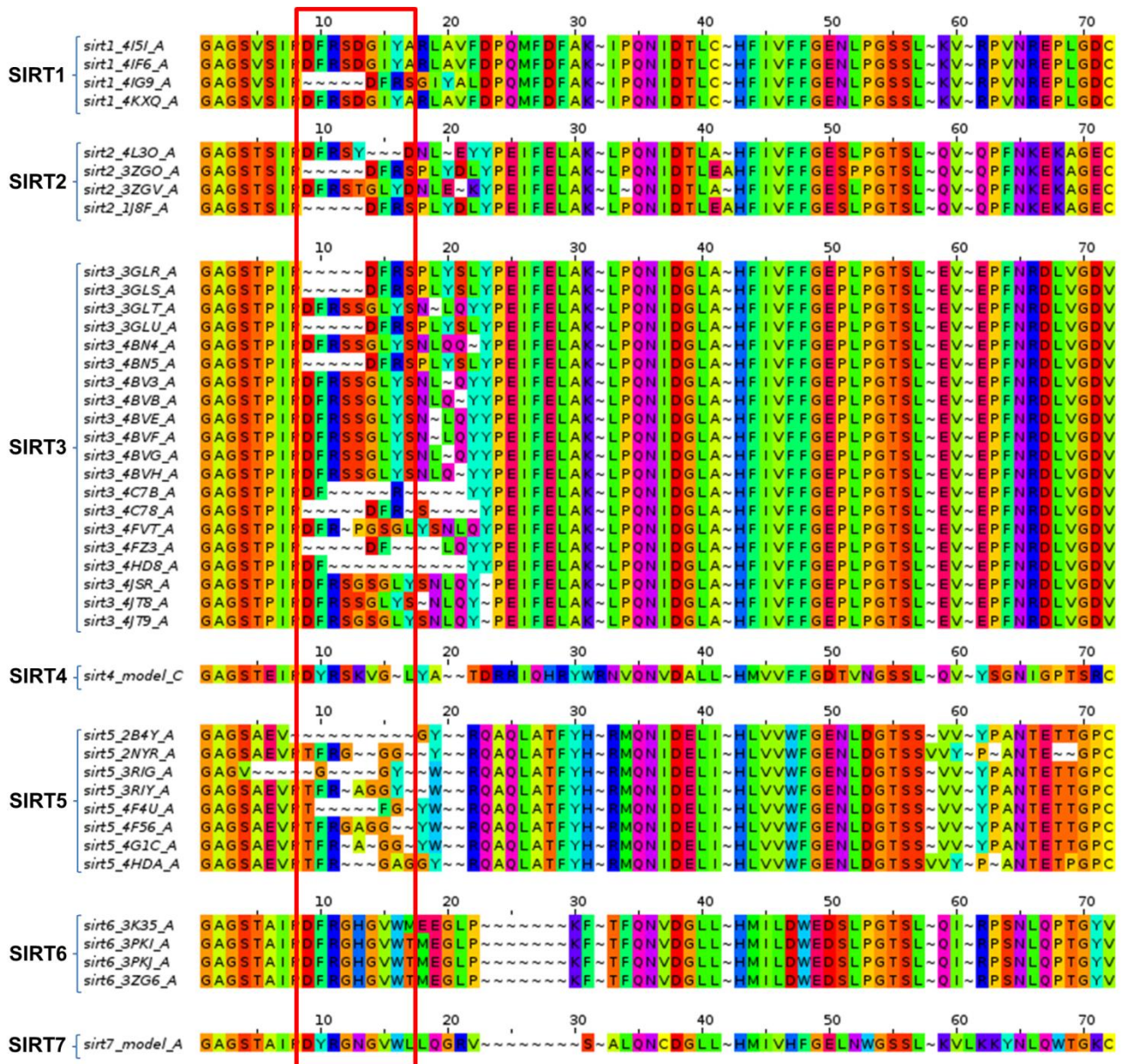


Figure 5.4. Structural alignment of available three-dimensional structures of human sirtuins. Residues are color-coded using Taylor classification. The red box highlights the area of the cofactor binding loop

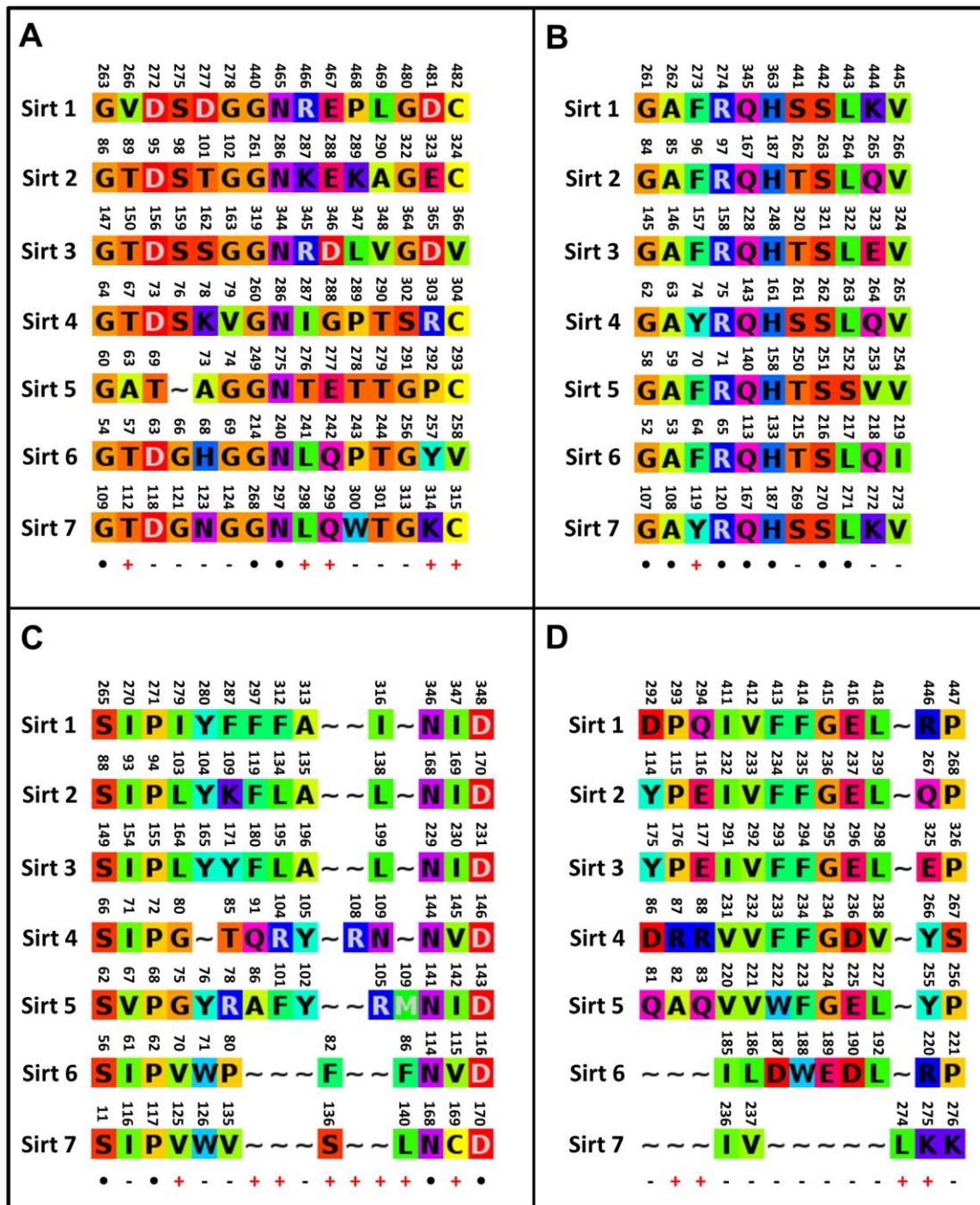


Figure 5.5. Structural alignment of human sirtuins. The alignments were generated using residues in a range of 4Å from the ligand and considering a three-dimensional superposition. The residues were color-coded using Taylor classification and numbered following gene sequences taken from the Uniprot database. The last line of each alignment suggests the estimated importance of each residue in selectivity: black dot (•) indicates residues conserved in all sirtuins, while black minus (-) and red plus (+) indicates residues respectively with poor or higher probability to be involved in selectivity. A) Structural alignment of residues comprising adenine binding pocket (pocket A). B) Structural alignment of residues comprising nicotinamide-ribose binding pocket (pocket B). C) Structural alignment of residues comprising nicotinamide binding pocket (pocket C). D) Structural alignment of residues comprising substrate binding pocket.

Overall, we identified 18 residues in the active site (red plus in Figure 5.5) that could have a significant impact on ligand selectivity and that should be taken into account while designing new sirtuin modulators. The pharmacophoric features and the position in the active site relative to the cofactor and a reference inhibitor (SRT1720) was depicted in Figure 5.6 while the complete information about aminoacidic differences for all possible couples of sirtuin isoforms was reported in a double-entry table in Figure 5.7 that encodes similarities and differences among the whole sirtuin family.

Complementary to the results obtained with the sequence alignment of the deacetylase domain, the structural superposition of sirtuin active sites reveal that catalytic cores can be divided into different clusters. SIRT1, SIRT2 and SIRT3 (group 1) are characterized by high similarity in the active sites, with few different residues located mainly in the adenine pocket and in the substrate pocket. Likewise, SIRT6 and SIRT7 (group 2) show significant similarity, with a total of 6 variable residues, while both SIRT4 and SIRT5 (group 3) show several aminoacidic variations compared to all other sirtuins. Based on these observations, it is possible to hypothesize the design of selective ligands for sirtuins belonging to different identified groups, while we predict that the selectivity within a single group is harder to achieve. For example, inhibitors of SIRT6 or SIRT7 could be likely selective versus SIRT1 or SIRT2 due to the important aminoacidic differences that characterize the active site of these isoforms. On the contrary, ligands resulting in a high selectivity for SIRT1 over SIRT2, or SIRT6 over SIRT7, are expected to be difficult to obtain on the basis of the intrinsic similarities in their aminoacidic composition. Certainly this similarity does not preclude the possibility to obtain ligand selective that exploit other structural features such as preferential conformational behavior and specific shape of the catalytic core (see below). Figure 5.8 depict these concepts showing the difference in the active site among sirtuins belonging to the same group (Figure 5.8A and Figure 5.8B) and belonging to different groups (Figure 5.8C). From the pharmacophoric point of view, the sirtuin active site (Figure 5.6) is characterized by a high number of hydrophobic interactions (green boxes), especially in proximity of the reference ligand SRT1720 that lie in the nicotinamide and the substrate binding pocket. This is especially evident for SIRT1, SIRT2 and SIRT3 (group 1, as defined above). Taking into consideration the differences among each sirtuin isoform, these interactions are primarily replaced with polar interactions (blue boxes) or with sequence gaps (gray boxes), the latter implying the presence of small but significant variations in the shape and dimension of the catalytic core. On the contrary, the adenine binding pocket and

the nicotinamide-ribose binding pocket show mainly polar or charged features (blue and purple/red respectively), often involving hydrogen bonding with the cofactor molecule. In these cases, the differences among sirtuin isoforms involve charge shifting (positive to negative or *vice versa*) or substitutions with hydrophobic features; in both cases, the result is a variation of the surface properties of the active site.

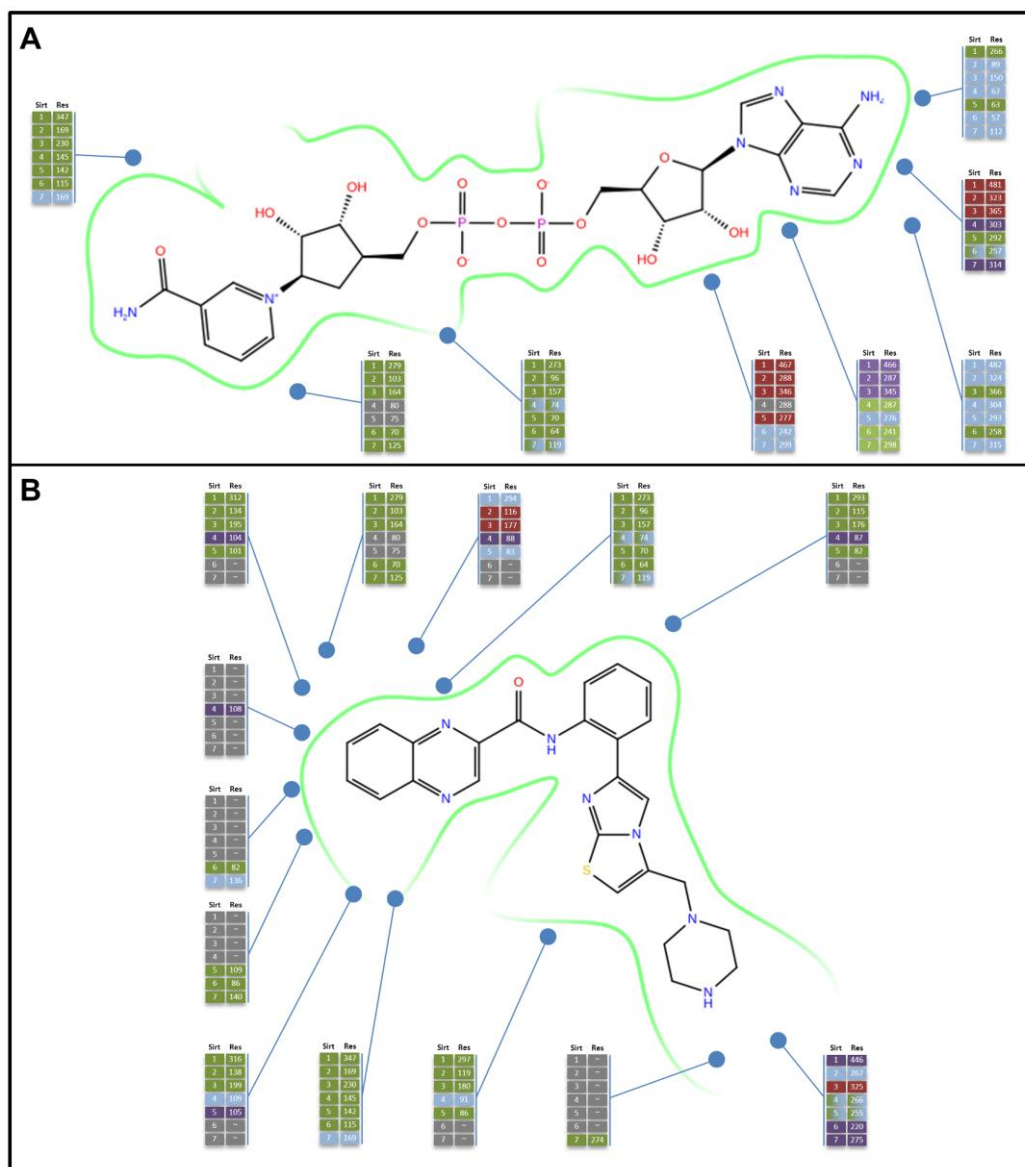


Figure 5.6. Pharmacophoric features of catalytic core residues of sirtuin family. The green line represents the active site surface and the blue dots the position of important residues in the catalytic core. For each dot a small table reports the residue number for each sirtuin, color-coded by pharmacophoric features: green for hydrophobic, blue for polar, purple for positive charge, red for negative charge and gray for absent residues or glycines. The green/blue cells represent tyrosine residues. Some residues can interact with both ligand and cofactor and are reported in both parts of the figure.

A) Ligand interaction diagram of NAD⁺. B) Ligand interaction diagram of SRT1720.

	Sirt 1	Sirt 2	Sirt 3	Sirt 4	Sirt 5	Sirt 6
Sirt 2	V266/T89 Q294/E116 R446/Q267					
Sirt 3	Q294/E177 C482/V366 R446/E325 V266/T150	C324/V366 Q267/E325				
Sirt 4	V266/T67 I279/G80 F273/Y74 E467/G288 R466/I287 D481/R303 F312/R104 Q294/R88 P293/R87 I316/N109 F297/Q91 R446/Y266 ~/R108	L103/G80 F96/Y74 E288/G288 K287/I287 E323/R303 L134/R104 E116/R88 P115/R87 ~/R108 L138/N109 F119/Q91 Q267/Y266	L164/G80 F157/Y74 D346/G288 R345/I287 V366/C304 D365/R303 L195/R104 E177/R88 P176/R87 ~/R108 L199/N109 F180/Q91 E325/Y266			
Sirt 5	I279/G75 R466/I287 D481/P292 I316/R105 R446/Y255	L103/G75 K287/T276 E323/P292 T89/A63 E116/Q83 ~/M109 L138/R105 Q267/Y255	L164/G75 R345/T276 V366/C293 D365/P292 T150/A63 E177/Q83 ~/M109 L199/R105 E325/Y255	Y74/F70 G288/E277 I287/T276 R303/P292 T67/A63 R88/Q83 ~/M109 N109/R105 R104/F101 R87/A82 R108/~ A86/Q91		
Sirt 6	E467/Q242 R466/L241 C482/V258 D481/Y257 V266/T57 F312/~ Q294/~ P293/~ ~/F82 ~/F86 I316/~ F297/~	E288/Q242 K287/L241 C324/V258 E323/Y257 L134/~ E116/~ P115/~ ~/F82 ~/F86 L138/~ F119/~ Q267/R220	D346/Q242 R345/L241 D365/Y257 L195/~ E177/~ P176/~ ~/F82 ~/F86 L199/~ F180/~ E325/R220	G288/Q242 R303/Y257 C304/V258 Y74/F64 G80/V70 R104/~ R88/~ R87/~ N109/~ Q91/~ R108/~ ~/F82 ~/F86 Y266/R220	E277/Q242 P292/Y257 C293/V258 G75/V70 A63/T57 F101/~ Q83/~ A82/~ R105/~ A86/~ ~/F82 M109/F86 Y255/R220	
Sirt 7	I347/C169 F273/Y119 E467/Q299 R466/L298 D481/K314 V266/T112 F312/~ ~/S136 ~/L140 I316/~ F297/~ ~/L274 Q294/~ P293/~	I169/C169 F96/Y119 E288/Q299 K287/L298 E323/K314 L134/~ E116/~ P115/~ ~/S136 ~/L140 L138/~ F119/~ ~/L274 Q267/K275	I230/C169 F157/Y119 D346/Q299 R345/L298 D365/K314 V366/C315 L195/~ P176/~ E177/~ L199/~ F180/~ ~/S136 ~/L140 ~/L274 I230/C169 E325/K275	V145/C169 G80/V125 G288/Q299 I287/L298 R303/K314 R104/~ R87/~ R88/~ N109/~ Q91/~ ~/S136 ~/L140 ~/L274 V145/C169 Y266/K275	I142/C169 V70/Y119 E277/Q299 T276/L298 P292/K314 G75/V125 A63/T112 F101/~ F82/~ Q83/~ R105/~ A86/~ ~/S136 ~/L274 Y255/K275	V115/C169 F64/Y119 Y257/K314 V258/C315 F82/S136 ~/L274

Figure 5.7. Selectivity hot-spots table. Each cell reports the aminoacidic differences between a couple of sirtuins that are supposed to be important for selectivity. For each difference, the first residue refers to the sirtuin in the row and the second refers to the sirtuin in the column.

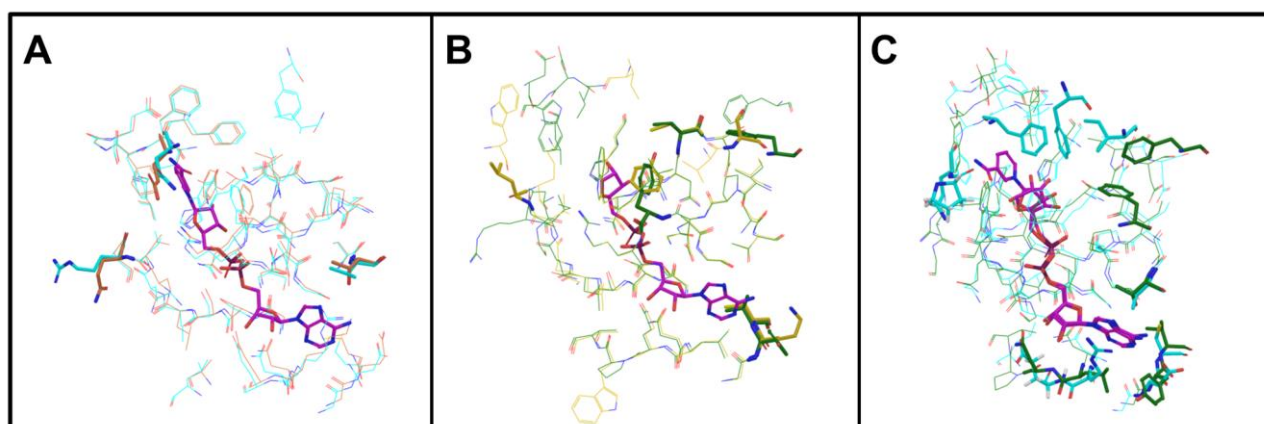


Figure 5.8. Structural comparison of SIRT1, SIRT2, SIRT6 and SIRT7. Residues classified as important for selectivity are drawn in thick tube. Reference ligands are reported to help the identification of active site pockets. A) Structural comparison of SIRT1 (cyan) and SIRT2 (orange). Reference ligand (purple) is NAD^+ taken from PDB code 4I5I. B) Structural comparison of SIRT6 (dark green) and SIRT7 (lime green). Reference ligand (purple) is ADPR taken from PDB code 3K35. C) Structural comparison of SIRT1 (cyan) and SIRT6 (dark green), with the same reference ligands of A and B (purple).

It is worth mentioning that compound selectivity for SIRT1 vs. SIRT2 was studied by previous works and several examples of fairly selective inhibitors were reported in the last few years^{252–258}. The rationale for this selectivity was investigated using classical structural-activity relationships (SAR) and, occasionally, with the help of molecular modeling techniques that were used to predict the active site residues involved. The same techniques were recently applied by our group for the discovery of selective SIRT6 inhibitors²⁵⁹. Nevertheless, despite the amount of structural information appeared in the literature in the last years, the mechanisms underlining ligand selectivity towards cognate sirtuin isoform is still not fully understood. In fact, the selectivity could be the result of a combination of different effects not related to the single residue modifications in the active site but, for instance, different kinetic profiles, conformational changes of the proteins, presence of allosteric sites as well as subcellular location of protein targets and their level of expression in specific tissues. As an example, the isoform selectivity of EX-527 (**1**, Figure 5.1) appears to be based on kinetic differences of catalysis, suggesting that selectivity could also vary under different physiological conditions, such as substrate availability²³². However, such effects are difficult to be estimated *a priori* and experimental determinations are needed elucidate selective behaviors, whereas aminoacidic composition that alter active site properties could be considered in structural analyses, like the one herein presented, that could be used for the rational design of new small-molecule modulators or for the development of analog compounds using standard SARs.

The structural model of human sirtuin family that we obtained clearly suggests several functional hot-spots that could be exploited to improve selectivity of newly identified sirtuin ligands. Nonetheless, it is important to note that approximations to generate this model have been taken into account and further experimental structural insights could contribute to refine our conclusions. In particular, it is important to note that conformational variations of the proteins, e.g the open and closed forms, could play a role in term of ligand selectivity while our model is based on the principle that all sirtuin family members can adopt both forms depending on the bound substrate, ligand and cofactor. Similarly, an experimental validation is still awaited for SIRT4 and SIRT7 that still have no three-dimensional structure representative in the Protein Data Bank and, for the time being, they needed to be modeled by homology. In the same way, the presence of allosteric sites, or ligands able to induce isoform-specific conformational variations have not been described yet. Finally, the model was built by including residues within a distance range compatible with reference ligands and cofactors (i.e. SRT1720 and NAD⁺) taken from the few crystallographic structures available; clearly, the discovery of additional ligands and their three-dimensional structure in complex with sirtuins might provide additional information on new interacting residues extending outside the range encompassed by our model.

5.4 Conclusions

The broad involvement of sirtuins in several pathological conditions has raised a strong interest in the development of specific inhibitors or activators to explore disease models that are dependent on sirtuin functions. Selective modulators, able to modify the enzymatic activity of single sirtuin isoforms could be used as chemical probes to elucidate the role of each sirtuin isoform in biological activities but also as a starting point to develop more efficient targeted therapies. Our study is the first effort to summarize in a comprehensive structural model the selectivity hot-spots among sirtuin family members, providing a simple tool to estimate the selectivity of a small molecule ligand between two or more isoforms. Starting from a putative binding mode of a ligand into the active site of one sirtuin isoform, experimental (i.e. X-ray or NMR) or molecular modeling (docking, molecular dynamics) techniques, could be used in combination to our model to allow understanding at a glance the active site residues that most likely are involved in ligand selectivity and how to design suitable pharmacophoric variations to improve the activity profiles. Although based on approximations and simplifications, this model constitute valuable tool to better understand the complexity of the sirtuin machinery and to advance the search for selective small-molecule modulators.

5.5 Experimental Section

In Silico techniques

Sequence alignment and principal component analysis. The sequences of the seven human sirtuins were retrieved from Uniprot database as reported in Table 5.2. The multiple sequence alignment was generated using T-Coffee method²⁶⁰ implemented in Jalview²⁶¹, followed by a manual revision to ensure the maximum accuracy. The alignment was then exported in FASTA format and converted to CSV format, using a bash shell script, to make it suitable for further steps. The PCA analysis was carried out using Simca-P software version 11.2 (Umetrics, Sweden). All variables with zero variance (conserved residues) were automatically excluded from the model and the first two principal components were calculated and used to generate the score plot reported in Figure 5.3.

Seq	Uniprot Code	Tot Residues	Catalytic HIS	Nucleotide Binding	Metal Binding	Deacetylase Domain
Sirt1	Q96EB6	747	363	261-280, 345-348, 440-442, 465-467	371,374,395,398	244 - 498
Sirt2	Q8IXJ6	389	187	84-104, 167-170, 261-263, 286-288	195,200,221,224	65-340
Sirt3	Q9NTG7	399	248	145-165, 228-231, 319-321, 344-346	256,259,280,283	126-382
Sirt4	Q9Y6E7	314	161	62-82, 143-146, 260-262, 286-288	169,172,220,223	45-314
Sirt5	Q9NXA8	310	158	58-77, 140-143, 249-251, 275-277	166,169,207,212	41-309
Sirt6	Q8N6T7	355	133	52-71, 113-116, 214-216, 240-242	141,144,166,177	35-274
Sirt7	Q9NRC8	400	187	107-126, 167-170, 268-270, 297-299	195,198,225,228	90-331

Table 5.2. Human sirtuins sequences available in Uniprot database.

Protein preparation. The crystal structures of human sirtuins (Table S1) were retrieved from PDB Database and submitted to a standard preparation procedures (protein preparation wizard) as included in the software package Maestro (Version 9.3, Schrödinger, LLC). Any water molecules, ions and crystallization mediums were removed (except for zinc ion) while substrates, ligands and cofactors were kept, if present. Each structure was optimized using PROPKA and minimized until an RMSD of 0.2 Å.

Structure-based alignment. The prepared structures were then aligned using the Protein Structure Alignment tool included in Maestro, using backbone as reference atoms. The Multiple Sequence Viewer tool was then used to align sequences according to structure superposition, and to generate

an alignment based only on structure superposition and not on sequence conservation. The structural alignment was restricted by selecting residues falling into a range of 4 Å from reference ligands, namely the SRT1720 and Carba-NAD structures taken from PDB code 4BN5; these reference ligands are able to fill up completely all active site pockets, and therefore were chosen among the other available structures. Due to the large number of three-dimensional structure included in the model, and to the high level of complexity of the structural alignment, the results obtained of automated tools were excluded to avoid inaccuracies and processed thorough a manual revision of the alignment. The alignment reported in Figure 4 was generated starting from the global alignment by selecting 7 representative structures, one for each sirtuin isoform. In particular, the following PDB codes were selected: 4I5I (SIRT1), 3ZGV (SIRT2), 3GLT (SIRT3), 3RIY (SIRT5), 3K35 (SIRT6), supplemented by the homology models for SIRT4 and SIRT5.

6. Discovery of new SIRT3 modulators

SIRT3 emerged as a protein of particular interest to the aging field due to its mitochondrial localization and association with exceptional long lifespan in humans. SIRT3 deacetylates and activates many mitochondrial enzymes involved in fatty acid β -oxidation, amino acid metabolism, the electron transport chain (ETC), and antioxidant defenses²⁶².

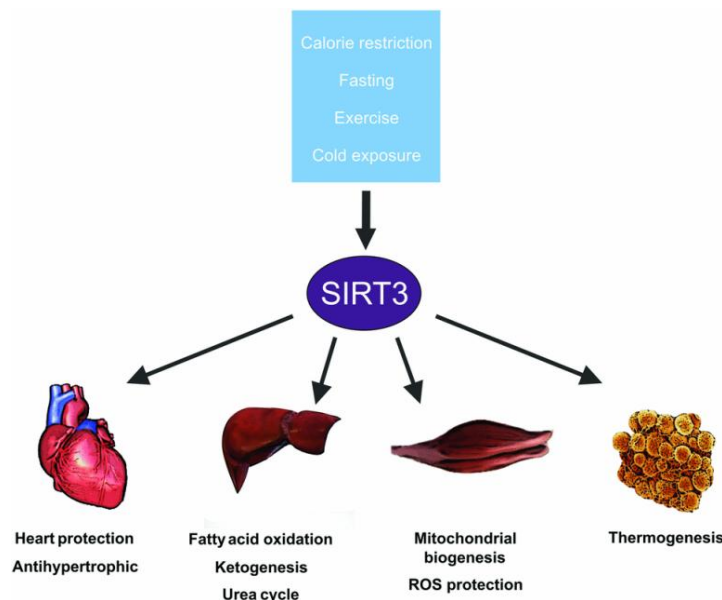


Figure 6.1. Main physiological and pathological processes regulated by SIRT3²⁶²

The study of mice with a targeted deletion of SIRT3 has been a valuable tool for clarifying the physiological role of SIRT3. One pivotal observation was a striking hyperacetylation of mitochondrial proteins in SIRT3^{-/-} mice, a pattern not observed in SIRT4^{-/-} or SIRT5^{-/-} mice²⁶³. Moreover, incubation of mitochondrial extracts from SIRT3^{-/-} mice with a recombinant wild-type form of SIRT3 effectively reversed this state of hyperacetylation. Collectively, these observations suggest that SIRT3 might be the main deacetylase in mitochondria. Keeping with its localization in mitochondria, SIRT3 is involved in the control of the mitochondrial ATP-production machinery through effects on the respiratory chain. A study in SIRT3^{-/-} mice showed abnormally reduced (nearly 50%) ATP levels in tissues that normally exhibit high ATP levels, such as heart, liver, kidney and skeletal muscle; notably, tissues where the expression of SIRT3 is normally elevated²⁶⁴. This reduction in ATP levels was not observed in tissues such as the pancreas where SIRT3 is expressed at low levels. It is likely that SIRT3 regulates ATP levels through the regulation of respiratory complex I activity, given that: (i) several components of complex I show increased acetylation in SIRT3^{-/-} mice; (ii) SIRT3 can physically interact with at least one of the known

subunits of complex I, the 39-kDa protein NDUFA9; and (iii) incubation of exogenous SIRT3 with mitochondria augments complex I activity. In addition to directly regulating the activity of the respiratory chain, SIRT3 participates in the production of reduced cofactors through activation of two enzymes: succinate dehydrogenase and IDH2 (isocitrate dehydrogenase 2), an NADP-dependent isoenzyme of IDH. Overall, SIRT3 appears to control the rate of mitochondrial ATP synthesis directly by controlling the activity and amount of mitochondrial respiratory and oxidative phosphorylation machinery.

Investigations of the mechanism of carcinogenesis in mice lacking Sirt3 have resulted in several important observations regarding the mechanistic connection between aberrant mitochondrial metabolism and carcinogenesis: (i) Sirt3 regulates HIF-1 α activity, resulting in an altered cellular metabolism that supports cell proliferation; (ii) Sirt3 directly regulates MnSOD enzymatic activity via acetylation, and the aberrant acetylation of MnSOD in cells lacking Sirt3 increases cellular ROS; and (iii) Sirt3 knockout mice develop estrogen-positive mammary tumors. Furthermore, SIRT3 expression is decreased in many different types of human cancers, and heterozygous loss of SIRT3 occurs in 40% of human breast malignancies, suggesting that knockout mice are the first murine model for the most common subtype of breast cancer observed in older, postmenopausal women²⁶⁵. SIRT3 exerts a profound protective action against oxidative stress-dependent pathologies; the identification of compounds capable of modulating SIRT3 activity is expected to provide promising strategies for ameliorating the aging-related metabolic syndrome such as cancer, cardiac dysfunction and neural degeneration.

6.1 Targeting SIRT3 with structure-based drug design techniques

In this study, we took advantage of the availability of SIRT3 crystal structure and performed a high-throughput molecular docking screen with the goal of identifying selective chemical scaffolds able to modulate activity of SIRT3. At the time of this study, several different X-ray structures were available in public domain (see Table 5.1 in chapter 5) in apo form or in complex with cofactor and/or inhibitor molecules.

When structurally compared, the structures showed to be similar in terms of the overall protein conformation but the shape of the active site modifies slightly depending on presence or absence of substrate and cofactor molecules. We therefore decided to use an “Ensemble Docking” approach in our virtual screening. Usually, docking software uses a rigid receptor model in which ligands are allowed to move flexibly but the protein remains rigid; because different ligand chemotypes may

induce different receptor conformations, as in the case of SIRT3, potent ligands whose chemotype induces one receptor conformation may score poorly against another receptor conformation. Ensemble docking mitigates this problem by allowing users to dock a single ligand library against multiple rigid receptor conformations, and collect the best score for each molecule.

So we used 5 X-ray structures of SIRT3 available in the Protein Data Bank; four accounts for conformational variations in the active site (PDB codes 3GLS, 3GLT, 3GLR, 3GLU) and one (PDB code 4C78) was used to define a putative allosteric activation site. This second binding site is located on the surface of Sirt3 and connected through two helices to peptide-binding active site loops. In Sirt1, this site appears to comprise a residue that is essential for its activation by small molecules and it therefore constitutes a candidate for the long-sought allosteric activator binding site. We screened a large database of commercial compounds¹³² in a high-throughput docking screening campaign (Figure 6.2). The best scoring compounds were visually inspected and the final candidate selection was done taking in account the interactions of each molecule in the active sites, the structural diversity and specific physicochemical properties of molecules. Hit compounds were purchased and tested for their ability to inhibit or activate SIRT3 using fluorescence-based assay in the Laboratory of Dr. Diego Albani (Istituto di Ricerche Farmacologiche Mario Negri). Active compounds were also tested for their ability to modify acetylation pattern in mitochondria. 31 molecules were purchased and tested using fluorescence-based assay; after removing of interfering compounds (>10% of interference) we identified 2 putative activators and 3 putative inhibitors. The best results were obtained for compound 20 and compound 24 (Table 6.1 and Figure 6.3).

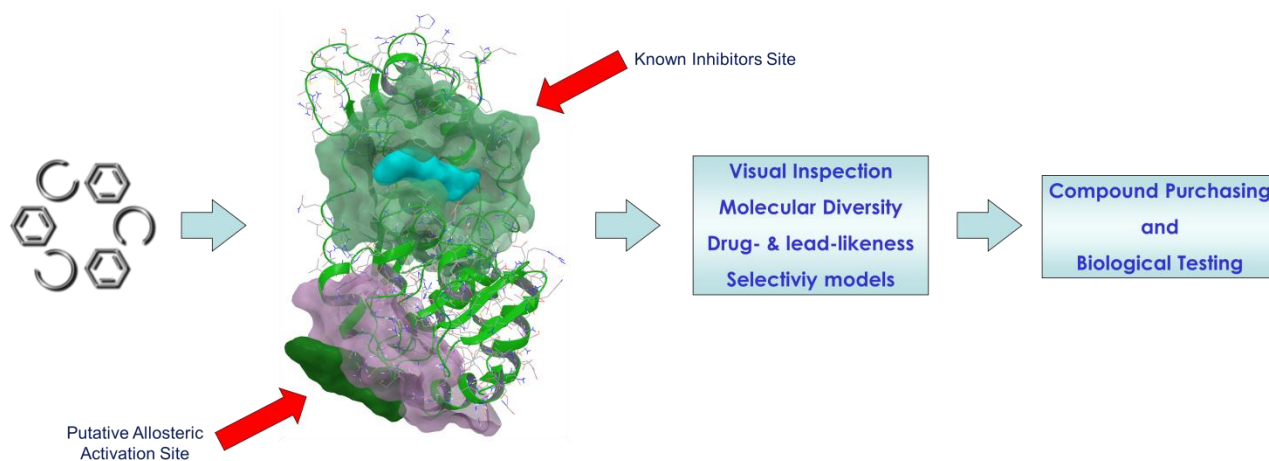


Figure 6.2: Molecular design workflow of new Sirtuin-3 inhibitors and activators

Compound	Activity	Results
CPD 20	Inhibitor	IC50 = 21 uM
CPD 24	Activator	EC50 = 22 uM

Table 6.1. Results of biological testing

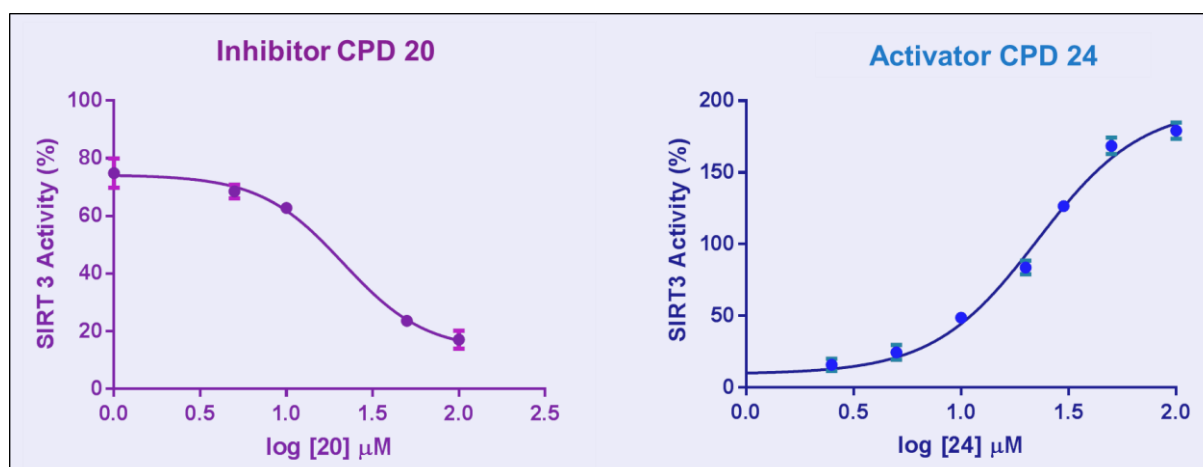


Figure 6.3. Dose-Response curves for active compounds

6.2 Evaluation of acetylation pattern of mitochondrial proteins

To confirm the SIRT3 activation and inhibition by the identified compounds, we evaluated the acetylation pattern of mitochondrial proteins. In particular, neuroblastoma SH-SY5Y cells were treated with compound 20 and compound 24 at 10uM for 24h, and then the mitochondrial lysate were analyzed by western blot using a generic antibody able to recognize acetylated lysines as antigen, and the mitochondrial channel VDAC as loading control. Both total acetylated lysines and acetylation pattern of ETC Complexes 1 and 4 were analyzed.

As reported in Figures 6.4 and 6.5, cells treated with compound 20 (inhibitor) shows an acetylation level significantly higher than control, while cells treated with compound 24 (activator) shows an acetylation level significantly lower than control.

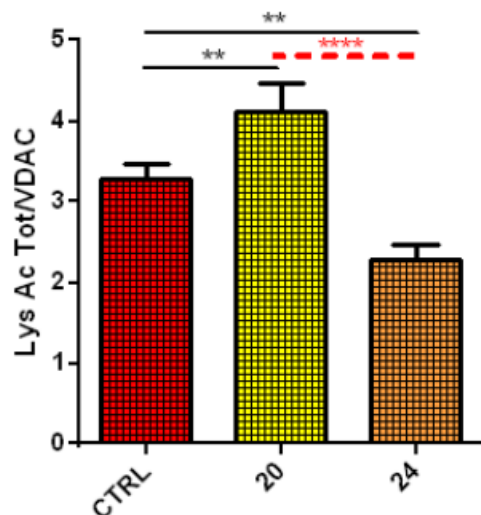


Figure 6.4. Total acetylated lysines/VDAC (One way-ANOVA, Tukey's post-hoc test; ** p<0,01; **** p<0,0001)

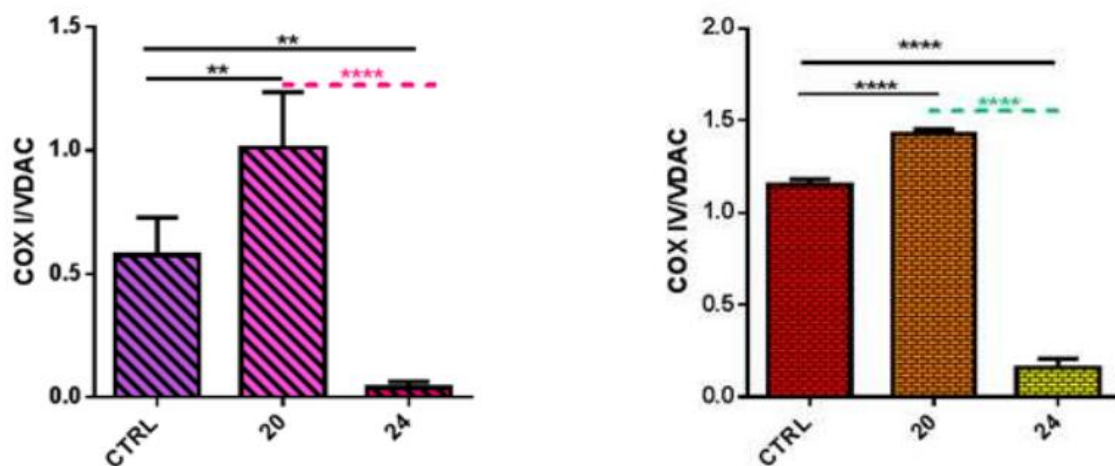


Figure 6.5. Acetylation pattern of ETC Complexes 1 (COX I) and Complex 4 (COX IV) vs VDAC (One way-ANOVA, Tukey's post-hoc test; ** p<0,01; **** p<0,0001)

6.2.1 Evaluation of acetylation pattern of a specific protein target of SIRT3

To better confirm the modulation of SIRT3 activity by active compounds, we evaluated the acetylation pattern of a known target of SIRT3, the mitochondrial superoxide dismutase (SOD2) protein. The test was conducted as above but using a specific SOD2 antibody. Before this test, we also confirmed, by co-immunoprecipitation, that in our model SIRT3 and SOD2 are interacting proteins, and that compounds 20 and 24 do not alter the expression level of SOD2 protein (data not shown). The results shows in Figure 6.6 confirm the alteration of acetylation pattern by both the activator and the inhibitor, strongly reinforcing the hypothesis of a direct interaction of these molecules with SIRT3.

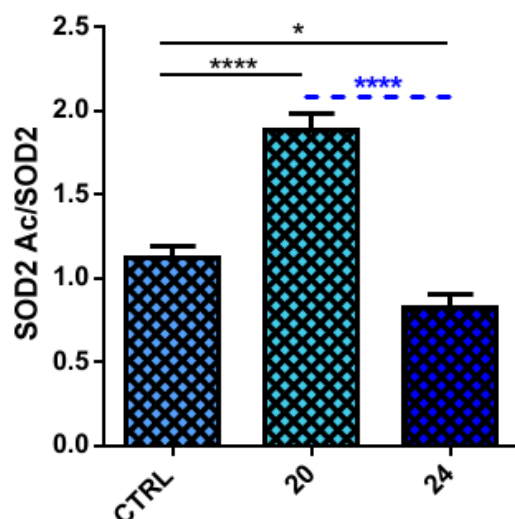


Figure 6.6. Acetylated SOD2 vs non-acetylated SOD2 (One way-ANOVA, Tukey's post-hoc test; * $p < 0,05$; **** $p < 0,0001$)

6.3 Evaluation of cell response to toxic stimulation

We tested the ability of the activator molecule, compound 24, to modify the cell response to toxic stimuli using two different oxidative compounds. SH-SY5Y cells were treated with compound 24 at 10uM for 24h and then with hydrogen peroxide or 6-hydroxydopamine (6-OHDA) at 75uM overnight. Then the cellular viability was measured using colorimetric assay. As reported in Figure 7, cells pre-treated with compound 24 show cell viability comparable to control, confirming the protective role of this compound against oxidative stress induced by two different toxic stimuli.

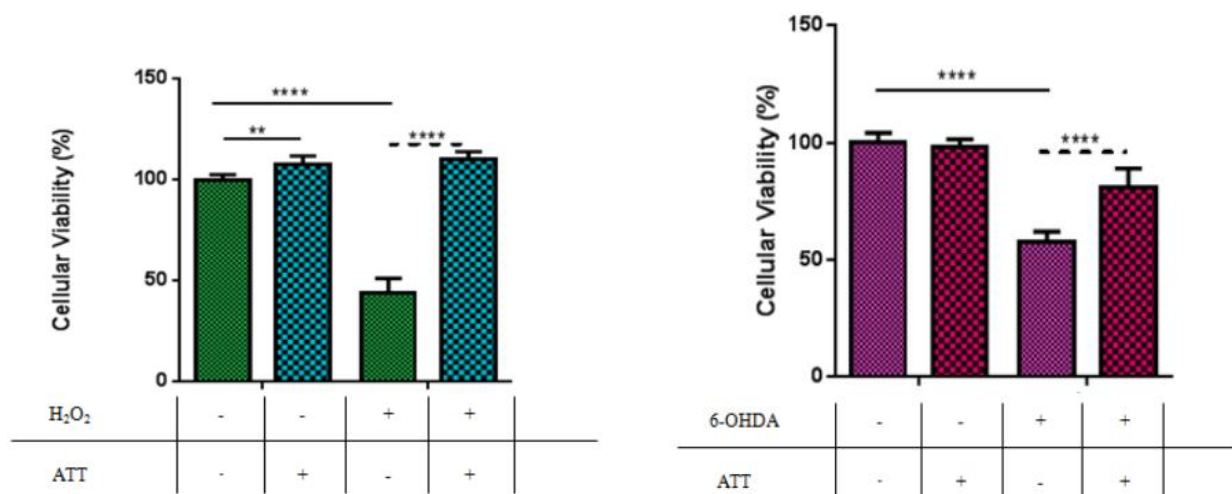


Figure 6.7. Cell response to toxic stimuli in absence or presence of activator compound 24. (Two way- ANOVA, Tukey's post-hoc test; ** $p < 0,01$; **** $p < 0,0001$)

6.4 Conclusions

This virtual screening approach led us to the discovery of new putative modulators of SIRT3 with interesting in-vitro and cellular activity. The activator compound 24 is of special interest since no specific SIRT3 activators are reported in literature so far.

The results, that need to be confirmed by other *in vivo* testing, could represent a good starting point for the development of new therapeutic strategies in many SIRT3-related pathologies.

6.5 Experimental Section

In silico techniques.

Several crystal structures of the SIRT3 in different conformation was used as a template for virtual screening purposes (PDB id: 3GLS, 3GLT, 3GLR, 3GLU and 4C78). These structures were prepared with standard preparation procedures (protein preparation wizard) as included in the software package Maestro¹³⁴. The docking software Glide¹³⁵ was used to perform a high-throughput virtual screening experiment. A docking grid was obtained by centering a 25 Å box in the centroid of the ADP-ribose ligand, as present in the template crystallographic structure of the human SIRT3. Although many water molecules are present in the crystal structure, none of these seems to be involved in stable interactions with ligand- or NAD⁺-binding, therefore all waters were removed from the grid. Standard precision (SP) docking was used to perform a first round of virtual screening. The top 1500 molecules, sorted by Glide score, were further refined with the extra-precision (XP) docking. Docking results were ranked based on the Glide score and the first 500 hits were considered for visual inspection. Compounds were visualized by taking into account several structural and physico-chemical rules, such as the qualitative evaluation of ligand-protein interactions within the active site, probability of suggested protonation and tautomeric states, stereochemistry complexity, compound availability, chemical diversity, drug-likeness and synthetic accessibility.

Compound Sources. We screened in silico the Asinex subset of the CoCoCo databases. Selected molecules were purchased in milligram quantities from chemical vendor. Purity of compounds was $\geq 95\%$, as declared by the chemical vendor.

Biological assays (Laboratory of Dr. Albani, Istituto Mario Negri - Milano)

Cell Lines. SHSY5Y cell line, derived from the original line SK-N-5H (obtained by biopsy from the bone marrow of a patient with neuroblastoma), was used for testing. Cells were maintained at 37°C

in a humidified atmosphere with 95% air and 5% CO₂. SHSY5Y cells grow in acceptance of polypropylene flasks (T75, Falcon) in DMEM medium (Invitrogen) supplemented with fetal bovine serum 10% (Gibco), 2 mM L-glutamine and 1% Penicillin-Streptomycin 1% (Invitrogen).

In vitro assays. Effects on enzymatic activity were tested with a standard kit from Cayman Chemical. SIRT3 Direct Fluorescent Screening Assay Kit provides a convenient fluorescence-based method for screening SIRT3 inhibitors or activators. The procedure requires only two easy steps, both performed in the same microplate. In the first step, the substrate, which comprises the p53 sequence Gln-Pro-Lys-Lys(ϵ -acetyl)-AMC, is incubated with human recombinant SIRT3 along with its cosubstrate NAD⁺. Deacetylation sensitizes the Substrate such that treatment with the Developer in the second step releases a fluorescent product. The Fluorophore can be analyzed with an excitation wavelength of 350-360 nm and an emission wavelength of 450-465 nm.

Western Blotting. About 20 μ g of total protein extract was subjected to gradient SDS-PAGE electrophoresis (5–12%) and transferred to a nitrocellulose membrane. The membrane was incubated overnight with a primary antibody (anti-SIRT3, Anti-SOD2, Anti-VDAC or Anti-Ac-Lys), for 1 hour with a horseradish peroxidase-conjugated secondary antibody and ECL-detected. The resulting impressed film was quantified using a digital image analyser.

7. Discovery of new SIRT6 inhibitors

SIRT6 is a sirtuin family member with a role in intermediary metabolism, genome stability and inflammation²⁶⁶. SIRT6 regulates gene expression as a transcriptional co-repressor by physically interacting with transcription factors, such as NF- κ B¹⁵², HIF1 α ²⁶⁷, and MYC²⁶⁸ and by deacetylating histone H3 lysine 9 (H3K9) and 56 (H3K56) at target gene promoter. In line with this notion, SIRT6 deficiency results in an increased expression of genes controlled by these transcription factors, including pro-inflammatory genes through NF- κ B activity, glycolytic genes and the glucose transporter GLUT-1 due to increased HIF1 α activity, and genes involved in ribosome biogenesis due to de-repressed MYC-dependent transcription. Another mechanism through which SIRT6 may regulate cell signaling and gene transcription is through the production of Ca²⁺-mobilizing nucleotides, such as O-acetyl-ADP ribose (OAADPR), as a result of its catalytic activity^{245,269}. Last, but not least, SIRT6 has also been ascribed deacylation activity, which would be key to its ability to promote TNF- α secretion, and mono-ADPribosyltransferase activity, which would be self-directed but also used to modify other proteins, such as PARP1^{270,271}.

Consistent with these molecular roles of SIRT6, SIRT6-deficient mice are viable at birth but rapidly succumb to hypoglycemia after weaning²⁷². In particular, SIRT6-deficient animals were found to clear glucose from blood much faster than their wild-type littermates and to exhibit increased glucose uptake in the muscle and in brown adipose tissue, a phenotype that can be reversed through HIF1 α inhibition²⁶⁷. In addition, defective production of TNF- α and of other pro-inflammatory cytokines has also been observed in cells with reduced or absent SIRT6 expression^{271,273,274}.

Overall, taking into account SIRT6 biological functions, small molecule inhibitors of this enzyme hold potential for applications in metabolic disorders, such as diabetes (as blood glucose-lowering agents), in inflammatory conditions, and in cancer (as chemosensitizers)²⁶⁶. In addition, such compounds would complement the already available genetic tools and represent a valuable resource to study SIRT6-dependent biological processes *in vitro* and *in vivo*. In this context, the recent availability of SIRT6 crystal structure represents an important tool for structure-based *in silico* screenings and for the general understanding of the mode of action of SIRT6 and of its chemical modulators²⁴⁵.

7.1 Structure-based in silico screening

In this study, we took advantage of the availability of SIRT6 crystal structure and performed a high-throughput molecular docking screen with the goal of identifying selective chemical scaffolds with inhibitory activity on SIRT6.

At the time of this study, four different X-ray structures were available in public domain (PDB accession codes 3PKI, 3PKJ, 3K35 and 3ZG6)^{229,245,271}, one in complex with 2-N-acetyl-ADP-ribose (3PKJ) and the other in complex with ADP-ribose. When structurally compared, the four structures showed to be similar in terms of the overall protein conformation and shape of the active site. We therefore selected the 3K35 complex as the reference structure for in silico screens because of its higher resolution. A deeper analysis and a comparison with other sirtuin structures co-crystallized with the natural antagonist nicotinamide (NAM) revealed a different conformation of the Phe62 side chain that partially occludes the so-called nicotinamide pocket (or pocket C)²³⁰ impairing the binding of any ligand, including NAM itself. Because of this conformational constraint, and in order to maximize the chances to identify new potential scaffolds with the ability to bind in this position of the active site, the conformation of this side chain was modified using a custom procedure (see experimental section). The resulting model of SIRT6, after a standard protein preparation procedure, was used as template to virtually screen the Asinex compound dataset, as prepared in the CoCoCo database^{132,133}. The first hundreds hits were visually inspected to prioritize compounds that reproduced, at least in part, the binding mode of known substrates, cofactors and inhibitors, and to comply with simple physicochemical rules such as Lipinski's rule-of-five²⁷⁵. The structure of known SIRT1/SIRT2 binding compounds was also taken into account in order to select for compounds with high diversity and increased chances to be specific for SIRT6. Finally, sample availability from compound providers was also verified, leading to a final list of 20 compounds that were purchased and experimentally tested in the laboratories of Prof. Santina Bruzzone (University of Genova) for biochemical assays and Prof. Alessio Nencioni (University of Genova) for cellular and other functional assays. A commercial kit exploiting SIRT6 NAD⁺-dependent deacetylase activity was used to assess the effect of the selected compounds on this enzyme. The percentage of SIRT6 activity inhibition obtained with each compound at a 200 μ M concentration is reported in Table 7.1.

Among the 20 compounds tested, 4 led to a significant inhibition of SIRT6 deacetylase activity, ranging from 12 to 100%, thus giving a remarkable hit-rate obtained with the virtual screening protocol. Ten compounds resulted inactive at the concentration used in the assay, while 6

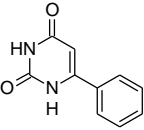
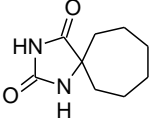
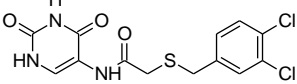
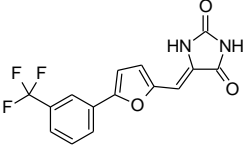
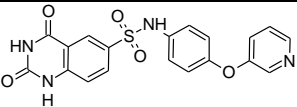
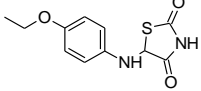
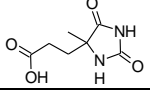
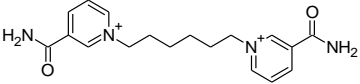
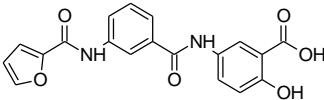
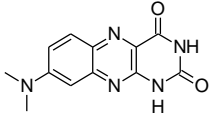
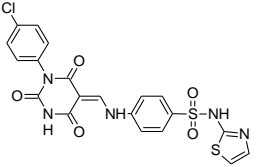
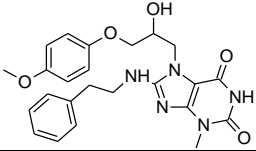
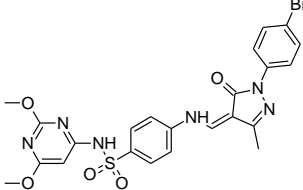
compounds could not be tested due to interferences with the fluorescence-based assay. None of the active compounds identified include substructures described as Pan Assay Interference Compounds (PAINS)²⁷⁶.

We subsequently determined the IC₅₀ values of the active compounds (Table 7.2). Consistent with the results of the preliminary screening, three compounds were found to inhibit SIRT6 activity in the low micromolar range (5, 9, and 17), while compound 16 was the less potent as it showed an IC₅₀ in the millimolar range.

Figure 7.1 reports the predicted binding modes of the four active molecules identified with the virtual screening. Compound 5 and compound 9 are both predicted to bind the NAM binding pocket (pocket C) and part of the substrate binding pocket, while compounds 16 and 17 are predicted to bind the adenine binding pocket (pocket A) and the ribose binding pocket (pocket B). Compound 5 is characterized by the presence of a quinazolinone group that is predicted to establish an extended hydrogen bond network with Val113 and Asp114, similar to the observed binding of the NAM moiety in other sirtuin complexes^{277,278}, and an additional hydrogen bond with the backbone carbonyl of Pro60. The aromatic part of 5 quinazoline ring is predicted to form a stacking interaction with Phe62 and the pyridine moiety to interact with His131 and, in part, with Trp186.

Compound 9 has a different chemical structure but a very similar pharmacophore compared to 5; in fact, it undergoes the same interaction network within the SIRT6 active site in which the salicylic moiety take place of the quinazoline ring and a furan ring replace the pyridine group. Notably, the predicted binding mode of 9 assumes that the salicylic group is in a protonated form. However, since the estimated pKa of this group is 2.73, a deprotonated form could also be hypothesized, which would likely prevent the formation of the hydrogen bond with Asp114 and favour the formation of a hydrogen bond with the amino group of Asn112 (Figure 7.2).

Compound 16 is predicted to form a number of hydrogen bonds with different residues in the NAD⁺-binding active site, as observed in the ADPR-SIRT6 complexes. Namely, such interactions are predicted to occur with Val256, Thr55, Asn238, Ser214 and Phe62. Notably, 16 also shows a double hydrogen bond with Asp61 side chain which is not observed in the available ADPR-SIRT6 complexes. The triazolyl-pyrimidine moiety of 16 fills up the adenine binding pocket and is packed between the hydrophobic residues Gly52 and Leu239; this functional group is able to reproduce, at least in part, the key structural binding features of the adenine moiety of NAD⁺, while the pyrazine-2-carboxamide group replaces the phosphate and ribose groups of the coenzyme.

Compound ID	Compound Structure	Asinex ID	% inhibition of SIRT6 at 200 μ M
1		BAS00130267	NI
2		BAS00565226	NI
3		BAS09175153	NI
4		BAS02804575	ND
5		SYN17739303	100 \pm 4
6		BAS07297446	NI
7		BAS06501826	NI
8		BAS00229902	NI
9		BAS13555470	62 \pm 7
10		BAS00780431	ND
11		BAS00620938	ND
12		BAS02378913	NI
13		BAS00324098	ND

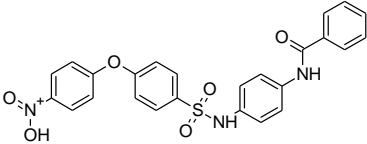
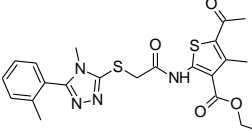
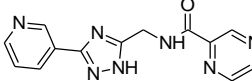
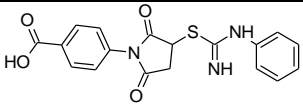
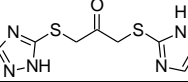
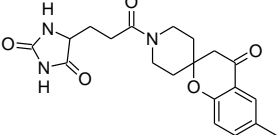
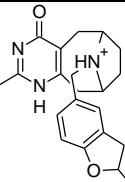
14		BAS00127176	NI
15		BAS01918477	ND
16		SYN10366754	12±3
17		BAS00417531	66±6
18		BAS09805329	NI
19		SYN13238554	ND
20		LEG19281134	NI

Table 7.1 Structures and SIRT6 inhibition activities of compounds selected with in silico techniques. NI = no inhibition and ND = not determined (interfering with the assay).

Compound 17 is predicted to form hydrogen bonds with Val256, Gln240 and Arg63, while hydrophobic interactions are observed between its benzoate moiety and the residues Gly52 and Leu239. Notably, these interactions are also observed in the binding of NAD⁺. In this case, the adenine binding pocket is predicted to be occupied by the benzoate moiety, while the succinimide and imino-phenyl groups are located in the ribose binding pocket. This compound was purchased and tested as a racemic mixture, as available from the vendor. However, it should be mentioned that docking results suggest a favorable binding for the R enantiomer.

7.2 Selectivity profiling

In order to evaluate the selectivity of the most interesting SIRT6 inhibitors, their IC₅₀ values were also determined for SIRT1 and SIRT2 by using commercially available kits. Compounds 9 and 17 proved to be the most selective compounds towards SIRT6, their IC₅₀ values being almost 20 times higher for SIRT1, and approximately 9 times higher for SIRT2 (Table 7.2). Compound 5 showed moderate SIRT6/SIRT1 selectivity, with an IC₅₀ value approximately three times higher for SIRT6,

and almost no selectivity over SIRT2; similar results were also obtained for compound 16, which showed poor or no selectivity over the other two sirtuins.

The analysis of previously solved sirtuin structures showed the presence of the so-called cofactor binding loop which adopts different conformations depending on the ligands bound in the active site²³⁰. SIRT6 is the only sirtuin isoform lacking this loop which is replaced by an ordered helix which confers a less flexible binding pocket²⁴⁵. This distinctive feature of SIRT6 entails the presence of relevant modifications in the active site that might be exploited to design selective inhibitors. Figure 7.3 shows a superposition of SIRT6, SIRT1 and SIRT2 active sites with the predicted binding poses of compounds 5 and 16 reported as reference. In fact, the presence of specific binding site residues in SIRT1 and SIRT2 determine differences in the shape and properties of the cavity compared to SIRT6. Specifically, the NAM binding pocket of SIRT1 and SIRT2 (Figure 7.3 A) shows the presence of bulky and hydrophobic residues, such as Phe119/Phe297, Leu103/Ile279 and Ile316, which have not cognate representation in the SIRT6 binding site, thus reducing the volume cavity and most probably leading to steric clash with the SIRT6 inhibitors. Similarly, the adenine binding pocket (Figure 7.3 B) shows also remarkable differences which modify the binding site properties: Leu239 in SIRT6 is substituted by Lys287/Arg466, and Gly64 is replaced by Ser98/Ser275. Taken together with the predicted binding poses, these differences can justify the selectivity ratio between SIRT6 and SIRT1/SIRT2 for the two most selective compounds, 9 and 17. Conversely, no structural explanation for the weak selectivity of compounds 5 and 16 can be proposed. Among other hypothesis, the lower selectivity of compound 5 could be explained with a higher conformational flexibility allowing this molecule to adapt more easily to the binding site of different sirtuins without losing key interactions. In the case of 16, its low activity (IC₅₀ for SIRT6 in the millimolar range) makes it difficult to speculate about possible determinants of its lack of selectivity for the different sirtuins.

Compound ID	SIRT6	SIRT1	SIRT2	ratio SIRT1/SIRT6	ratio SIRT2/SIRT6
5	106±16	314±19	114±5	2.96	1.07
9	89±5	1578±47	751±23	17.7	8.44
16	1339±54	1470±29	2291±69	1.10	1.71
17	181±15	3466±208	1744±52	19.15	9.63

Table 7.2. Determination of IC₅₀ (μM) for compounds 5, 9, 16 and 17 on SIRT6, SIRT1 and SIRT2 and fold-selectivity SIRT1/SIRT6 and SIRT2/SIRT6.

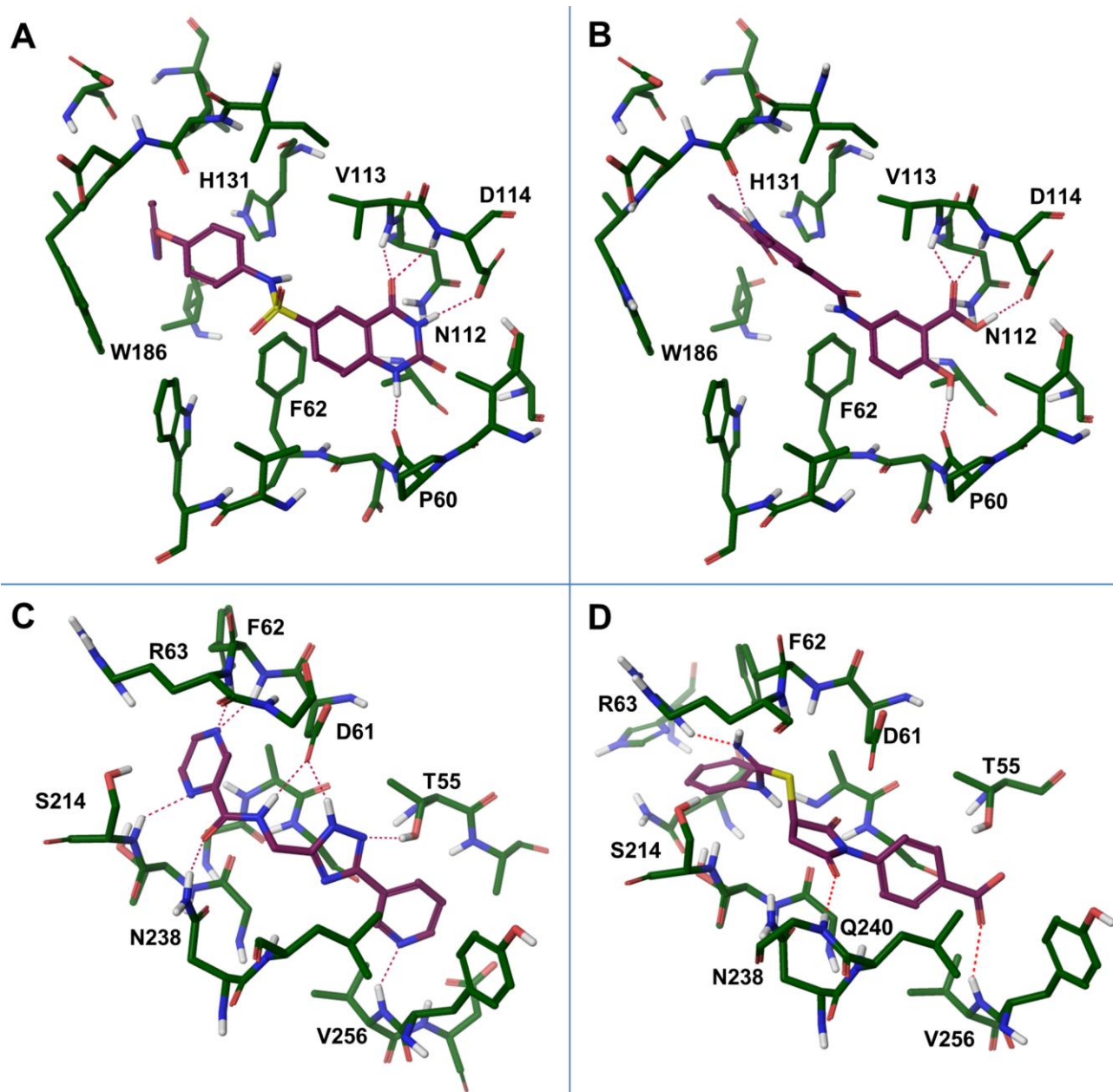


Figure 7.1. Putative binding mode of active inhibitors. Predicted binding mode of compound 5 (A), compound 9 (B), compound 16 (C) and compound 17 (D). Hydrogen bonds are represented as red dotted lines.

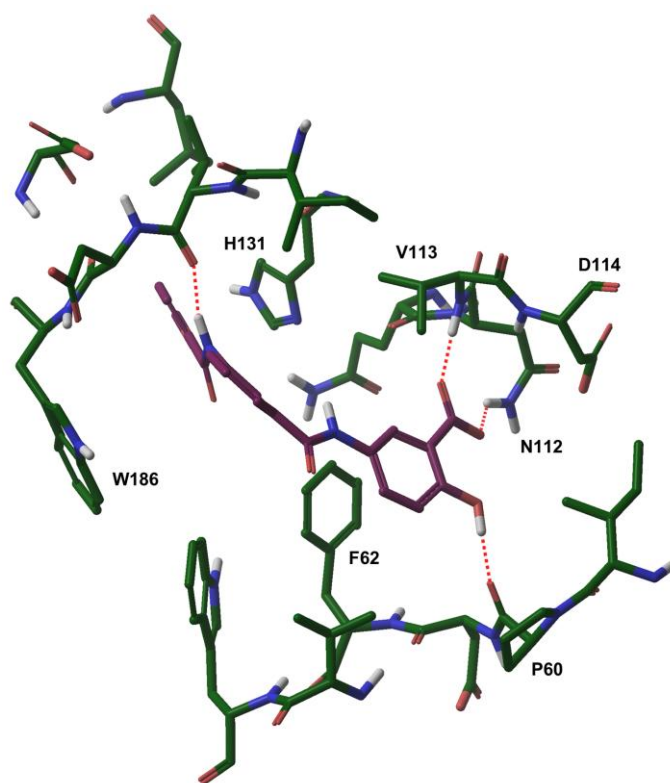


Figure 7.2. Alternative predicted binding modes of compound 9 in its deprotonated state.

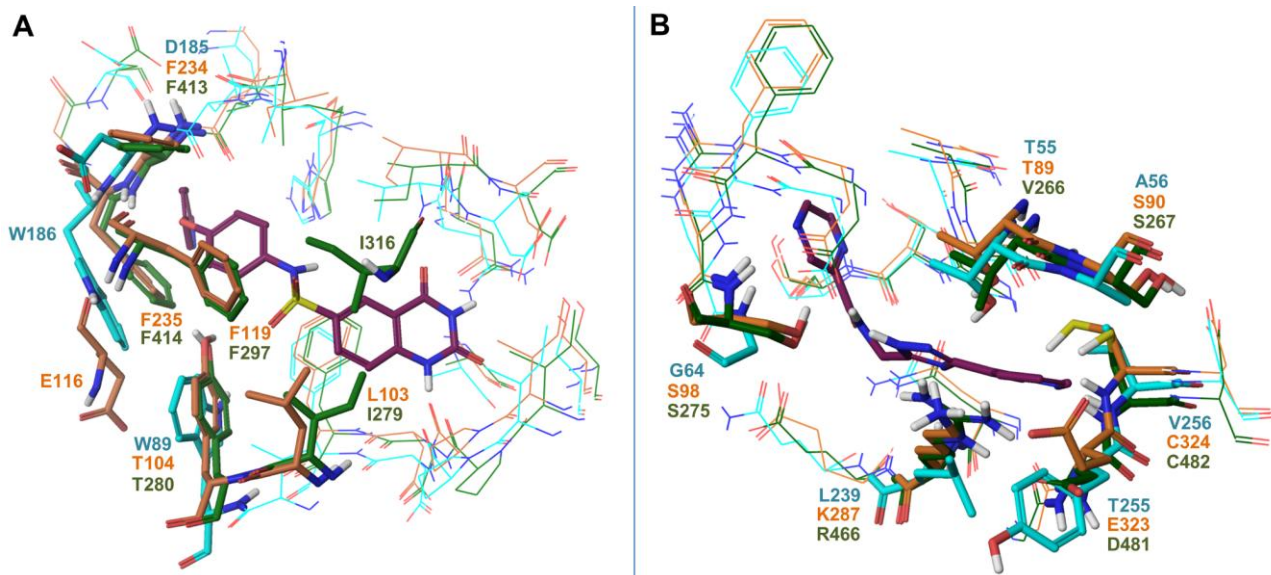


Figure 7.3. Superposition of binding sites of SIRT6 (cyan), SIRT1 (green), SIRT2 (orange) and the predicted binding mode of two reference compounds (maroon). Different residues among sirtuin structures are drawn in thick tube and labelled using the same colour coding. A) Superposition of the nicotinamide binding pocket and the predicted binding mode of compound 5. B) Superposition of the adenine binding pocket and the predicted binding mode of compound 16.

7.3 Biological characterization of the identified SIRT6 inhibitors

5, 9, and 17 were selected for further biological evaluations while 16 was excluded due to its low potency and specificity. In particular, experiments were performed to determine whether 5, 9, and 17 are active in intact cells and whether they achieve the biological effects that are predicted to occur as a result of SIRT6 inhibition. The acetylation status of H3K9, a known target of SIRT6 deacetylase activity²⁷⁹ was used as the initial reading frame to monitor the activity of the SIRT6 inhibitors in human cells (BxPC-3, pancreatic adenocarcinoma). Figure 7.4A shows a time course experiment in which H3K9 acetylation in response to 9 (100 μ M) was monitored over time, while the quantification of similar experiments performed with 5 and 17, in addition to 9, is shown in Figure 7.4B. The results demonstrate that all of the three identified SIRT6 inhibitors increased H3K9 acetylation, suggesting that they all are cell permeable and active in cultured cells. Notably, in response to all compounds, H3K9 acetylation appeared to peak at 18h of exposure and to decline afterward, suggesting that complex mechanisms may intervene in regulating H3K9 acetylation in response to sustained SIRT6 inhibition.

Subsequently, we focused on the ability of the identified SIRT6 inhibitors to increase glucose uptake in cultured cells and to reduce TNF- α secretion, two effects that have both been detected in SIRT6-deficient cells^{174,266,267,269,273}. Indeed, 5, 9 and 17 effectively increased the uptake of radioactive glucose in BxPC-3 cells (Table 7.3).

By comparison, specific down-regulation of SIRT6 expression by RNA interference determined an approximately 3-fold increase in glucose uptake. A similar enhancement in glucose uptake was also observed with 5, 9 and 17 in L6 rat myoblasts (Table 7.3). To gain insight into the mechanism through which SIRT6 inhibition increases glucose uptake in cultured cells, we monitored the levels of the glucose transporter GLUT-1 in BxPC-3 cells given previous evidence that SIRT6 represses GLUT-1 expression by opposing HIF1 α -dependent transcription and that SIRT6 deletion leads to increased GLUT-1 levels²⁶⁷. A strong increase in GLUT-1 expression in response to both 5 and 9 was detected in total cell lysates by Western blotting (Figure 7.5 A, B). Similar results were obtained with 17 which, in time course experiments, demonstrated to substantially increase GLUT-1 expression in BxPC-3 cells starting from 6h of exposure (Figure 7.5 C). Finally, upregulated GLUT-1 expression at the cell surface in cell treated with 5 or 9 could be documented by flow cytometry (Figure 7.5 D, E).

Finally, we also evaluated whether 5, 9 and 17 would prevent TNF- α secretion by cultured BxPC-3 cells stimulated with phorbol myristate acetate (PMA), as predicted based on the reported role of SIRT6 in TNF- α production^{271,273,274} and on previous data from our own laboratories on the effect of SIRT6 silencing in this cell line²⁶⁹. Indeed, all of the three SIRT6 inhibitors effectively reduced PMA-induced TNF- α secretion (Table 7.3). Overall, these results indicate that the SIRT6 inhibitors identified in this study have the potential to recreate the biological effects that are commonly observed in response to SIRT6 ablation or silencing.

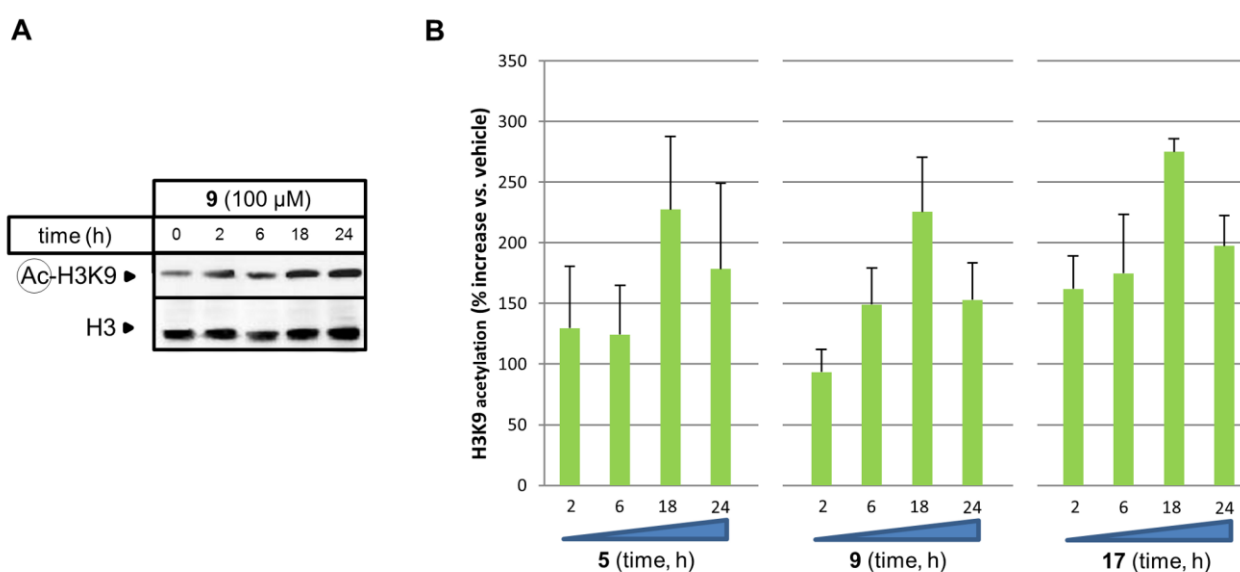


Figure 7.4. Compounds 5, 9, and 17 increase H3K9 acetylation in cultured cells. 4×10^5 BxPC3 cells were plated in 6-well plates and allowed to adhere for 24h. Thereafter, cells were stimulated with $100 \mu\text{M}$ 5 (B), 9 (A, B), or 17 (B) or the respective amounts of vehicle DMSO for the indicated time amounts. Finally, cells were used for protein lysate generation and total H3 and acetylated H3K9 levels were detected by immunoblotting. In B, the levels of acetylated H3K9 were quantified, normalized to total H3 levels, and expressed as percentage increase vs. vehicle-treated cells.

Compound ID	Glucose Uptake		TNF- α release
	BXPC3 cells (rel to NT)	L6 cells (rel to NT)	% Inhibition on BXPC3 cells
5	1.30 ± 0.21	1.98 ± 0.23	73 ± 10
9	1.11 ± 0.08	1.20 ± 0.12	50 ± 16
17	3.09 ± 0.49	1.55 ± 0.19	53 ± 13

Table 7.3. Evaluation of biological effects of the identified SIRT6 inhibitors.

Despite the emerging pathophysiological role of SIRT6 in human disease and its potential as a therapeutic target²⁶⁶, few SIRT6 modulators have been identified so far. Yasuda et al.²⁸⁰ identified the fenugreek seed extract as able to inhibit SIRT6 deacetylase activity, but, aside for quercetin and vitexin that are known promiscuous sirtuin modulators³, the specific component responsible for this biological activity was not clarified. A set of five small molecules that exert a partial inhibitory activity on SIRT6 (approximately by 25% at 100 μ M) was reported by Schliker et al.²⁴⁰. However, these compounds were classified as semi-specific and were not further investigated. More recently, a series of peptides and pseudopeptides was reported as SIRT6 inhibitors, with the most potent compound exhibiting an IC_{50} in the micromolar range, but showing no selectivity for SIRT6 versus SIRT1 and SIRT2²⁸¹. Our study represents an important advancement in this research area since it reports for the first time a number of active, structurally diverse, non-peptide, selective SIRT6 inhibitors. The most active compounds (5, 9 and 17) are able to inhibit SIRT6 deacetylase activity in the micromolar range, as expected for not yet optimized compounds and consistently with the typical results of an *in silico* screening²⁸². The SIRT6/SIRT1 selectivity ratio for two of these compounds (9 and 17) is also remarkable, showing a SIRT6 activity respectively 17 and 19 fold higher than SIRT1 activity (Table 7.2). Since no previous knowledge on specific SIRT6 inhibitors was available, our selection was based on the conformations of the reaction cofactor, of the substrate, and/or of product of this enzyme. As a consequence, many of the compounds selected from the virtual screening are characterized by the presence of small saturated nitrogen rings, such as uracil or hydantoin groups. These are able to form a hydrogen bond network in the active site similar to the one formed by the natural product/inhibitor NAM, but in some cases unable to reproduce the aromatic interactions (see for example compounds 1-3). All of these compounds, with the exception of compound 5, showed no activity on SIRT6, demonstrating that this chemical feature alone is not sufficient to improve potency on SIRT6. On the contrary, quinazoline or salicylate derivatives (compounds 5 and 9) both reproduce NAM interactions, but also show extra features, such as a partial filling of the substrate and cofactor binding pockets, and lead to a marked SIRT6 inhibition. The other two active compounds, 16 and 17, are both predicted by docking software to bind mainly the adenine binding pocket, suggesting a possible binding competition with NAD. However, these molecules also show chemical features that are similar to NAM, such as the pyrazine-2-carboxamido group in compound 16 and the succinimidobenzoate group in compound 17. Therefore their ability to bind the NAM binding pocket should be also considered. Certainly, complementing *in silico* data with information that could be obtained with crystallographic complexes and/or extensive structure-activity relationship studies, will contribute to better explain

the fine mechanism underlying SIRT6 inhibition by these small molecules. From a biological point of view, it is worth to emphasize that compound 5, 9, and 17 were all able to reduce TNF- α secretion as would be expected based on the current knowledge on the role of SIRT6 in TNF- α production^{269,271,273,274}. Thus, it is conceivable that such compounds could find potential application in the treatment of inflammatory conditions in which TNF- α secretion plays an important pathophysiological role, such as arthritis or Crohn disease. In addition, a strong increase in GLUT-1 expression that was accompanied by a consistent increase in glucose uptake was also observed in cultured cells treated with these compounds. This data is in line with the observation of high GLUT-1 levels in the muscle and of increased tissue glucose uptake and consequent hypoglycemia in SIRT6^{-/-} mice^{267,283}. These properties make the identified SIRT6 inhibitors, or derivatives of them, particularly appealing for their possible applications as blood glucose-lowering drugs. In particular, their ability to upregulate GLUT-1, which is not reliant on insulin for its expression²⁸⁴, could make them suitable for treating patients with insulin-resistant diabetes.

7.4 Conclusions

SIRT6 is emerging as a possible therapeutic target for a wide range of conditions, including diabetes, immune-mediated disorders and cancer^{230,266}. Nevertheless, no selective small-molecule SIRT6 inhibitor has been identified to date. In this study, we made use of in silico design approaches to identify novel and selective scaffolds that would bind and inhibit SIRT6 selectively. We report several drug-like compounds that show in vitro activities in the low micromolar range of concentration and have some degree of selectivity for SIRT6 versus other sirtuins. A structural analysis of the ligand binding modes suggests that the selectivity and potency of the identified chemical scaffolds are susceptible to be further improved. In conclusion, since the identified SIRT6 inhibitors show a favorable drug-likeness profile and their biological annotation has already revealed strong activity in cell line models, these compounds can be considered as highly promising leads for the development of future SIRT6-based therapeutics.

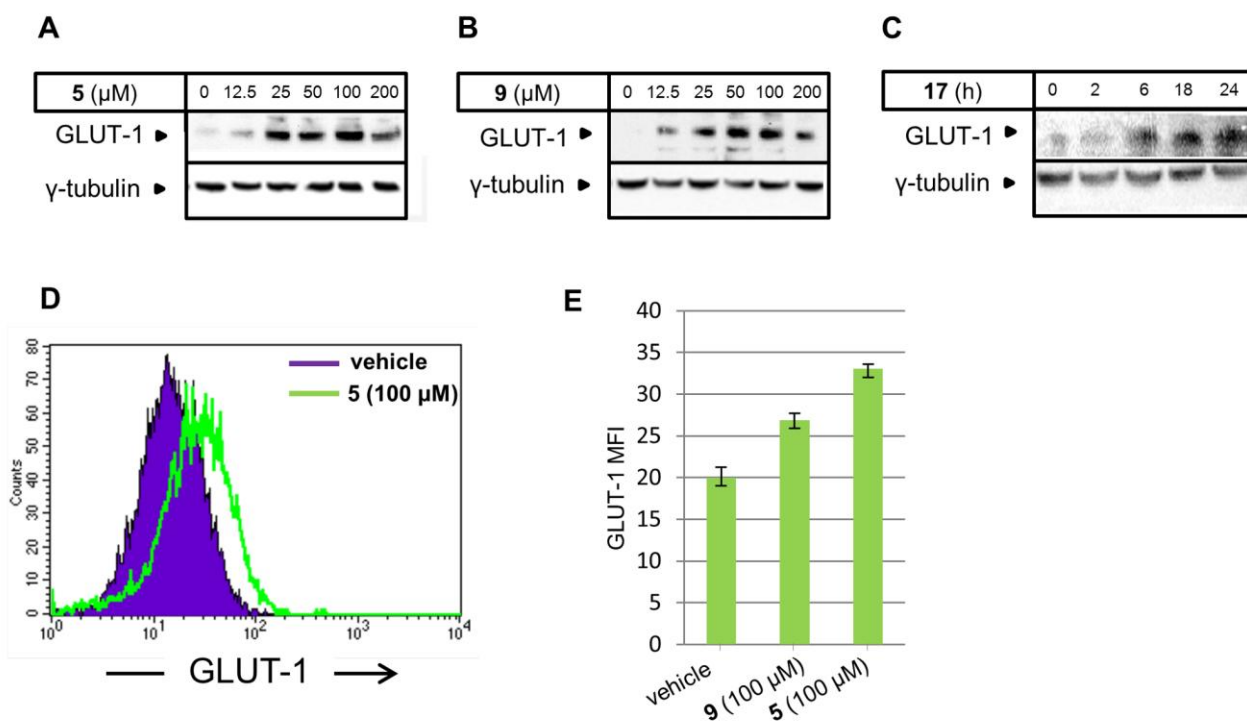


Figure 7.5. Compounds 5, 9, and 17 increase GLUT-1 expression in cultured cells. A, B, 4 x10⁵ BxPC-3 cells were plated in 6-well plates and allowed to adhere for 24h before being stimulated for 24h with 5 or 9 at the indicated concentrations. Thereafter, cells were used for protein lysate generation and subsequent detection of GLUT-1 and γ -tubulin by immunoblotting. C, BxPC-3 cells were plated as above and then stimulated for the indicated time amounts with 17 (200 μ M). Subsequently, cells were used for protein lysate preparation and GLUT-1 and γ -tubulin were revealed by immunoblotting. D, E, BxPC-3 cells were plated and treated with 100 μ M 5 or 9 as in A, B. After 24h of exposure to the compounds, cells were detached and GLUT-1 expression at the cell surface was detected by flow cytometry.

7.5 Experimental section

In silico techniques.

The crystal structure of the SIRT6 in complex with ADP-ribose was used as a template for virtual screening purposes (PDB id: 3K35). This structure was prepared with standard preparation procedures (protein preparation wizard) as included in the software package Maestro¹³⁴. In order to allow searching ligands that are able to target the NAM pocket, we corrected the partially occluded structure of the human SIRT6 by aligning it to the structure of the *Archeoglobus fulgidus* SIR2, which is co-crystallized with NAM (PDB id: 1YC2). The NAM molecule was merged in the template of human SIRT6 and the Phe62 residue was minimized to allow the binding of NAM in the C pocket. The final conformation of the Phe62 side chain was incorporated in the final template that was used for the docking grid generation. The docking software Glide¹³⁵ was used to perform a

high-throughput virtual screening experiment. A docking grid was obtained by centering a 25 Å box in the centroid of the ADP-ribose ligand, as present in the template crystallographic structure of the human SIRT6. Although many water molecules are present in the crystal structure, none of these seems to be involved in stable interactions with ligand- or NAD⁺-binding, therefore all waters were removed from the grid. Standard precision (SP) docking was used to perform a first round of virtual screening. The top 1500 molecules, sorted by Glide score, were further refined with the extra-precision (XP) docking. Docking results were ranked based on the Glide score and the first 500 hits were considered for visual inspection. Compounds were visualized by taking into account several structural and physico-chemical rules, such as the qualitative evaluation of ligand-protein interactions within the active site, probability of suggested protonation and tautomeric states, stereochemistry complexity, compound availability, chemical diversity, drug-likeness and synthetic accessibility. Finally, the active compounds were filtered for Pan Assay Interference Compounds (PAINS) using FAF-Drugs2^{285,286}.

Compound Sources. We screened in silico the Asinex subset of the CoCoCo databases. Selected molecules were purchased in milligram quantities from chemical vendor and ID are reported in Table 7.1. Purity of compounds was $\geq 95\%$, as declared by the chemical vendor.

Biological Assays (biochemical assays: Prof. Santina Bruzzone, University of Genova. Cellular and other functional assays: Prof. Alessio Nencioni, University of Genova)

Cell lines. BxPC-3 cell line (human pancreatic ductal adenocarcinoma) was purchased from ATCC (LGC Standards S.r.l., Milan, Italy) and maintained in RPMI1640 medium supplemented with 10 % FBS, 50 IU/ml penicillin and 50 µg/ml streptomycin (Lonza Milano S.r.l., Treviglio, Italy). BxPC-3 cells were transduced with the empty plasmid pRETROSUPER (pRS), or with a validated RNA-interference construct (sh2 SIRT6)²⁶⁹, and cultured as above. Rat L6 myoblasts were obtained from Prof. Beguinot (University of Napoli Federico II, Naples, Italy) and maintained in DMEM with 10% FBS, 100 IU/ml penicillin and 100 µg/ml streptomycin. Cells were maintained in a humidified 5% CO₂ atmosphere at 37°C.

In vitro assays and IC₅₀ determination. The identified molecules were tested as sirtuin inhibitors using commercial kits for SIRT6, SIRT1 and SIRT2 (Cayman, Ann Arbor, MI), following manufacturer's instructions. IC₅₀ values were determined using the same commercial kit assays. All compounds were solubilized at 50 mM concentration in DMSO. The concentrations of the compounds for IC₅₀ determination were in the range from 8 µM to 5 mM. IC₅₀ were determined

from the logarithmic non linear regression curves in GraphPad Prism (GraphPad Software, La Jolla, CA). Three independent IC₅₀ measurements were performed for each compound.

Immunoblotting. BxPC-3 cells (pancreatic ductal adenocarcinoma) were incubated for the indicated amounts of time with the specified compounds or with the corresponding amount of vehicle DMSO (the final concentration of DMSO that was added to the medium to test the effects of a compound at 100 µM concentration ranged between 2‰ and 6‰, depending on the compound). Thereafter, cells were lysed in lysis buffer (50 mM Tris-HCl, pH 7.5, 150 mM NaCl, 1% NP40 and protease inhibitor cocktail). Thirty µg of proteins were loaded on a 15% polyacrilamide gel and separated by SDS-PAGE. Proteins were subsequently transferred to polyvinyl difluoride (PVDF) membranes and the expression of total or modified proteins were detected using the following primary antibodies: anti-acetylated H3K9 (rabbit polyclonal, H9286, Sigma Aldrich), anti-histone H3 (rabbit polyclonal, 9715, Cell Signaling Technology), anti-GLUT-1 (mouse monoclonal, SPM498, Abcam). Following incubation with the appropriate secondary antibodies and ECL detection (GE Healthcare, Milano, Italy), band intensity was quantified with the ChemiDoc imaging system (Bio-Rad, Milan, Italy). H3K9 acetylation was normalized to total H3 levels and expressed as percentage of H3K9 acetylation vs. vehicle-treated cells.

Flow cytometric GLUT-1 detection. For flow cytometric detection of GLUT-1 expression at the cell surface, adherent cells were trypsinized and washed in cold PBS. 5 x 10⁵ cells were subsequently fixed for 10 min in 100% methanol at -20°C. Thereafter, cells were washed in cold PBS, resuspended in 100 µl cold culture medium and incubated with or without 2.5 µl anti-GLUT-1 antibody (SPM498, Abcam) for 30 min at 4°C. Subsequently, cells were washed in cold PBS and incubated in 100 µl cold culture medium with 10 µl anti-mouse IgG2a (a kind gift of Dr. Alessandro Poggi, IRCCS AOU San Martino IST, National Cancer Institute, Genoa, Italy) for 30 min at 4°C. Finally, cells were washed twice with cold PBS and analysed using a FACS Calibur (Becton Dickinson) by acquiring 10.000 events/sample.

TNF-α ELISA. BxPC-3 cells (3 × 10⁵ cells/well) were seeded in 6-well plates and allowed to adhere for 24 h. Thereafter, cells were incubated overnight with SIRT6 inhibitors (100 µM) or vehicle. Thereafter, to induce cytokine secretion, cells were stimulated for 24 h with PMA. Finally, supernatants were collected and assayed for TNF-α using commercially available DuoSet® ELISA kits (R&D Systems, Minneapolis, MN).

Glucose uptake assay with [¹⁴C]-2-deoxy-d- in BxPC-3 and L6 cells. BxPC-3, pRS and sh2 SIRT6 BxPC-3 and L6 cells (6x10⁵/well), seeded in 12-well plates, were treated in triplicate for 18 h with

or without the different compounds (200 μ M, final concentration), in complete medium. The cells were then washed twice with 1 ml of PBS buffer and glucose transport was measured by the addition of 0.5 mM d-glucose/[¹⁴C]-2-deoxy-d-glucose (0.5 μ Ci/well) in 0.4 ml KRH buffer (129 mM NaCl, 5 mM NaHCO₃, 4.8 mM KCl, 1.2 mM KH₂PO₄, 1 mM CaCl₂, 1.2 mM MgSO₄, 10 mM Hepes, 0.5% bovine serum albumin) for 5 min at 37°C. Glucose uptake was stopped by immediately removing the labeling mix and washing the cells 3 times with ice-cold PBS. Cells were then lysed with 0.1% sodium dodecyl sulfate (SDS), and each lysate was used for scintillation counting in a Beta-Counter LS 6500 (Beckman-Coulter, Krefeld, Germany). Unspecific uptake in the presence of 20 μ M cytochalasin B and 200 μ M phloretin was subtracted from each experimental value.

8. Optimization of SIRT6 inhibitors - Quinazolinodione derivatives

We have identified a series of novel and selective SIRT6 inhibitors with a favorable drug-likeness profile and strong activity in cell line models. Nevertheless, selectivity and potency of the identified chemical scaffolds are susceptible of further improvement (see chapter 6). In particular, a quinazolinodione derivative (Figure 8.1) was found to inhibit SIRT6 activity in the low micromolar range, but showed moderate SIRT6/SIRT1 selectivity (the IC_{50} value for SIRT6 was approximately three times lower compared to the IC_{50} for SIRT1), and close to no selectivity over SIRT2. The goal of the present study was to obtain a better understanding of the structure-activity relationship (SAR) of this promising hit compound identified in our previous work, to improve its potency and selectivity as a SIRT6 inhibitor and to assess the value of 1 and its analogs as chemosensitizers.

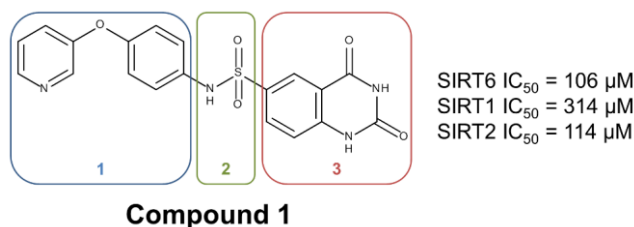


Figure 8.1. Chemical structure and activity data of the reference compound. The colored boxes indicate the parts of the molecule that were considered to identify interesting analogues.

8.1 Selection of analog candidates for biological testing

Using the chemical structure of compound 1 as a reference, and taking into account its predicted binding mode into the SIRT6 active site, as described in our previous study, we screened a collection of commercial compounds (the CoCoCo database)^{132,133} to identify analogues that could be easily purchased and tested, with the final goal to shed more light on the structure-activity relationship of this compound series. These derivatives were selected from the database using different substructure searches aimed to explore modifications on each fragment of the reference structure. Three main fragments were identified in the reference compound, the pyridine-3-yloxyphenyl moiety, a sulfonamide linker, and the quinazolinodione group (Figure 8.1, boxes 1, 2 and 3, respectively), and available modification of each fragment were independently searched for in the CoCoCo database. The starting list of approximately 450 analog compounds was then filtered by removing duplicates and by checking sample availability from compound providers, leading to a

final list of 88 compounds. The putative binding mode and the calculated binding score of these candidate molecules into the SIRT6 active site were predicted using molecular docking (see experimental section). Out of the thirteen representative compounds that were finally selected, seven presented variations of the pyridine-3-yloxyphenyl moiety (compounds 2-8 in Table 8.1), five presented variations of the quinazolinedione group (compounds 10-14 in Table 8.2), and one compound was chosen as it presented a variation of the sulfonamide linker (compound 9 in Table 8.1). To obtain independent assessments of the effect of these compounds on SIRT6 activity, two commercially available assays were utilized to determine the IC₅₀s of the identified thirteen compounds (Table 8.1, 8.2), namely a fluorescence-based and a luminescence-based assay, both of which are able to detect SIRT6 deacetylase activity. Assays were performed in the laboratory of Prof. Santina Bruzzone (University of Genova). Overall, an excellent agreement between the IC₅₀ values was obtained with the two methods and the use of the luminescence-based assay was of special value for those compounds that, having an intrinsic fluorescence, could not be assayed with the fluorescence-based kit.

Among the seven derivatives with the modified pyridine-3-yl-oxyphenyl moiety, five showed an improved activity on SIRT6 compared to 1, while two compounds showed a striking decrease of activity. The substitution of the oxyphenyl group with more hydrophobic substituents, such as benzyl (compound 8), ethylphenyl (compound 3) or even methylindole (compound 4) seemed to improve the compounds' inhibitory activity, while the replacement of the same group with a polar non-aromatic ring such as a pyrrolidine (compound 7) strongly reduced the inhibitory activity. The change in the substitution position from 3-yl to 4-yl (compounds 3) appeared to be almost irrelevant, with the exception of the introduction of a metamethylindole (compound 6), which caused a complete loss of activity. The substitution of sulfonamide linker with a sulfonate was tolerated (compound 9), indicating that the presence of a donor function is not essential to determine inhibitory activity. The methylation of the quinazolinedione group was also found not to be detrimental for the inhibitory activity, as demonstrated by compound 8. Finally, the replacement of the quinazolinedione group was found to be detrimental for SIRT6 inhibition in all cases with the exception of compound 10, whose activity was comparable to the reference compound. The results obtained in these SAR studies are only partially explained by the predicted binding mode of the tested molecules. In fact, compound 2 and compound 6 both show a predicted binding mode that is similar to the reference compound 1 (Figure 8.2A and 8.2B); both are predicted to bind the nicotinamide (NAM) binding pocket, also known as pocket C, and part of the substrate binding pocket. Both compounds maintain the extended hydrogen bond network with Val113, Asp114, and

Pro60, as well as the stacking interaction with Phe62, formed by the quinazolinedione group. The imidazole ring replaces the pyridine moiety of compound 1 forming interactions with His131 and with Trp186. Compound 6 also shows an additional hydrogen bond with the backbone carbonyl of Asp185. While the increase in activity reported for compound 2 compared to reference compound 1 can be explained by the better fit of methyl-imidazole moiety compared to oxy-pyridinyl group in the hydrophobic region comprised among His131 and Trp186, the remarkable drop in activity reported for compound 6 is apparently not attributable to its predicted binding mode since the substitution of the phenyl and of the *o*-oxy-pyridinyl moieties with a benzyl and a *m*-methylimidazole, respectively, seems to be perfectly tolerated, if not even preferred. Similarly, compound 7 is predicted to bind SIRT6 in a similar way compared to other active compounds in this series, also forming an additional hydrogen bond with Leu184 (Figure 8.2C), but shows a ten-fold reduction in terms of potency of SIRT6 inhibition compared to the reference compound, which wouldn't be explained by this predicted binding mode. The binding pose of compound 8 represents a particular paradigm in our binding hypothesis since it presents a double methylation of quinazolinedione group and therefore lacks two hydrogen-bond donor features that are considered to be key interactions in the proposed binding mode. In line with this model, the docking pose of 8 reveals an unfavorable binding in which the NAM pocket is occupied by the pyridine ring and the quinazolinedione group is directed towards the substrate binding pocket (Figure 8.2D). Despite these predictions, this molecule falls in the same activity range of the reference compound, indicating that other mechanisms or alternative/additional bindings may occur, underlying 8's ability to bind and inhibit SIRT6. Efforts aimed at identifying a more reliable binding model, such as the binding in adenine pocket or the presence of additional pockets, were unfortunately not useful to explain this behavior (data not shown).

Comp ID	R1	R2	R3	X	SIRT6 IC50 (μM) Fluorescence Assay	SIRT6 IC50 (μM) Luminescence Assay
1	-H	-H		NH	106±16	136±12
2	-H	-H		NH	60±4	ND
3	-H	-H		NH	37±2	55±4
4	-H	-H		NH	ND	82±4
5	-H	-H		NH	137±7	137±8
6	-H	-H		NH	ND	2872±546
7	-H	-H		NH	ND	517±77
8	-CH3	-CH3		NH	49±4	38±3
9	-H	-H		O	ND	127±14

Table 8.1. Structures and SIRT6 inhibition activities of compounds with modified pyridine-3-oxo-phenyl fragment or with modified linker. ND = not determined (interfering with the assay).

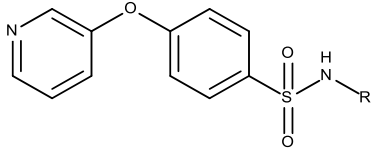
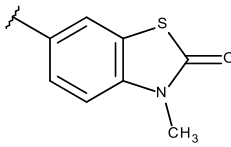
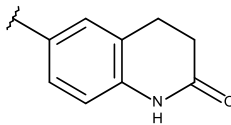
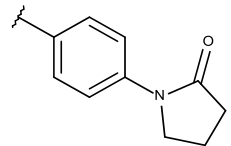
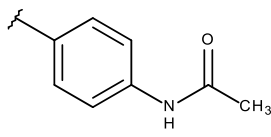
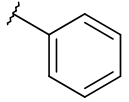
			
Compound ID	R	SIRT6 IC50 (μM) Fluorescence Assay	SIRT6 IC50 (μM) Luminescence Assay
10		77±14	102±10
11		270±47	275±7
12		441±23	ND
13		297±15	242±23
14		ND	300±9

Table 8.2. Structures and SIRT6 inhibition activities of compounds with modified quinazolidinedione fragment. ND = not determined (interfering with the assay).

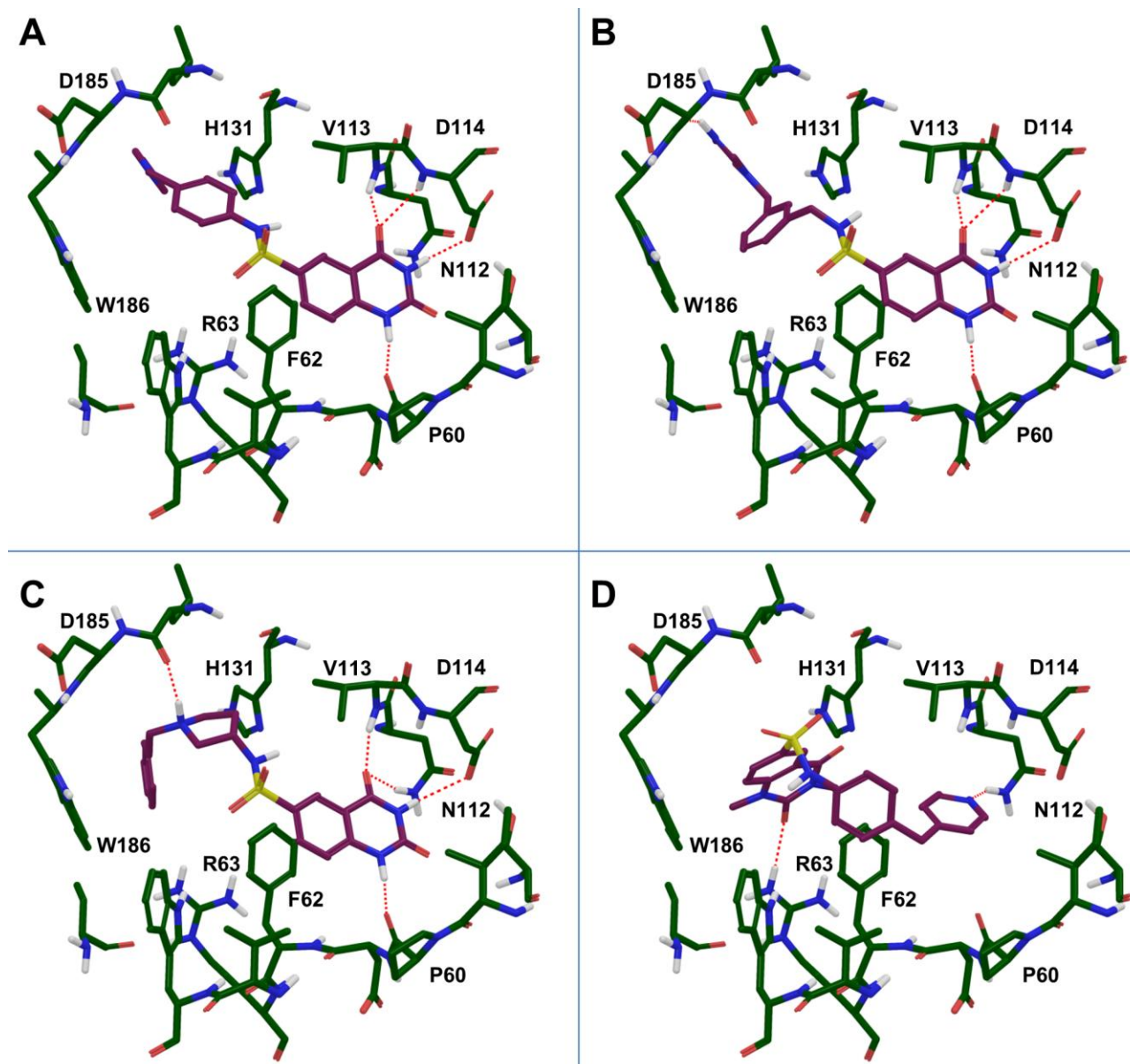


Figure 8.2. Putative binding mode of SIRT6 inhibitors derived from **1**. Predicted binding mode of compound **2** (A), compound **6** (B), compound **7** (C) and compound **8** (D). Hydrogen bonds are represented as red dotted lines.

8.2 Selectivity profiling

In order to evaluate the selectivity of the most interesting SIRT6 inhibitors of this series, their IC_{50} values for SIRT1 and SIRT2 were also determined using commercially available kits and compared to the results obtained with the reference compound **1**.

Compound **2** showed a SIRT6/SIRT1 selectivity ratio that was comparable to reference compound **1**, and a slightly better selectivity SIRT6 over SIRT2. Conversely, compounds **3** and **8** proved to be the most SIRT6/SIRT1 selective, their IC_{50} values being respectively almost 12 times and more

than 100 times higher for SIRT1, respectively, while showing a moderate SIRT6/SIRT2 selectivity. A distinctive feature of SIRT6 is the lack of the so-called cofactor binding loop, a structural element identified in previously solved sirtuin structures and which can adopt different conformations depending on the ligands bound in the active site²³⁰. In SIRT6, this element is replaced by an ordered helix that reduces the flexibility of the active site itself²⁴⁵, making its structure unique among sirtuins, which, in turn can be exploited for designing selective inhibitors, as demonstrated in our previous study²⁵⁹. This feature is likely to play a main role in explaining the selectivity of the reported compounds even if the predicted binding poses are still not sufficiently accurate to provide a conclusive structural explanation for each binding mode. For instance, the remarkable SIRT6/SIRT1 selectivity of compound **8** should be ascribed to the double methylation of quinazolidinedione fragment that is well tolerated in SIRT6 and in SIRT2 but clearly not permitted in SIRT1, suggesting the occurrence of different binding modes in each sirtuin isoform.

Compound ID	SIRT6	SIRT1	SIRT2	ratio SIRT1/SIRT6	ratio SIRT2/SIRT6
1	106±16	314±19	114±5	2.96	1.07
2	60±4	238±12	159±4	3.97	2.65
3	37±2	424±26	85±3	11.46	2.30
8	49±4	6521±130	242±16	133.08	4.94

Table 8.3. Determination of IC₅₀ (μM) on SIRT6, SIRT1 and SIRT2 for compounds 1, 2, 3 and 8 and of the selectivity ratios SIRT1 IC₅₀/SIRT6 IC₅₀ and SIRT2 IC₅₀/SIRT6 IC₅₀ for the same compounds

8.3 Mechanism for SIRT6 inhibition by quinazolidinediones

In order to better clarify the mechanism underlying SIRT6 inhibition by the reference compound **1** and by the compound **3**, which is the analog with the lowest IC₅₀, we evaluated the NAD⁺ saturation curves in enzymatic reactions utilizing recombinant SIRT6. We also explored the inhibition mechanism of compound **1** and **3** by varying the concentration of the substrate peptide, which contains an acetylated Lysine as a substrate for SIRT6 activity. As shown in Fig. 8.3A, V_{max} was not altered by the presence of compound **1**, indicating a competitive inhibition by this compound with respect to the coenzyme. The same holds true for compound **3** (Fig. 3B), which also appeared to competitively inhibit SIRT6 deacetylase activity. Similar results were obtained by varying the concentration of substrate peptide (Fig. 8.3C and 8.3D) since both compounds inhibited SIRT6 through competition with the peptide substrate. The results of these competition experiments are consistent with SIRT6 inhibition by compounds **1** and **3** occurring through their binding in the nicotinamide pocket and in the substrate pocket, in agreement with our previous hypothesis for compound **1**²⁵⁹.

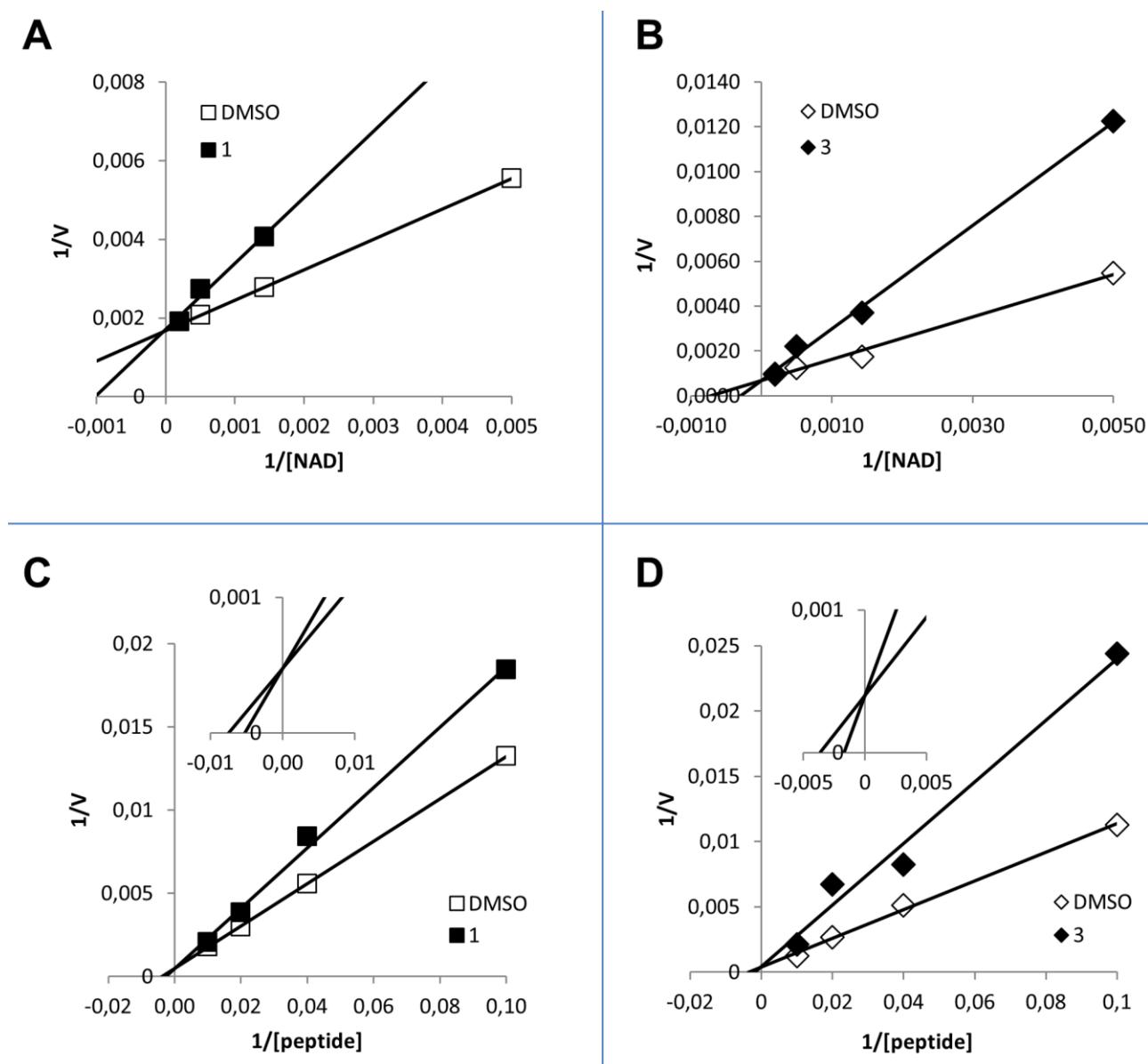


Figure 8.3. Mechanism of SIRT6 deacetylase activity inhibition by compounds **1** and **3**. NAD^+ (A and B) or peptide (C and D) saturation curves were generated incubating recombinant SIRT6 in the presence or absence of 50 μM compound **1** or **3**, and varying the concentrations of NAD^+ or of the peptide, respectively. Inset in panels C and D, magnification of line intersections. SIRT6 activity was determined using the chemiluminescent assay kit.

8.4 Biological evaluation of quinazolidione SIRT6 inhibitors

Having identified analogs that, as compared to the reference compound **1**, exhibited improved potency and specificity (compounds **2**, **3**, and **8**), we set out to determine whether they would also be active in mammalian cells, recreating the biological effects that are predicted to occur as a consequence of SIRT6 inhibition. In particular we aimed at confirming an increase in histone 3 lysine 9 (H3K9) acetylation, an increase in cellular glucose uptake, and a reduction in $TNF-\alpha$

production²⁶⁶. These assays were performed in the laboratory of Prof. Alessio Nencioni (Univ. Genova).

An increase in H3K9 acetylation in BxPC-3 cells (pancreatic ductal adenocarcinoma) could be observed with all of the three compounds, the strongest effect being achieved with compound **3**. A representative time course experiment evaluating acetylated H3K9 levels in cells treated with **3** is shown in Figure 4. Notably, similar to what observed with **1**, H3K9 acetylation peaked at 18 h of exposure and started decreasing afterward, suggesting the existence of feedback mechanisms regulating H3K9 acetylation in cells in response to sustained SIRT6 inhibition. Compounds **3** and **8** significantly increased the uptake of radiolabeled glucose in both BxPC-3 and L6 myoblasts (Table 8.4) and a similar enhancement in glucose uptake was also observed in L6 myoblasts by evaluating the uptake of a fluorescent glucose analog, 2-[N-(7-nitrobenz-2-oxa-1,3-diazol-4-yl)amino]-2-deoxy-D-glucose (2-NBDG), whereas no stimulation of glucose uptake by compound **2** could be detected. Compound **3** could not be tested with 2-NBDG, due to interference with the method (see Experimental Section). A strong inhibition of TNF- α production by **2** and **3** could be documented in BxPC-3 cells stimulated with PMA. Compounds **1**, **3** and **8** inhibited TNF- α production in human peripheral blood mononuclear cells (PBMC) stimulated with phytohemagglutinin (PHA) or with allogeneic antigen-presenting cells (in mixed leukocyte reaction, MLR) (Table 8.4). **2** only reduced TNF- α production by PBMC stimulated in MLR while its effect on PHA-stimulated TNF- α release did not reach statistical significance ($p=0.07$), possibly because of the high inter-donor variability.

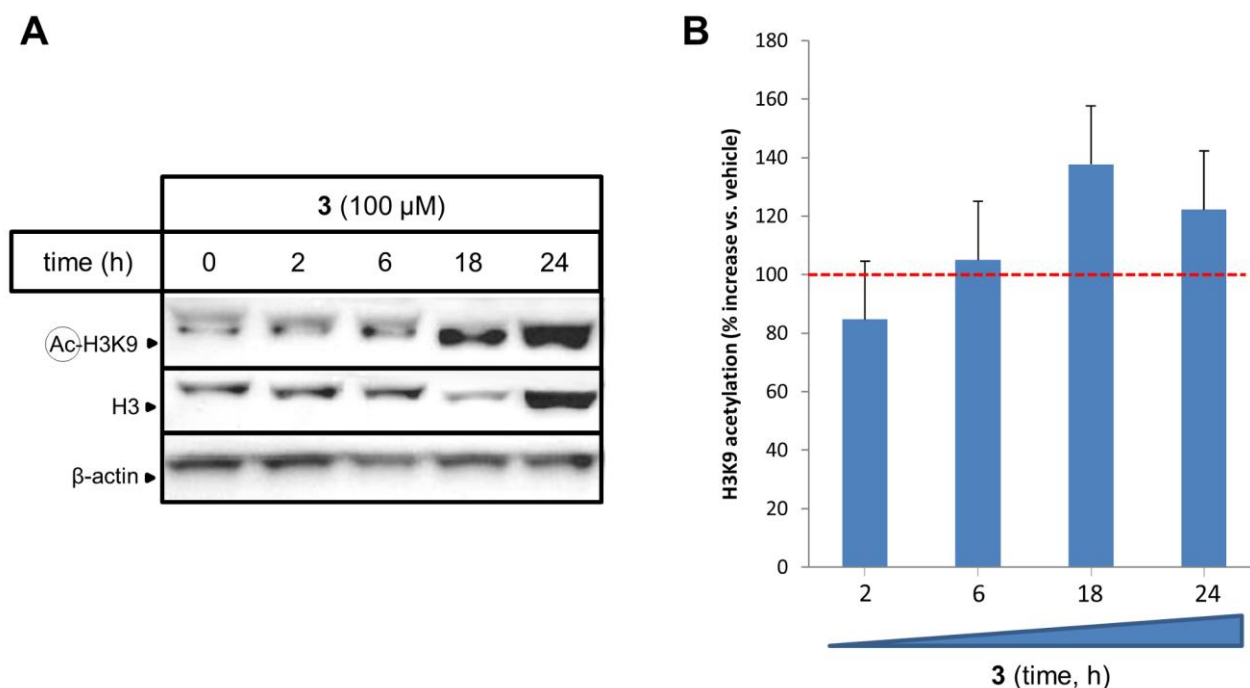


Figure 8.4. Compound 3 increases H3K9 acetylation in cultured cells. A, B. 2×10^5 BxPC-3 cells/well were seeded in 6-well plates, allowed to adhere overnight and subsequently stimulated with **3** for the indicated amounts of time. Thereafter, cells were used for cell lysate preparation and acetylated H3K9, total H3 and β -actin were detected by immunoblotting. Band intensities were quantified and acetylated H3K9 signals were normalized to those of the corresponding total H3 bands and, finally, to the corresponding intensities that were obtained with vehicle DMSO. A, one representative experiment out of three is presented. B, results are presented as means \pm SD of three separate experiments.

<i>Compound ID</i>	<i>H3K9 acetylation (normalized to control)</i>	<i>Radiolabelled glucose uptake in BxPC-3 cells (normalized to control)</i>	<i>Radiolabelled glucose uptake in L6 cells (normalized to control)</i>	<i>2-NBDG uptake in L6 cells (normalized to control)</i>	<i>% inhibition of TNF-α production in BxPC-3 cells</i>	<i>% inhibition of TNF-α production in human PBMC (PHA)</i>	<i>% inhibition of TNF-α production in human PBMC (MLR)</i>
1	2.2 \pm 0.5*	1.3 \pm 0.2*	2.0 \pm 0.3*	2.4 \pm 0.5*	73 \pm 10	52 \pm 37*	47 \pm 26*
2	1.5 \pm 0.2*	0.6 \pm 0.3	0.8 \pm 0.2	0.7 \pm 0.4	25 \pm 8	31 \pm 31 ^{n.s.}	21 \pm 16*
3	1.4 \pm 0.2*	1.2 \pm 0.2*	2.8 \pm 0.4*	I	72 \pm 18	44 \pm 28*	27 \pm 17*
8	1.6 \pm 0.3*	1.9 \pm 0.3*	4.0 \pm 0.4*	3.1 \pm 0.5*	ND	39 \pm 27*	30 \pm 19*

Table 8.4. Biological evaluation^a of quinazolinone SIRT6 inhibitors. I = interfering with the assay; ND = not determined. *, $p < 0.05$ compared to control, vehicle-treated cells; n.s., not statistically significant.

8.5 Quinazolinone inhibitors sensitize cancer cells to chemotherapeutics

SIRT6 deficient cells exhibit increased sensitivity to chemotherapeutics and to γ -irradiation^{272,287–289}. Thus, we decided to evaluate whether SIRT6 inhibitors would sensitize pancreatic cancer cells to a commonly administered chemotherapeutic, such as gemcitabine. To obtain the proof-of-concept that reduced SIRT6 activity could indeed be effective to this aim, we first exposed BxPC-3 cells in which SIRT6 had been silenced by RNA interference²⁶⁹ to titrated concentrations of the chemotherapeutic. As predicted, in SIRT6-silent BxPC-3, gemcitabine caused a more pronounced reduction in cell viability as compared to the control BxPC-3 (Figure 8.6A). Drawing from these experiments, we assessed the effect of **2** and **3** on the anticancer activity of gemcitabine in plain BxPC-3 cells. The two SIRT6 inhibitors were tested at concentrations that were close to their IC₅₀ (30 and 60 μ M) and, while essentially not affecting BxPC-3 cell growth as single agents, they caused a striking enhancement of gemcitabine activity when used in combination with this chemotherapeutic (Figure 8.5).

Within the DNA damage response, SIRT6 was shown to specifically cooperate with PARP1 in ensuring double strand break repair²⁷⁰. Thus, we reasoned that SIRT6 inhibitors could possibly achieve a potentiation of the activity of PARP inhibitors, such as olaparib, in cancer cells. The BRCA2-deficient pancreatic cancer cell line Capan-1 was chosen for these experiments since BRCA1/2 deficient tumors represent an important clinical indication for PARP inhibitors in oncology²⁹⁰. The proof-of-concept that SIRT6 inhibitors could indeed be effective to this end was first obtained by silencing SIRT6 in Capan-1 cells (Figure 8.6B) since SIRT6-silent Capan-1 did exhibit an increased sensitivity to olaparib as compared to the control cells, particularly for concentrations ranging between 0.5 and 4 μ M (Figure 8.6C). Drawing from these findings, we used confocal microscopy and flow cytometry to monitor DNA damage, as detected by γ H2AX staining, in Capan-1 treated with olaparib, SIRT6 inhibitors, and their combination. Both types of studies readily demonstrated that, even though single-agent olaparib, **1** or **3**, did induce some degree of DNA damage, the combination of olaparib with a SIRT6 inhibitor led to a much more pronounced γ H2AX expression (Figure 8.7A-C). These findings were paralleled by results of viability assays in which **1** and **3** were found to effectively increase olaparib's anticancer activity in Capan-1 cells (Figure 8.7C-D). A cooperative inhibition of Capan-1 cell viability was also obtained by combining SIRT6 inhibitors with NU1025, an unrelated PARP inhibitor (data not shown).

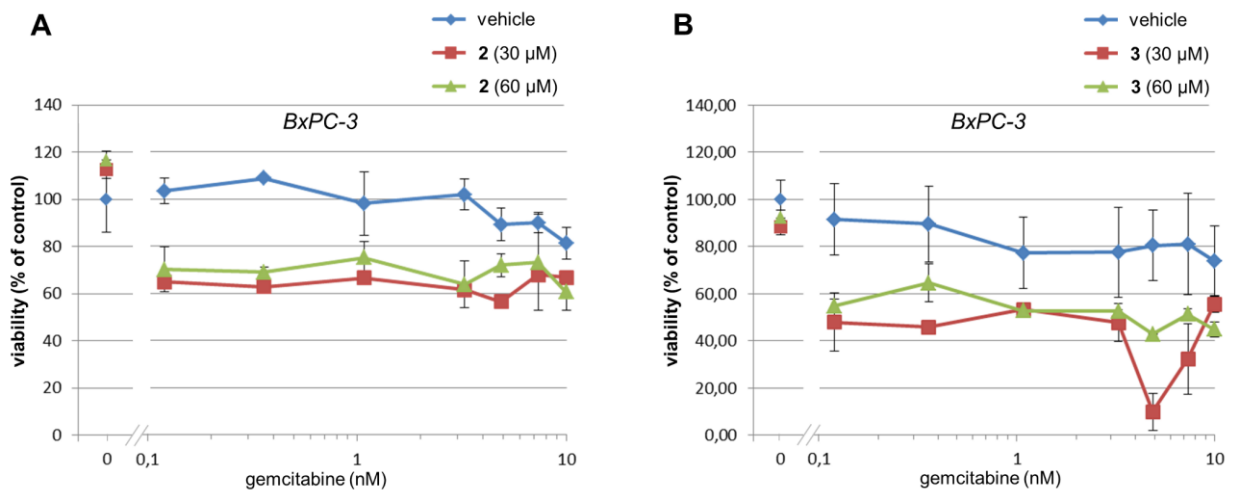


Figure 8.5. SIRT6 inhibitors sensitize pancreatic cancer cells to gemcitabine. A, B, 5×10^3 BxPC-3 cells/well were plated in 96-well plates, allowed to adhere overnight and subsequently incubated with **2** or **3** at the indicated concentrations or with vehicle DMSO (vehicle) for 2 h. Thereafter, cells were treated with or without the indicated concentrations of gemcitabine. 72 h later, cell viability was quantified utilizing CellTiter96 Aqueous1. Results are means \pm SD of three separate experiments. The lower inset of each panel presents the CIs that were calculated for each concentration of gemcitabine in combination with **2** or **3** at the indicated concentration.

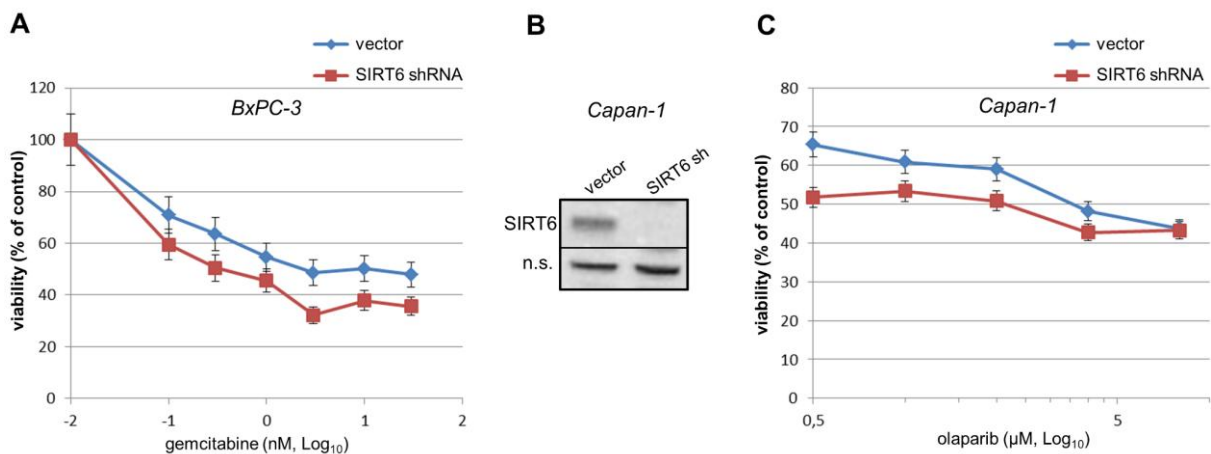


Figure 8.6. SIRT6 silencing sensitizes cancer cells to gemcitabine and to olaparib. 5×10^3 BxPC-3 that were either engineered to express an anti-SIRT6 shRNA (SIRT6 shRNA) or a control vector (vector) were plated in 96-well plates and allowed to adhere overnight. Thereafter, cells were treated with or without the indicated concentrations of gemcitabine. 72 h later, cell viability was quantified utilizing CellTiter96 Aqueous1. B, Capan-1 cells were transduced with a vector (pRS) expressing an anti-SIRT6 shRNA (SIRT6 shRNA) or with a control vector (pRS, vector). Successfully infected cells were selected with puromycin and used for protein lysate generation. SIRT6 levels were detected by immunoblotting while a non-specific immune band (n.s.i.b.) was used as a loading control. C, 10^3 Capan-1 cells that were either engineered to express an anti-SIRT6 shRNA (SIRT6 shRNA) or a control vector (vector) were plated in 96-well plates and allowed to adhere overnight. Thereafter, cells were treated with or without the indicated concentrations of olaparib. 7 days later, cell viability was quantified utilizing CellTiter96 Aqueous1. A, C, Results are means \pm SD of three separate experiments. B, One representative experiment out of three is presented. *:p<0.05; n.s.: not statistically significant.

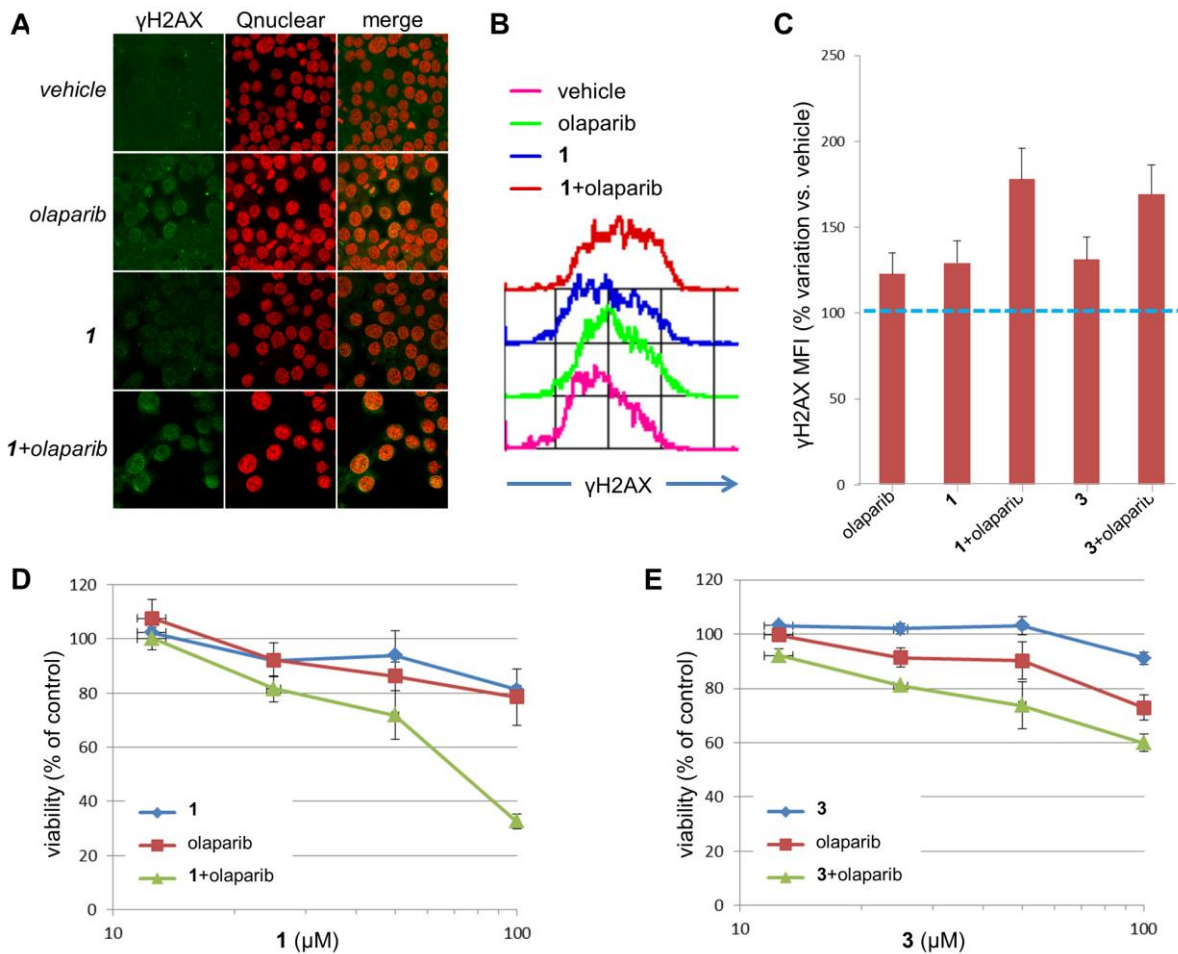


Figure 8.7. SIRT6 inhibitors cooperate with olaparib to induce DNA damage and cytotoxicity in BRCA2-deficient Capan-1 cells. A. γ H2AX levels, nuclei staining (Qnuclear), and their overlap were detected by confocal microscopy in Capan-1 cells treated with vehicle DMSO, **1**, olaparib, or the combination **1** + olaparib. B. γ H2AX levels in Capan-1 cells treated with vehicle DMSO, **1**, olaparib, or the combination **1** + olaparib were detected by flow cytometry. C. Mean fluorescence intensities (MFI) of γ H2AX staining in Capan-1 cells treated with vehicle DMSO, **1** (100 μ M), **3** (100 μ M), olaparib (8 μ M), or the combinations were normalized to the MFI measured in cells treated with vehicle DMSO and expressed as percentage variation vs. vehicle. D, E, 103 Capan-1 cells/well were plated in 96-well plates, allowed to adhere overnight and subsequently incubated in the presence of the concentrations of **1** or **3** indicated on the x axis or of vehicle DMSO. Olaparib was administered (or not) according to a 1:1 titration starting from 8 μ M, the latter concentration being the one that was combined to the highest concentration of **1** or **3**. Viability was detected 7 days later using CellTiter96 Aqueous1. Cooperative indexes (CI) for each drug combination are indicated within each panel. A, B, One representative experiment out of three is presented. C-E, results are means \pm SD of three separate experiments.

8.6 Conclusions

Here we reported on the identification of new derivatives of a quinazolinone SIRT6 inhibitor (**1**) with improved potency as compared to this reference compound. Three compounds have been identified (**2**, **3**, **8**) which exhibit an IC_{50} for SIRT6 of 60, 37 and 49 μ M, respectively, versus 106 μ M of compound **1**. Although further efforts are clearly still required to increase the potency of these sirtuin inhibitors, it should be noticed that these improvements were paralleled by concomitant progresses in terms of isoform selectivity. Indeed, weakly selective compounds such as **1** (SIRT2/SIRT6 IC_{50} ratio of 1.07) could result in major disadvantage when specific SIRT6 inhibition was to be sought for clinical uses. With the newly identified SIRT6 inhibitors a significant improvement in terms of selectivity profile has been achieved since compounds **2**, **3**, and **8** exhibit a SIRT2/SIRT6 IC_{50} ratio ranging between 2.3 (for **3**) and 4.9 (for **8**). Notably, the SIRT1/SIRT6 IC_{50} ratio has also been improved, since, starting from the 2.9 value of **1**, we were able to increase it to 3.9, 11.4, and 133 with compound **2**, **3**, and **8**, respectively.

A qualitative SAR was performed and allowed us to highlight some structural changes that appear to critically affect the activity of **1** and its derivatives, although a complete understanding of the SAR for this compound series is still unclear. An obvious explanation for the inability of our SAR studies to explain the activity of all of the analogs of **1** that were evaluated could be the ability of some of these compounds to exert their biological effects through different binding modes, even when small structural changes apply. Nevertheless, the competition experiments on the most active compounds clearly indicated the active site of the enzyme as the putative binding site, excluding the presence of allosteric inhibition. For a conclusive assessment of the fine mechanisms underlying SIRT6 inhibition by the identified compounds, particularly by those whose inhibitory activity would not be predicted based on the *in silico* model such as **8**, *in silico* data should be complemented with specific, corroborating experiments, such as site-directed mutagenesis or X-ray crystallography.

Extensive biological evaluations were undertaken to assess the ability of the newly identified SIRT6 inhibitors to produce the effects that would be expected as a consequence of SIRT6 inhibition. As previously described for **1**, **2**, **3**, and **8** all proved to be active in cultured cells as shown by increased acetylation of H3K9, a well-known target of SIRT6 deacetylase activity²⁷⁹. **3** and **8** successfully recreated the effects of SIRT6 knock-down and of treatment with **1** in that they increased glucose uptake in cultured cells^{259,267}. In addition, similar to **1**, **2**, **3**, and **8** all reduced TNF- α production by BxPC-3 cells, as well as by cultured human PBMC that were either stimulated with the mitogen

PHA or in mixed leukocyte reaction. Therefore, these findings are all consistent with the effects that SIRT6 inhibition is predicted to cause in cells and suggest possible applications of the identified compounds (or of derivative of them) as blood sugar lowering agents or as anti-inflammatories.

A specific focus of this study was to assess whether the identified SIRT6 inhibitors would be effective as enhancers of the activity of chemotherapeutics (i.e. gemcitabine) and of PARP inhibitors, as would be predicted based on the well-known roles of SIRT6 in DNA repair and on its emerging roles in carcinogenesis^{269,288,291–293}. **2** and **3** proved to be extremely active at potentiating the anti-proliferative activity of gemcitabine in BxPC-3 pancreatic cancer cells, while for **1** and **3** a striking potentiation of olaparib's activity could also be documented. These experiments represent the first proof-of-concept that small-molecule SIRT6 inhibitors can be used to sensitize tumor cells to commonly used anticancer agents and mandate further evaluations of these agents in *in vivo* tumor models and in combination with other cancer therapeutics.

8.7 Experimental section

In silico techniques.

Structure database management and substructure searches were conducted using Instant JChem from Chemaxon (ver. 5.11.5, 2012, <http://www.chemaxon.com>). The crystal structure of the SIRT6 in complex with ADP-ribose was used as a template for virtual screening purposes (PDB id: 3K35). This structure was prepared with standard preparation procedures (protein preparation wizard) as included in the software package Maestro (Version 9.3, Schrödinger, LLC, New York, NY, 2012). In order to allow searching ligands that are able to target the nicotinamide binding pocket, we corrected the partially occluded structure of the human SIRT6 using a special procedure previously reported²⁵⁹. The docking software Glide (Version 5.8, Schrödinger, LLC, New York, NY, 2012) was used to perform a high-throughput virtual screening experiment. A docking grid was obtained by centering a 25 Å box in the centroid of the ADP-ribose ligand, as present in the template crystallographic structure of the human SIRT6. Although many water molecules are present in the crystal structure, none of these seems to be involved in stable interactions with ligand- or NAD⁺-binding, therefore all waters were removed from the grid. Extra Precision (XP) docking was used to obtain a binding pose for each ligand.

Biological Assays (biochemical assays: Prof. Santina Bruzzone, University of Genova. Cellular and other functional assays: Prof. Alessio Nencioni, University of Genova)

Cell Lines. BxPC-3 and Capan-1 cells line were purchased from ATCC (LGC Standards S.r.l., Milan, Italy) and maintained in RPMI1640 medium supplemented with 10% FBS, 50 IU/mL penicillin and 50 µg/mL streptomycin (Lonza Milano S.r.l., Treviglio, Italy). Rat L6 myoblasts, obtained from Prof. Beguinot (University of Napoli Federico II, Naples, Italy), were cultured as previously described¹⁹. Cells were maintained in a humidified 5% CO₂ atm at 37°C.

In Vitro Assays and IC₅₀ Determination. The compounds were tested as sirtuin inhibitors with commercial kits: for SIRT6, SIRT1, and SIRT2, fluorescence-based assay kits (Cayman, Ann Arbor, MI) were used, following manufacturer's instructions; for SIRT6, a luminescence-based assay kit was used (Enzo Life Sciences, Vinci-Biochem, Vinci, Italy). For the luminescence-based kit, SIRT6 was recombinantly produced (see below). IC₅₀ values were determined using these commercial kit assays. All compounds were solubilized at 50 mM concentration in DMSO (except for compounds 2, 8 and 13 that were solubilized at 16 mM concentration in DMSO). The concentrations of the compounds for IC₅₀ determination were in the range from 4 µM to 1 mM. IC₅₀s were determined from the logarithmic nonlinear regression curves in GraphPad Prism (GraphPad Software, La Jolla, CA). Three independent IC₅₀ measurements were performed for each compound.

Determination of inhibition mechanism. NAD⁺ saturation curves were generated with recombinant SIRT6, in the presence or absence of compounds 1 or 3 (50 µM, final concentration) with increasing concentrations of NAD⁺ (ranging from 200 µM to 5 mM) and a constant peptide concentration (100 µM), or with increasing concentrations of peptide (ranging from 10 to 100 µM) and a constant NAD concentration (2 mM). SIRT6 activity was determined using the commercially available, chemiluminescent assay kit (Enzo Life Sciences).

Production of recombinant SIRT6. Human recombinant SIRT6 production was carried out as described by others²⁰, with a slight modification: SIRT6 purification was obtained with a His GraviTrap Talon® (GE Healthcare, Uppsala, Sweden).

Immunoblotting. Cells were lysed in lysis buffer (50 mM Tris-HCl, pH 7.5, 150 mM NaCl, 1% NP40, and protease inhibitor cocktail). Thirty microgram amounts of proteins were loaded on a 15% polyacrilamide gel and separated by SDS-PAGE. Proteins were subsequently transferred to polyvinyl difluoride (PVDF) membranes, and the expression of total or modified proteins was

detected using the following primary antibodies: anti-acetylated H3K9 (rabbit polyclonal, H9286, Sigma-Aldrich), anti-histone H3 (rabbit polyclonal, 9715, Cell Signaling Technology), anti-SIRT6 (S4197, Sigma-Aldrich), or anti- β -actin-HRP (sc-47778, Santa Cruz Biotechnology). Following incubation with the appropriate secondary antibodies and ECL detection (GE Healthcare, Milano, Italy), band intensity was quantified with the ChemiDoc imaging system (Bio-Rad, Milano, Italy). H3K9 acetylation was normalized to total H3 levels and expressed as percentage of H3K9 acetylation vs. vehicle-treated cells.

Glucose Uptake Assay with [¹⁴C]-2-Deoxy-D-glucose or with d-glucose analog 2-NBDG. Glucose uptake was evaluated as previously described¹⁴ in BxPC3 and L6 cells incubated for 18 h in the presence or absence of the different compounds (100 μ M, final concentration). In addition, glucose uptake in L6 cells was evaluated with a fluorescent d-glucose analog, 2-NBDG. L6 cells (2×10^6 /well) were seeded in 96-well plates, treated in triplicate for 18 h with or without the different compounds (200 μ M, final concentration), in complete medium. The cells were then washed twice with 0.2 ml of KRH buffer (129 mM NaCl, 5 mM NaHCO₃, 4.8 mM KCl, 1.2 mM KH₂PO₄, 1 mM CaCl₂, 1.2 mM MgSO₄, 10 mM HEPES, 0.5% bovine serum albumin) and glucose transport was measured by the addition of 200 μ M 2-NBDG in 50 μ l KRH buffer for 10 min at 37°C. Glucose uptake was stopped by removing the buffer and washing the cells twice with KRH buffer; 100 μ l of the same buffer were then added and fluorescence was evaluated with a fluorescence plate reader (Fluostar Optima, BMG Labtechnologies GmbH, Offenburg, Germany; excitation 485 nm, emission 520 nm). Unspecific uptake in the presence of 20 μ M cytochalasin B and 200 μ M phloretin was subtracted from each experimental value. In addition, autofluorescence of cells incubated or not with the different compounds was evaluated: compound 2 proved to increase cell autofluorescence by itself.

TNF- α ELISA. TNF- α levels in cell supernatants were measured by a commercially available ELISA kit (TNF- α DuoSet, R&D Systems) according to the manufacturer's instructions.

PBMC isolation and stimulation. Peripheral blood mononuclear cells (PBMC) were isolated from buffy coats of healthy blood donors (n=4) by density gradient centrifugation using Ficoll-Paque PLUS (density 1.077 g/ml; GE Healthcare, Uppsala, Sweden). PBMCs were cultured in round-bottomed 96-well plates (Nunc, Roskilde, Denmark) in RPMI-1640 medium supplemented with 10% fetal calf serum, glutamine and penicillin-streptomycin (Biochrom, Berlin, Germany) in a humidified atmosphere with 5% CO₂ at 37°C. 5×10^4 effector PBMC were either stimulated with 10 μ g/ml PHA for 3 days or with 5×10^4 γ -irradiated (40 Gy) allogeneic PBMC (mixed leukocyte

reaction, MLR) for 7 days. Thereafter, supernatants were harvested and TNF- α concentration was detected by commercially available ELISA. Cultures were set up in the presence of either 200 μ M 1, or 100 μ M 2, 3, or 8, or of vehicle DMSO (CTR). Cell viability, as measured by FACS-assessment of propidium iodide exclusion, was on average 84%, 71%, 81%, 85%, 82% for CTR, 1, 2, 3, and 8, respectively, in PHA-stimulated cells, and 71%, 57%, 70%, 73%, 74% for CTR, 1, 2, 3, and 8, respectively, in cells stimulated in MLR.

Viability assays. 5×10^3 cells/well were plated in 96 well plates. Following stimulation with the indicated stimuli, viability was detected at the indicated time points using CellTiter96 Aqueous1 (Promega) according to the manufacturer's instructions. The cooperative index (CI) was calculated as the sum of the specific cell deaths induced by the single agents divided by the specific cell death in response to the combination. CI values <1 , $= 1$ and >1 indicate a synergistic, additive or infra-additive effect respectively.

Retroviral transduction. Empty pRETROSUPER (pRS) was from Dr. Thijn Brummelkamp (Netherlands Cancer Institute, Amsterdam, The Netherlands), while pRS SIRT6 sh2 was a kind gift from Dr. Katrin F. Chua (Department of Medicine, Stanford University School of Medicine, Stanford, CA). 1.5×10^6 Phoenix cells were plated in 4 ml of medium in 6-cm dishes and allowed to adhere for 24 h. Thereafter, cells were transfected with 4 μ g of plasmid DNA using TransIT-293 (Mirus Bio, Madison, WI) according to the manufacturer's instructions. Viral supernatants were harvested after 36, 48, and 60 h and used to infect Capan-1 cells (5×10^5) in 10-cm dishes in the presence of 5 μ g/ml protamine sulfate. Successfully infected cells were selected using 1.5 μ g/ml puromycin.

Confocal microscopy. 3×10^4 Capan-1 cells were plated on glass coverslips (Thermo Scientific™ Nunc Lab-Tek II Chamber Slide System) and allowed to adhere overnight. Thereafter, cells were incubated for 24 h with 100 μ M 1 or vehicle DMSO. Subsequently, cells were treated with or without 8 μ M olaparib. 24 h later, cells were then fixed with 4% paraformaldehyde, washed, saturated and incubated with anti- γ H2AX primary antibody (Ser139, JBW301, Millipore) over night at 4°C. Nuclei were counterstained with Qnuclear™ Deep Red Stain (Life Technologies, Monza, Italy). After that, glass coverslip were mounted using Prolong Gold antifade reagent (Life Technologies Ltd, Paisley, UK). The images were collected using a three-channel TCS SP2 laser-scanning confocal microscope (Leica Microsystems, Wetzlar, Germany).

Flow cytometric γ H2AX detection. 10^5 Capan-1 cells/well were plated in 6-well plates, allowed to adhere overnight and subsequently treated with 100 μ M 1 or 3, or with vehicle DMSO for 24h.

Thereafter, cells were stimulated with or without 8 μ M olaparib for additional 24 h. Finally, cells were trypsinized and γ H2AX levels were detected with the FITC-conjugated anti- γ H2AX primary antibody according to the instructions of the manufacturer. The mean fluorescence intensity of each sample was normalized to the MFI of cells treated with vehicle DMSO and expressed as % variation versus vehicle.

9. Optimization of SIRT6 inhibitors – Salicylate derivatives

Using the same methodology reported for optimization of quinazolinedione derivatives, we tried to identify analogues of another scaffold identified as active in our previous study, with the same final goal to shed more light on the structure-activity relationship of this compound series. These derivatives were selected from a database of commercially available compounds (CoCoCo Database) using different substructure searches aimed to explore modifications on each fragment of the reference structure. A final list of 26 derivatives of reference compound were purchased from vendors and tested in vitro using a commercial kit exploiting SIRT6 NAD⁺-dependent deacetylase activity. The percentage of SIRT6 activity inhibition obtained with each compound at a 200 μ M concentration is reported in Table 8.1.

Among the 26 compounds tested, 17 led to a significant inhibition of SIRT6 deacetylase activity (>10%), ranging from 17 to 100%, thus giving a remarkable hit-rate obtained with the virtual screening protocol. Five compounds resulted inactive at the concentration used in the assay, while 4 compounds could not be tested due to interferences with the fluorescence-based assay. None of the active compounds identified include substructures described as Pan Assay Interference Compounds (PAINS)²⁷⁶. We subsequently determined the IC₅₀ values of the most active compounds (Table 7.2). Consistent with the results of the preliminary screening, five compounds were found to inhibit SIRT6 activity in the low micromolar range (3, 5, 9, 11 and 13); compounds 11 and 13 showed a remarkable increment of activity, resulting approx. four times more active than reference compound 1. In order to evaluate the selectivity of the most interesting inhibitors, their IC₅₀ values were also determined for SIRT1 and SIRT2 by using commercially available kits. Compounds 5, 11 and 13 proved to be fairly selective compounds towards SIRT6, their IC₅₀ values being more than 20 times higher for SIRT1 and for SIRT2 (Table 8.1).

Biological characterization of identified inhibitors is currently ongoing and will be completed in due course.

Compound ID	% Inhibition (200µM) KIT SIRT6	SIRT6 IC50 (µM)	SIRT1 IC50 (µM)	SIRT2 IC50 (µM)
1	62	89	1578	751
2	54			
3	89	122		
4	50			
5	100	34	783	453
6	44			
7	62			
8	70			
9	100	86		
10	17			
11	100	22	599	482
12	ND			
13	100	20	424	333
14	NI			
15	ND			
16	NI			
17	17			
18	ND			
19	5			
20	NI			
21	39			
22	NI			
23	54			
24	68			
25	18			
26	4			
27	ND			

Table 8.1. Structures and SIRT6, SIRT1 and SIRT2 inhibition activities of compounds selected with in silico techniques. NI = no inhibition and ND = not determined (interfering with the assay).

10. Interleukin 6 inhibitors

10.1 Biologic Functions of IL-6

Human IL-6 consists of 184 amino acids with two potential N-glycosylation sites and four cysteine residues; the core protein is about 20 kDa, and glycosylation accounts for the 21- to 26-kDa size of natural IL-6. In response to infections or tissue injuries caused by burns and traumas, IL-6 is promptly synthesized and activates an acute immune response (Figure 9.1). IL-6 induces the differentiation of activated B cells into immunoglobulin-producing plasma cells and acts as a growth factor for hybridoma and myeloma cells. In addition to B cells, IL-6 also affects T cells by inducing the specific differentiation of naive CD4⁺ T cells into effector T-cell subsets; in combination with TGF- β , IL-6 preferentially induces the differentiation of naive CD4⁺ T cells into Th17 cells, but inhibits the TGF- β -induced development of regulatory T cells (T-reg). The IL-6-induced dominance of Th17 cells over T-reg cells may account for the disruption of the immune tolerance that is involved in the development of autoimmune and inflammatory diseases. IL-6 stimulates hepatocytes to produce acute-phase proteins, such as C-reactive protein (CRP), serum amyloid A (SAA), fibrinogen, hepcidin, and α 1-antichymotrypsin, and it reduces the production of fibronectin, albumin, and transferrin²⁹⁴. IL-6 exerts other effects that are detected frequently in chronic inflammatory diseases. Bone marrow stromal cells produce IL-6 that stimulates the receptor activator of NF- κ B ligand (RANKL), which is essential for the differentiation and activation of osteoclasts, leading to bone resorption and osteoporosis. IL-6 also induces the production of VEGFs, resulting in angiogenesis and increased vascular permeability, which are pathologic features of cancers and of inflammatory lesions in the synovial tissues of rheumatoid arthritis. Moreover, it has been reported that IL-6 promotes keratinocyte proliferation and the synthesis of collagen in dermal fibroblasts and their differentiation into myofibroblasts, which may account for skin fibrosis in patients with systemic sclerosis. Mesangial cell proliferation and matrix overproduction are characteristic features of glomerular diseases, and IL-6 has been found in matrix deposits and may be involved in mesangial cell proliferation. Finally, IL-6 has been shown to interact with and affect various cells and organ systems, including the vascular endothelial cells, the endocrine system of the hypothalamic–pituitary–adrenal axis, and the neuropsychologic system.

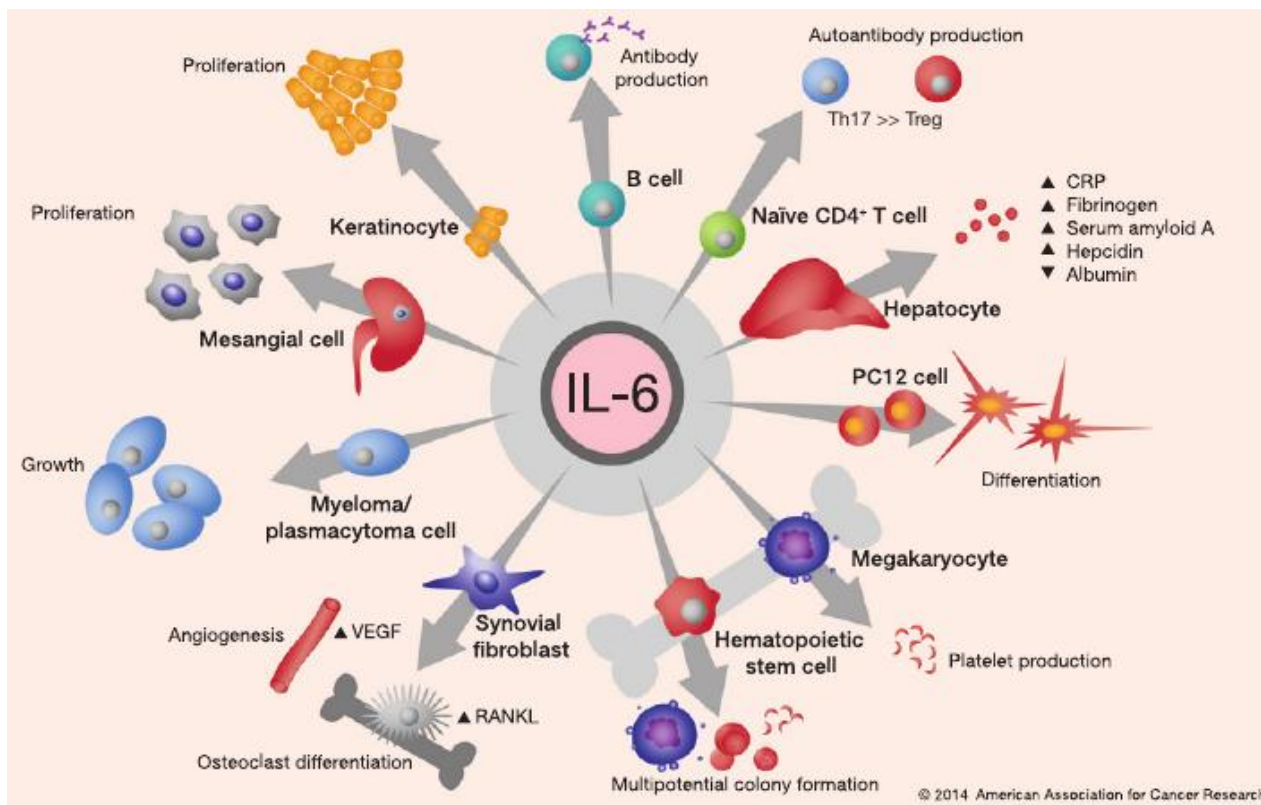


Figure 9.1. Pleiotropic activity of IL-6. Reproduced from Tanaka et al.²⁹⁵

10.2 IL-6 Signaling Pathway

The IL-6 receptor (IL-6R) exists in two forms, which are the membrane-bound and soluble forms. Signaling through membrane-bound IL-6R is called the classical or the cis-signaling pathway. The transmembrane IL-6R is an 80 kDa protein that contains the IL-6 binding site and a very short cytoplasmic domain. Its expression is restricted mainly to leukocytes and hepatocytes. After binding to IL-6, the complex IL-6/IL-6R recruits another transmembrane glycoprotein gp130, the signaling subunit of the functional IL-6R complex. In contrast to IL-6R, gp130 is ubiquitously expressed and is also the signaling subunit of other cytokine members in the IL-6 family. Through IL-6R and gp130, IL-6 signaling activates tyrosine kinases JAK1, JAK2, and TYK2, which leads to the phosphorylation of signal transducers and activators of transcriptions 1 and 3 (STAT1 and STAT3). The modulation and termination of this JAK/STAT3 pathway are regulated by the suppressor of cytokine signaling (SOCS) feedback inhibition and protein inhibitor of activated STAT (PIAS) proteins. In addition to the JAK–STAT3 pathway, IL-6 activates RAS–MAPK, and PI3K–AKT signaling pathways which also contribute to anti-apoptotic and tumorigenic function.

The presence of soluble IL-6R (sIL-6R) also allows IL-6 to function through a pathway known as trans-signaling²⁹⁶. The soluble IL-6R, is mainly produced by hepatocytes, neutrophils, macrophages, and some CD4⁺ T cells and forms a complex with IL-6 and interacts with cell surface gp130. The fully assembled, activated IL-6 receptor complex is a hexameric structure containing two of each IL-6, sIL-6R (or membrane-bound IL-6R), and gp130 molecules, and this complex activates signaling pathway in a broader range of cell types²⁹⁷. Both classical and trans-signaling are mediated by gp130, and both activate the identical intracellular pathway even if trans-signaling is considered as a potential danger signal because it enhances IL-6 responsiveness and inflammatory events. In normal cells, IL-6 production can be regulated by different signals including IL-1, tumor necrosis factor (TNF), interferons (IFNs), DNA viruses, RNA viruses, and bacterial endotoxin²⁹⁸. During acute inflammation, monocytes and macrophages are the main producers of IL-6 after activation of Toll-like receptors via a MyD88-dependent pathway, whereas T cells appear to be the major source of IL-6 during chronic inflammation.

10.3 IL-6 in aging and aging-related diseases

Inflammation is a physiological process that repairs tissues in response to endogenous or exogenous aggressions. Nevertheless, a chronic state of inflammation may have detrimental consequences. Aging is associated with increased levels of circulating cytokines and proinflammatory markers. Aged-related changes in the immune system, known as immunosenescence, and increased secretion of cytokines by adipose tissue, represent the major causes of chronic inflammation. This phenomenon is known as "inflamm-aging"²⁹⁹. IL-6 is called "a cytokine for gerontologists"³⁰⁰ because age is associated with its increased production, although changes in IL-6 levels reflected the inflammatory processes associated with aging, and not aging itself. The plasma levels of IL-6 are low or undetectable in most young people and start to increase in healthy people at about 50–60 years of age; this increase appears to be unexpectedly present in both persons who enjoyed successful aging and those who suffered pathological aging. This increase continues with age, until the extreme limit of human life, and high levels of IL-6 are found in a high percentage of centenarians in good shape. In sharp contrast, high levels of IL-6 have been referred to as the most powerful predictors of morbidity and mortality in the elderly^{301,302}.

Indeed, the increase in IL-6 with age is the consequence of the successful adaptation to a number of stresses, including infections, which unceasingly occur throughout life. This process occurs continuously, and in centenarians inflamm-aging eventually reaches levels very close to the threshold of morbidity and mortality, which indeed occur within months or a few years. Thus, the

beneficial effect of the defense system network (innate immunity, stress, and inflammation), devoted to the neutralization of dangerous/harmful agents early in life and in adulthood, turns out to be detrimental late in life, in a period largely not foreseen by evolution²⁹⁹.

IL-6 dysregulation is involved in age-related diseases such as cancer, lymphoma, cardiovascular disease, osteoporosis, Alzheimer's disease, diabetes, and atherosclerosis³⁰³.

10.4 IL-6 and cancer

IL-6 is one of the most ubiquitously deregulated cytokines in cancer, with over-expression of IL-6 observed in virtually every tumor that has been studied. Several investigators have reported an aberrant IL-6 pathway activation in a variety of human cancer cell lines and solid tumors, including epithelial tumors of ovary, breast and prostate as well as multiple myelomas, leukemias and lymphomas³⁰⁴. Preclinical and translational findings indicate that IL-6 plays an important role in diverse malignancies and provides a biologic rationale for targeted therapeutic investigations.

10.5 Pharmacological approaches to blockade of IL-6 signaling

In conventional therapy, a number of agents that inhibit the expression of IL-6 and its signaling are effective in treating IL-6-mediated disorders³⁰⁵. Corticosteroids may inhibit IL-6 production at the transcription level, and are routinely used in the treatment of chronic inflammatory and autoimmune diseases such as rheumatoid arthritis and lupus erythematosus. Nonsteroidal anti-inflammatory drugs (NSAIDs) are known immunoregulators, and may inhibit the expression of IL-6 and its activity while increasing the production of TNF- α , IFN- γ , IL-12, and IL-2. Based on the large number of studies conducted on biological activities of IL-6 and its pathological roles, targeted therapeutic strategies using IL-6 blockade by antibody drugs are in development for inflammatory and autoimmune diseases. Tocilizumab binds to the IL-6 binding site of membrane-bound human IL-6R and sIL-6R and neutralizes IL-6-mediated activities. The inhibition of the IL-6 pathway by tocilizumab is a clinical breakthrough in the treatment of rheumatoid arthritis and has been approved for RA in more than 90 countries worldwide.

Several small molecule compounds inhibiting IL-6 and its downstream targets have been developed and evaluated in preclinical and clinical studies of various human cancers, such as Atiprimod, a JAK2/JAK3 inhibitor, or Ruxolitinib, a JAK1/2 inhibitor; however, since STAT3 is not IL-6 specific as it is activated by all other cytokine signaling associated with gp130 and JAK1/2, these

drugs are not specific to inhibits IL-6 mediated effects. At the time of this study, no small molecule modulators of IL-6/IL-6R interaction have been reported in literature.

10.6 Drug repurposing

One approach to speeding up drug discovery is to find new uses for existing approved drugs. This is termed ‘drug repositioning’ or ‘drug repurposing’, and traditionally has occurred by serendipity³⁰⁶. Recently, repurposing of known drugs for new biological targets acquired popularity as a new medicinal chemistry paradigm. Indeed, finding new biological applications/therapies of existing drugs entails several advantages in respect to de novo design. The benefits of repositioning include the availability of chemical materials and previously generated data that can be used and presented to regulatory authorities and, as a result, the potential for a significantly more time- and cost-effective research and development effort than typically experienced when bringing a new drug to market. *In silico* methods, including target- and ligand-based strategies, are excellent complements to experimental techniques, and should be used alongside in vitro methods to drug repurposing, if for no other reason than to speed up the process of drug discovery at little additional cost.

10.7 Screening for IL6 – IL6 receptor interaction modulators

10.7.1 Screening of hexameric assembly IL-6/IL-6R/gp130 ligands

As a first approach we tried to identify small molecules able to bind potential interaction sites on the surface of the ternary complex formed by IL-6, IL-6R and gp130. The basic idea underlying this strategy is that the binding of an high affinity ligand may in fact lead to a destabilization of the complex of IL-6 with its receptor, and/or interfere with the binding of the ternary complex to effector proteins, and thus induce a reduced activation of the signaling pathway, and consequently of the biological effects of IL-6.

At the time of this study, only an X-ray structure of the complex between human IL-6, the extracellular binding domains of human IL-6 receptor, and the extracellular activation and binding domains of gp130 was available in public domain (PDB accession code 1P9M). The ternary complex forms a hexamer containing two IL-6, two IL-6R, and two gp130 that assemble sequentially and cooperatively. The hexamer is held together by 10 two-fold-related protein-protein interfaces, five of which are unique to each half of the hexamer, namely (according to Boulanger et al²⁹⁷) sites I, sites IIa and IIb, sites IIIa and IIIb.

The binding site I is localized between IL-6 and IL-6R and form the initial IL-6/IL-6R binary complex. IL-6R provides the majority of contact surface with IL-6, contributing more than 70% of the total buried surface area; of the 18 contact residues contributed by the IL-6R, PHE229 and PHE279 dominate the binding interface, and dock into two cavities on the IL-6 surface. Mutational data have identified Phe229 as a “hotspot” residue at the interface³⁰⁷. IL-6 also contributes several charge interactions within the site I interface surrounding the PHE229 residues, such as ARG179 and LYS171. The site II is separated into two spatially distinct interfaces: site IIa is located between the IL-6 A and C helical faces and the boundary between the D2 and D3 domains of gp130, and site IIb is located between the IL-6R D3 domain and the gp130 D3 domain. In site IIa, PHE169 contributes the largest fraction of the total buried surface area; this residue was originally identified as conserved in gp130, and as crucial for all cytokine interactions from mutational studies^{308,309}.

Site IIIa is a broad and discontinuous interface between IL-6 and gp130 where the tip of the IL-6 four-helix bundle (A/B loop and N-terminal region of D helix) abuts into the bottom sheet of the D1 domain of gp130. In site IIIb the tip of the gp130 D1 domain forms a large interaction surface with the side of the D2 domain of IL-6R. The critical residue in the site IIIa interface is TRP157 of IL-6 which has been defined by mutagenesis as being the critical aromatic site III signature residue^{310,311}.

The available model of the asymmetric unit (ternary complex IL-6/IL-6R/gp130) was obtained from PDB database and prepared using a standard protein preparation procedure (see experimental section); the 3D coordinates of the complete hexameric assembly, not available directly on PDB database, was obtained from PDBePISA service³¹² and prepared with the same procedure.

A systematic search using the software Sitemap was conducted on both the asymmetric unit and the hexameric assembly; the latter allowed finding potential active sites located also in the interfaces between the different asymmetric units.

From this search, we identified three putative sites (Figure 9.2):

- Site A: A long “tunnel” formed by the small cavity located at the intersection between the three subunit (Site I, Site IIIa, Site IIIb) and the cavity at the intersection of IL6-R and gp130 (Site IIb); although they are quite close, this two cavity could be considered two different sites (A1 and A2)
- Site B: A cavity between IL-6 and gp130, mainly on the surface of Site IIIa; adjacent to Site A, with small portion shared among the two sites

- Site C: A cavity at the interface between IL-6 and gp130, on the surface of Site IIa.

The active sites identified by sitemap was located near the interaction interfaces between the three subunits, and no other putative active sites seemed to be present on the external surface of the complex; the active site A was of special interest because located at the intersection of all the three subunits and included several interaction interfaces in its cavity. Due to its remarkable volume this site was split in two different sites to simplify the virtual screening procedure.

All the putative sites identified were used as template to virtually screen the Prestwick Chemical Library, as prepared in the CoCoCo database^{132,133}. This library contains 1200 small molecules that are 100% FDA approved drugs; the choice of this subset limits the chemical diversity compared to the whole CoCoCo database, which include more than 7M molecules, but entails the advantages of drug repurposing strategy (see above). The first hundred hits of each putative site were visually inspected to prioritize more interesting compounds; since no knowledge about active ligands was available, and physicochemical rules such as Lipinski's rule-of-five²⁷⁵ was not relevant since the screening is limited only to approved drugs, the selection was based on the quality of docking poses and on known pharmacological activities and side effects of screened drugs.

Unfortunately, this screening strategy was unsuccessful; the first positions of the docking output list, in which compounds are ranked based on estimated free energy of binding, are largely dominated by glycosidic compounds, which are highly hydrophilic and highly flexible molecules, such as aminoglycosides (neomycine, paromomycine), flavanone glycosides (hesperidin), and acarbose. This is probably due to the large number of charged residues which characterize the protein-protein interaction patches; the abundance of this kind of residues stabilize the binding between the three subunits, but also makes the hypothetical binding sites highly hydrophilic, and the scoring functions of docking software probably overestimate this contribution to the ligand binding affinity. At the same time, important hydrophobic pockets, which are certainly present on interaction surfaces, are not accessible by the potential ligands as they are in close contacts with the matching interaction surface on the nearby subunit. As a result, the docking software rewards only high hydrophilic molecules, adversely affecting the quality of screening results.

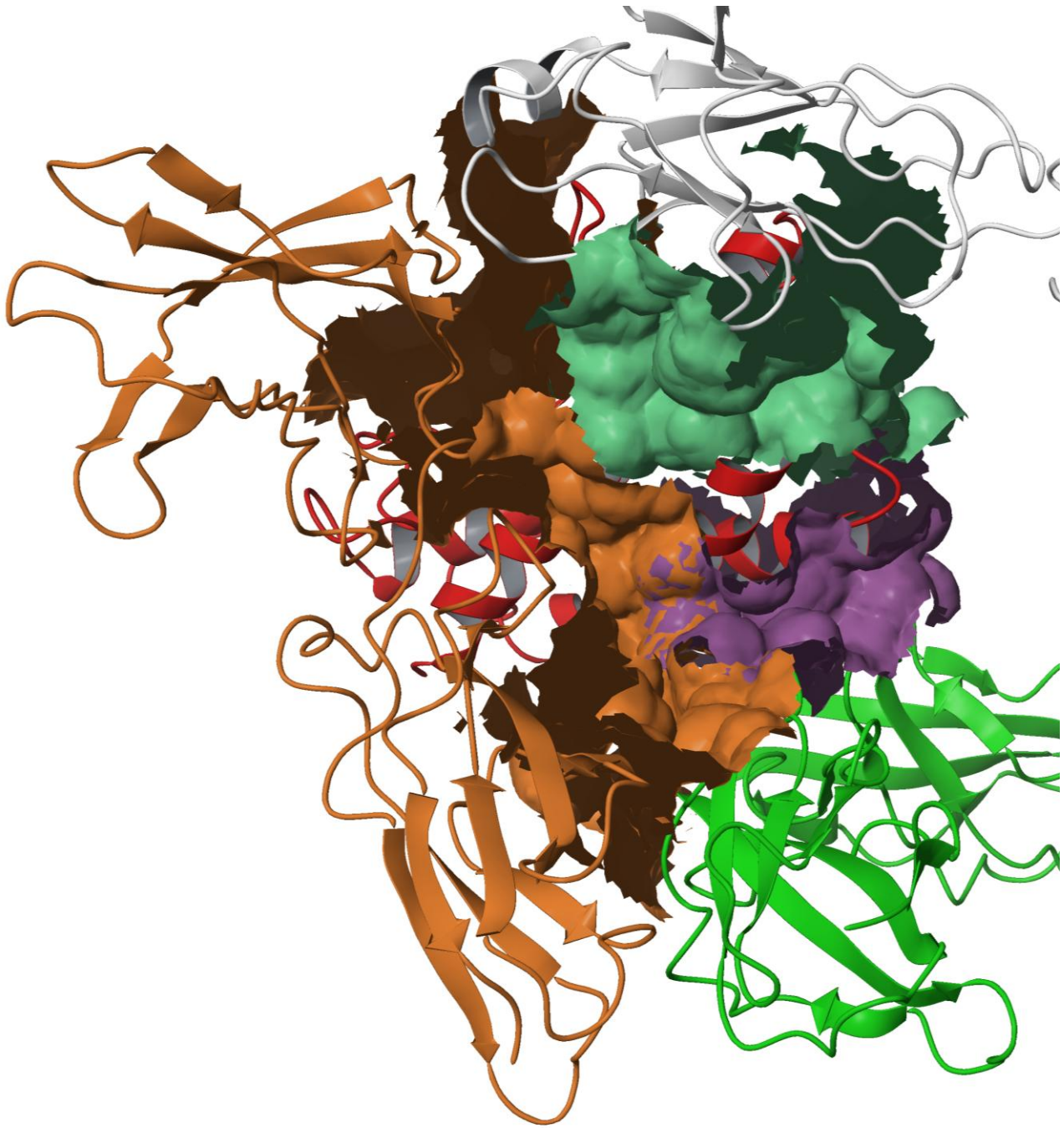


Figure 9.2. Putative binding sites identified on hexameric assembly of IL-6/IL-6R/gp130. Different subunits are represented using ribbons and labeled using different color: red for IL-6, orange for IL-6R, and green and gray for gp130 (2 symmetric subunits are observable). Putative sites are represented using colored surfaces: orange for Site A, purple for Site B and green for Site C.

10.7.2 Screening of Protein-Protein Interface inhibitors

Having regard to these unsatisfactory results, we tried a different screening strategy aimed to find potential inhibitors of ternary complex formation. The goal of this screening is to find some molecules able to bind the single interaction patches and therefore block the protein-protein interaction between the subunits. However, since the interaction patches are small and quite flat, and no defined cavity seems to be present, docking couldn't be the right method to use since it requires the presence of a putative active site to work properly. For this reason, we used a mixed structure-based and ligand-based approach based both on fragment docking search and on pharmacophore search. We implemented a method reported by Loving et al.³¹³ which use energetic analysis of structure-based fragment docking to elucidate key features for molecular recognition. This method requires three steps: i) docking of a focused library of diverse fragments, curated from the literature, as a set of probe molecules to find interaction sites; ii) mapping the energy terms computed by the docking scoring function onto individual ligand atoms to determine the most favorable pharmacophoric features for a given pose and generation of an energy-optimized pharmacophore; iii) pharmacophoric screening of ligand database. This approach combines strengths of both ligand- and structure-based methods; namely, energetic contributions to binding can be accurately computed from the structure-based docking, while the pharmacophore-based screening is fast and allows a great deal of control. Furthermore, there is no need for knowledge of known active compounds, as required in standard ligand-based methods.

The initial screening was conducted on site A as main target, since the interaction between IL-6 and IL-6R is the first interaction involved in the formation of the ternary complex, and it is needed for the interaction with gp130 (neither IL-6 nor IL-6R has affinity for gp130 alone)²⁹⁷, thus blocking of this interaction should impair the complex formation. The screening was based on the surface of IL-6 as reference, and centered using the position of phe299, residue known as one of the most important interaction residues from mutagenesis study (see above).

A 7-features pharmacophore was generated, including 1 aromatic ring, 2 hydrogen bond acceptor, 3 hydrogen bond donors and 1 negative charge (Figure 9.3A). A second pharmacophore was generated manually using as reference a selection of important residues of IL-6R that are likely to be responsible for binding to IL-6, considering both the three-dimensional structure and the mutagenesis data reported by Kalai et al.³⁰⁷. The selected IL6-R residues were: phe229, tyr230, arg231, glu277, glu278, and phe279. A 5-features hypothesis was generated, including 3 aromatic rings and 2 negative charges; the features was selected among all the available features considering

only the interactions clearly identified in the 3D structure and reported as important in the mutagenesis data (Figure 9.3B). A last 5-features hypothesis was generated by adding to the above hypothesis a negative charge feature that match the arg182 residue in IL-6 (Figure 9.3C). This residue show a high positive electrostatic potential due to the positive charge, and its side chain points toward the IL-6 surface, but no interactions with IL-6R residues are present; therefore we manually added an hypothetical negative feature able to account for the presence this IL-6 surface property. The excluded volume based on IL-6 receptor was added to all hypotheses, in order to simulate the surface of IL-6 interaction patch. All the generated hypothesis was used to search the multiconformer version of Prestwick database with the following restrictions:

- Pharmacophore 1 (fragment-based): hit molecules must match the aromatic ring and the negative charge features near phe279, and 1 feature among the remaining (total required matches: 3)
- Pharmacophore 2 (based IL6-R residues): hit molecules must match one of the two negative features and two out of the three aromatic features (total required matches: 3)
- Pharmacophore 3: (Pharmacophore 2 modified): hit molecules must match one of the three negative features and two out of the three aromatic features (total required matches: 3)

The hit molecules from each search was collected in a single list, and then subjected to energy minimization in the context of the IL-6 protein (see experimental section), in order to evaluate the stability of the ligand-protein interactions found by the pharmacophore search.

The final list of compound to buy was selected using the following parameters, in order of importance:

1. Quality of interactions between putative ligand and IL-6 surface
2. Stability of the complex after energy minimization
3. Minimum strain of binding conformation (flexible molecules were preferred against rigid molecules)
4. Molecular diversity

The final list of selected compound is reported in Table 9.1. The selected compounds exert their biological effect in physiological pathways not directly related to cytokine pathways. Interestingly, some of them are used in therapy as anti-inflammatory drugs, and methotrexate in particular is used in IL-6 related autoimmune disease including rheumatoid arthritis, although its exact mechanism of

action remains uncertain. The putative binding pose of zafirlukast, one of the most interesting compounds found in our screening, is reported in Figure 9.4.

10.8 Conclusion and perspective

It is challenging to design small molecules to disrupt multiple binding “hot spots” on the interface of protein–protein interaction. The approach to combine fragment docking and pharmacophore searches with drug repositioning could potentially help to design novel inhibitors targeting this kind of interactions.

During this study we analyzed the characteristics and properties of the surfaces of interaction between IL-6 and its receptor, and coded into a short series of pharmacophores that could be used to identify ligands capable of interacting specifically with the target protein. In the near future the selected compounds will be tested *in vitro* to measure the direct binding with IL-6 and the ability to reduce the pro-inflammatory effects of IL-6.

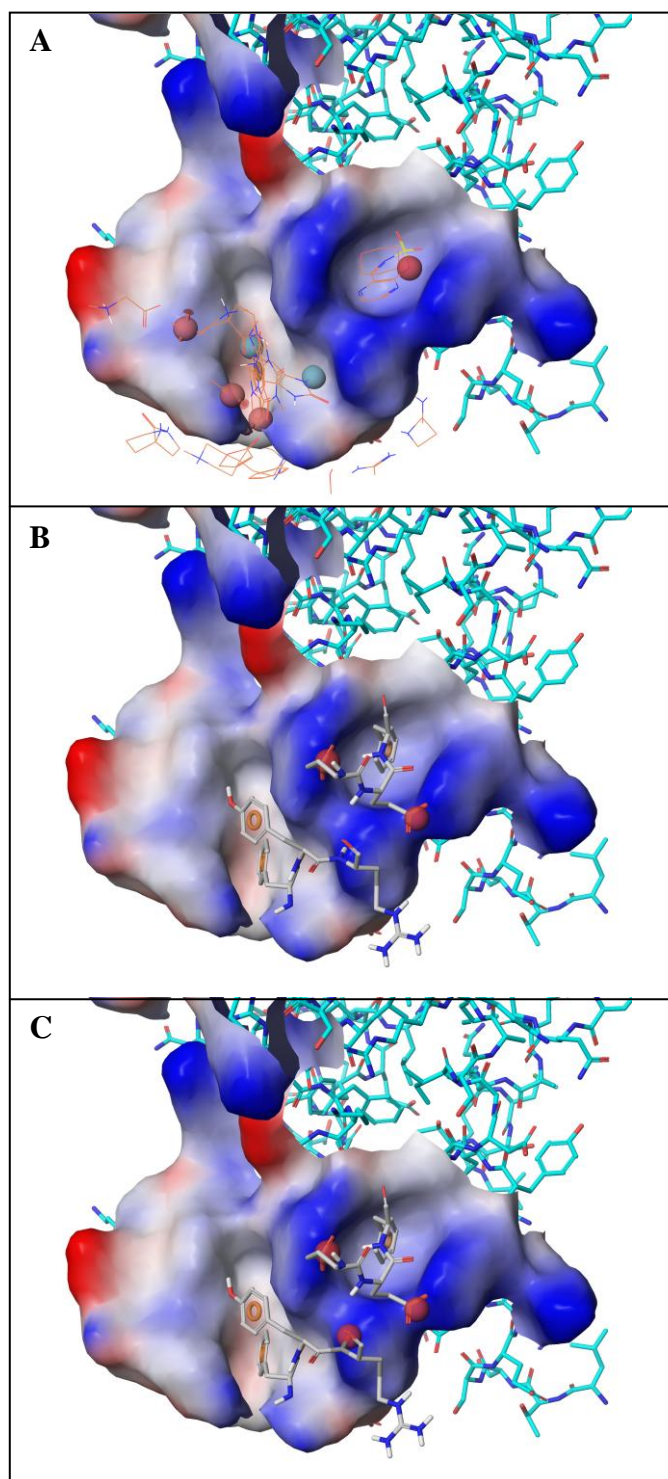


Figure 9.3. Pharmacophore used in virtual screening. Interaction patch of IL-6 with IL-6R is represented as a molecular surface colored according to electrostatic potential (blue = positive, red = negative, white = neutral). Pharmacophoric features are represented using colored balls (red for negative charges, blue for hydrogen bond donors and orange for hydrogen bond acceptors) and circles (aromatic rings). **A)** Pharmacophore 1, based on fragment-based docking; small molecular fragments are represented in orange. **B)** Pharmacophore 2, manually generated based on most important IL-6R residues, represented in gray. **C)** Pharmacophore 3, modified version of pharmacophore 2.

Prestwick ID	Chemical name	Pharmacological activity
Prestw-859	Fluvastatin sodium salt	HMG-CoA reductase inhibitor
Prestw-503	Cetirizine dihydrochloride	H1 receptor antagonist
Prestw-819	Moxalactam disodium salt	antibiotic (β-lactamic)
Prestw-658	Suxibuzone	NSAID
Prestw-1129	Benazepril HCl	ACE inhibitor
Prestw-1364	Zafirlukast	Leukotriene receptor antagonist
Prestw-135	Methotrexate	DHFR inhibitor

Table 9.1. Interesting compounds identified using virtual screening.

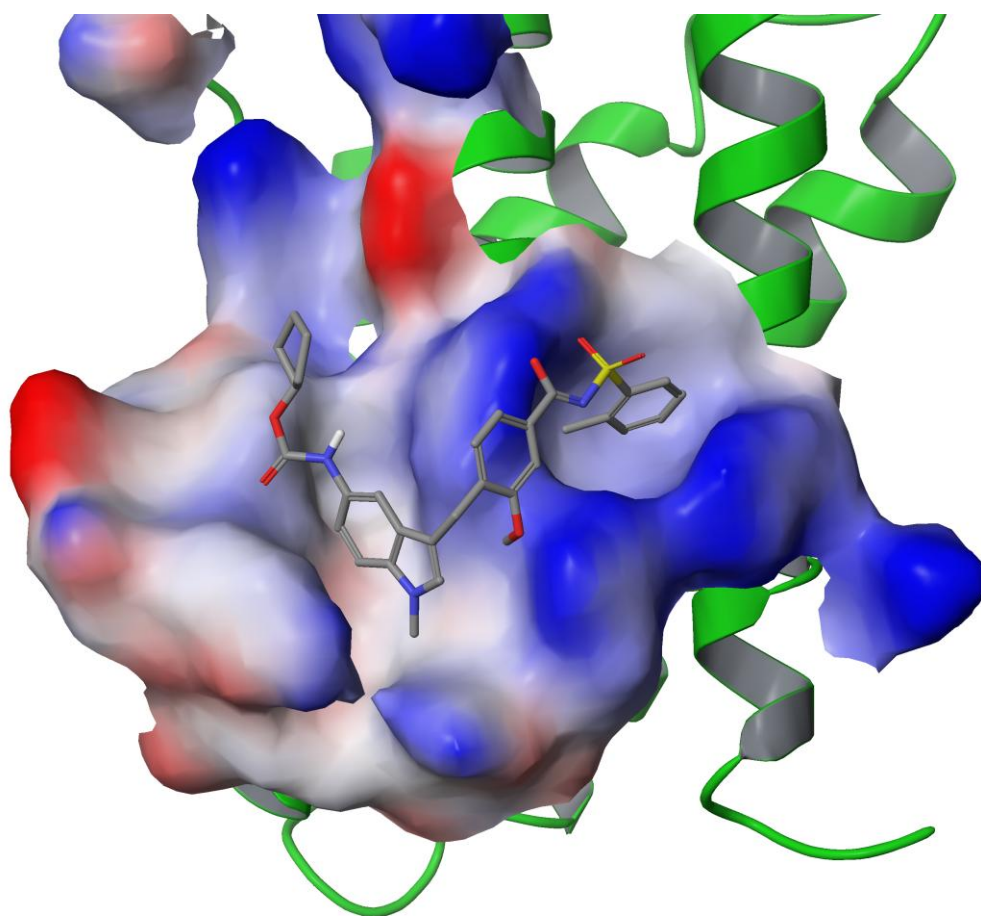


Figure 9.4. Putative binding mode of zafirlukast. Interaction patch of IL-6 with IL-6R is represented as a molecular surface colored according to electrostatic potential (blue = positive, red = negative, white = neutral).

10.9 Experimental section

In silico techniques.

The crystal structure of the IL-6/IL-6R/gp130 ternary complex was used as a template for virtual screening purposes (PDB id: 1P9M). This structure was prepared with standard preparation procedures (protein preparation wizard) as included in the software package Maestro¹³⁴.

The docking grid was created using the IL-6 structure (chain B in structure) and centered using phe299 of IL-6R and a 12Å cube; this grid was large enough to include all the interaction surface of IL-6. The Schrodinger fragment library (available from www.schrodinger.com) was docked into the generated grid using the modified parameters reported in Loving et al³⁰⁶. Briefly, we increased the number of poses per ligand for the initial docking stage to 50,000, used a wider scoring window of 500.0 kcal/mol for keeping initial poses, and kept the best 1,000 poses per ligand for energy minimization. The keyword roughmin was added to the maxkeep line of the Glide input file, instructing Glide to bypass the sorting by the rough score and to minimize all maxkeep (50,000) poses on the Glide grid. This allows for a much larger number of poses to be scored with the more accurate scoring function in Glide. We also subjected the top 100 poses per fragment to post-docking minimization and requested the top 100 poses to be returned. The results of fragment docking were used to generate an e-pharmacophore using a ad-hoc script in Maestro; the fragments clustering was applied and a maximum of 7 features was required. The script extracts the energetic descriptors of the Glide XP score and assigns them to pharmacophore features. The resulting energy pharmacophore (e-Pharmacophore) hypotheses can be used directly in a Phase search or can be manually modified based on visualization and the energetics. The hit molecules from pharmacophoric search was collected in a single list, and then subjected to energy minimization in the context of the IL-6 protein; in particular, each molecule was minimized using the Embrace interface in Macromodel (version 9.9, Schrödinger, LLC, New York), keeping the receptor atoms frozen and with the ligand free to move, with a max of 5000 steps of minimization. Other options set as default.

11. Concluding remarks and future perspectives

This thesis describes the discovery of new compounds able to modulate activity of relevant targets involved in cancer and aging-related pathologies using a rational design approach. We demonstrated that *in silico* techniques, mainly virtual screening methods, can efficiently complement standard screening technologies, and maximize the number of hit molecules found.

In summary, we identified new moderately active and selective non-peptidic compounds able to inhibit the activity of both standard and immunoproteasome, as well as novel and selective scaffolds that would bind and inhibit SIRT6 selectively and can be used to sensitize tumor cells to commonly used anticancer agents such gemcitabine and olaparib. Moreover, our virtual screening approach led us also to the discovery of new putative modulators of SIRT3 with interesting in-vitro and cellular activity; the activator compound 24 is of special interest since no specific SIRT3 activators are reported in literature so far. Although the selectivity and potency of the identified chemical scaffolds are susceptible to be further improved, these compounds can be considered as highly promising leads for the development of future therapeutics.

In addition, two theoretical studies provided i) a simple tool to estimate the selectivity of a small molecule ligand between two or more sirtuin isoforms and ii) a deep analysis of the characteristics and properties of the surfaces of interaction between IL-6 and its receptor, encoded into a short series of pharmacophores that could be used to identify ligands capable of interacting specifically with the target protein.

For the future, the following issues would be of interest to investigate:

- In vitro testing of selected IL-6 putative inhibitors, to measure the direct binding with IL-6 and the ability to reduce the pro-inflammatory effects of IL-6
- Design and chemical synthesis of active compounds derivatives, with improved biological activity and better pharmacokinetic and pharmacodynamic profiles.
- In vivo proof-of-concept studies to measure the effect of the identified inhibitors/modulators in animal models of neurodegeneration (for SIRT3 activators) or type 2 diabetes (for SIRT6 inhibitors).

Acknowledgements

I wish to thank all the colleagues and friends who were involved in the projects here described and in particular:

Prof. C. Franceschi, Prof. S. Salvioli, Prof. M. Capri and all the other members of Immunology Lab (Dept. of Experimental, Diagnostic and Specialty Medicine) from the University of Bologna for *in vitro* testing of proteasome inhibitors and helpful discussion;

Dr. D. Albani and Dr. G. Forloni (Laboratory of Biology of Neurodegenerative Disorders - Department of Neuroscience - IRCCS - Istituto di Ricerche Farmacologiche "Mario Negri" Milano) for biological characterization of SIRT3 modulators;

Dr. S. Bruzzone (Department of Experimental Medicine, Section of Biochemistry, University of Genoa) and Dr. A. Nencioni (Department of Internal Medicine, University of Genoa) for biological characterization of SIRT6 inhibitors;

Dr. G. Varchi (Institute of Organic Synthesis and Photoreactivity ISOF-CNR, Bologna) for helpful discussion on SIRT6 inhibitors optimization and synthesis;

Last but not least, Dr. Alberto Del Rio and all members of BCI Lab for support and contribution to all projects.

References

1. Paul, S. M. *et al.* How to improve R&D productivity: the pharmaceutical industry's grand challenge. *Nat. Rev. Drug Discov.* **9**, 203–14 (2010).
2. Gupta, S. C., Sung, B., Prasad, S., Webb, L. J. & Aggarwal, B. B. Cancer drug discovery by repurposing: teaching new tricks to old dogs. *Trends Pharmacol. Sci.* **34**, 508–17 (2013).
3. Iskar, M., Zeller, G., Zhao, X.-M., van Noort, V. & Bork, P. Drug discovery in the age of systems biology: the rise of computational approaches for data integration. *Curr. Opin. Biotechnol.* **23**, 609–16 (2012).
4. Claus, B. L. & Underwood, D. J. Discovery informatics: its evolving role in drug discovery. *Drug Discov. Today* **7**, 957–66 (2002).
5. Tosato, M., Zamboni, V., Ferrini, A. & Cesari, M. The aging process and potential interventions to extend life expectancy. *Clin. Interv. Aging* **2**, 401–12 (2007).
6. Huang, J. *et al.* DAMPs, ageing, and cancer: The “DAMP Hypothesis.” *Ageing Res. Rev.* 1–14 (2014). doi:10.1016/j.arr.2014.10.004
7. Finkel, T., Serrano, M. & Blasco, M. a. The common biology of cancer and ageing. *Nature* **448**, 767–74 (2007).
8. Moffat, J. G., Rudolph, J. & Bailey, D. Phenotypic screening in cancer drug discovery - past, present and future. *Nat. Rev. Drug Discov.* **13**, 588–602 (2014).
9. Arrowsmith, J. A decade of change. *Nat. Rev. Drug Discov.* **11**, 17–8 (2012).
10. Bochtler, M., Ditzel, L., Groll, M., Hartmann, C. & Huber, R. The proteasome. *Annu. Rev. Biophys. Biomol. Struct.* **28**, 295+ (1999).
11. Voges, D., Zwickl, P. & Baumeister, W. The 26S proteasome: A molecular machine designed for controlled proteolysis. *Annu. Rev. Biochem.* **68**, 1015–1068 (1999).
12. Dahlmann, B. in *ESSAYS Biochem. VOL 41 UBIQUITIN-PROTEASOME Syst.* (Mayer, RJ and Layfield, R) **41**, 31–48 (2005).
13. Rechsteiner, M. & Hill, C. P. Mobilizing the proteolytic machine: cell biological roles of proteasome activators and inhibitors. *Trends Cell Biol.* **15**, 27–33 (2005).
14. Smith, D. M., Fraga, H., Reis, C., Kafri, G. & Goldberg, A. L. ATP Binds to Proteasomal ATPases in Pairs with Distinct Functional Effects, Implying an Ordered Reaction Cycle. *Cell* **144**, 526–538 (2011).
15. Weissman, A. M., Shabek, N. & Ciechanover, A. The predator becomes the prey: regulating the ubiquitin system by ubiquitylation and degradation. *Nat. Rev. Mol. CELL Biol.* **12**, 605–620 (2011).
16. Bech-Otschir, D. *et al.* Polyubiquitin substrates allosterically activate their own degradation by the 26S proteasome. *Nat. Struct. Mol. Biol.* **16**, 219–225 (2009).
17. Goldberg, A. L. Functions of the proteasome: from protein degradation and immune surveillance to cancer therapy. *Biochem. Soc. Trans.* **35**, 12–17 (2007).
18. Dahlmann, B. Role of proteasomes in disease. *BMC Biochem.* **8**, (2007).
19. Schmidt, F. *et al.* Quantitative proteome analysis of the 20S proteasome of apoptotic Jurkat T cells. *Amino Acids* **41**, 351–361 (2011).
20. Warren, E. H. *et al.* An antigen produced by splicing of noncontiguous peptides in the reverse order. *Science (80-.)*. **313**, 1444–1447 (2006).
21. Vigneron, N. *et al.* An antigenic peptide produced by peptide splicing in the proteasome. *Science (80-.)*. **304**, 587–590 (2004).
22. Dalet, A., Vigneron, N., Stroobant, V., Hanada, K. & den Eynde, B. J. Splicing of Distant Peptide Fragments Occurs in the Proteasome by Transpeptidation and Produces the Spliced

- Antigenic Peptide Derived from Fibroblast Growth Factor-5. *J. Immunol.* **184**, 3016–3024 (2010).
23. Hanada, K., Yewdell, J. W. & Yang, J. C. Immune recognition of a human renal cancer antigen through post-translational protein splicing. *Nature* **427**, 252–256 (2004).
 24. Dalet, A. *et al.* An antigenic peptide produced by reverse splicing and double asparagine deamidation. *Proc. Natl. Acad. Sci. U. S. A.* **108**, E323–E331 (2011).
 25. Liepe, J. *et al.* The 20S Proteasome Splicing Activity Discovered by SpliceMet. *PLoS Comput. Biol.* **6**, (2010).
 26. Vigneron, N. & Van den Eynde, B. J. Proteasome subtypes and the processing of tumor antigens: increasing antigenic diversity. *Curr. Opin. Immunol.* **24**, 84–91 (2012).
 27. Rock, K. L., York, I. A. & Goldberg, A. L. Post-proteasomal antigen processing for major histocompatibility complex class I presentation. *Nat. Immunol.* **5**, 670–677 (2004).
 28. Kloetzel, P. M. & Ossendorp, F. Proteasome and peptidase function in MHC-class-I-mediated antigen presentation. *Curr. Opin. Immunol.* **16**, 76–81 (2004).
 29. Kloetzel, P. M. Antigen processing by the proteasome. *Nat. Rev. Mol. CELL Biol.* **2**, 179–187 (2001).
 30. Groettrup, M., Kirk, C. J. & Basler, M. Proteasomes in immune cells: more than peptide producers? *Nat. Rev. Immunol.* **10**, 72–77 (2010).
 31. Muchamuel, T. *et al.* A selective inhibitor of the immunoproteasome subunit LMP7 blocks cytokine production and attenuates progression of experimental arthritis. *Nat. Med.* **15**, 781–U12 (2009).
 32. Basler, M., Dajee, M., Moll, C., Groettrup, M. & Kirk, C. J. Prevention of Experimental Colitis by a Selective Inhibitor of the Immunoproteasome. *J. Immunol.* **185**, 634–641 (2010).
 33. Hussong, S. A., Kapphahn, R. J., Phillips, S. L., Maldonado, M. & Ferrington, D. A. Immunoproteasome deficiency alters retinal proteasome's response to stress. *J. Neurochem.* **113**, 1481–1490 (2010).
 34. Jung, T. & Grune, T. The Proteasome and its Role in the Degradation of Oxidized Proteins. *IUBMB Life* **60**, 743–752 (2008).
 35. Grune, T., Merker, K., Sandig, G. & Davies, K. J. A. Selective degradation of oxidatively modified protein substrates by the proteasome. *Biochem. Biophys. Res. Commun.* **305**, 709–718 (2003).
 36. Farout, L. & Friguet, B. Proteasome function in aging and oxidative stress: Implications in protein maintenance failure. *Antioxid. Redox Signal.* **8**, 205–216 (2006).
 37. Pickering, A. M. *et al.* The immunoproteasome, the 20S proteasome and the PA28 alpha beta proteasome regulator are oxidative-stress-adaptive proteolytic complexes. *Biochem. J.* **432**, 585–594 (2010).
 38. Ding, Q. X., Martin, S., Dimayuga, E., Bruce-Keller, A. J. & Keller, J. N. LMP2 knock-out mice have reduced proteasome activities and increased levels of oxidatively damaged proteins. *Antioxid. Redox Signal.* **8**, 130–135 (2006).
 39. Seifert, U. *et al.* Immunoproteasomes Preserve Protein Homeostasis upon Interferon-Induced Oxidative Stress. *Cell* **142**, 613–624 (2010).
 40. Klare, N., Seeger, M., Janek, K., Jungblut, P. R. & Dahlmann, B. Intermediate-type 20 S proteasomes in HeLa cells: ``Asymmetric{}`` subunit composition, diversity and adaptation. *J. Mol. Biol.* **373**, 1–10 (2007).
 41. Schmidt, F. *et al.* Comprehensive quantitative proteome analysis of 20S proteasome subtypes from rat liver by isotope coded affinity tag and 2-D gel-based approaches. *Proteomics* **6**, 4622–4632 (2006).
 42. Kloss, A., Meiners, S., Ludwig, A. & Dahlmann, B. Multiple cardiac proteasome subtypes differ in their susceptibility to proteasome inhibitors. *Cardiovasc. Res.* **85**, 367–75 (2010).

43. Nitta, T. *et al.* Thymoproteasome Shapes Immunocompetent Repertoire of CD8(+) T Cells. *Immunity* **32**, 29–40 (2010).
44. Murata, S. *et al.* Regulation of CD8+ T cell development by thymus-specific proteasomes. *Science (80-.)*. **316**, 1349–1353 (2007).
45. Vasuri, F. *et al.* Studies on immunoproteasome in human liver. Part I: Absence in fetuses, presence in normal subjects, and increased levels in chronic active hepatitis and cirrhosis. *Biochem. Biophys. Res. Commun.* **397**, 301–306 (2010).
46. Stohwasser, R. *et al.* Biochemical analysis of proteasomes from mouse microglia: Induction of immunoproteasomes by interferon-gamma and lipopolysaccharide. *Glia* **29**, 355–365 (2000).
47. Vezzani, A., French, J., Bartfai, T. & Baram, T. Z. The role of inflammation in epilepsy. *Nat. Rev. Neurol.* **7**, 31–40 (2011).
48. Mishto, M. *et al.* Immunoproteasome expression is induced in mesial temporal lobe epilepsy. *Biochem. Biophys. Res. Commun.* **408**, 65–70 (2011).
49. Mishto, M. *et al.* Immunoproteasome and LMP2 polymorphism in aged and Alzheimer's disease brains. *Neurobiol. Aging* **27**, 54–66 (2006).
50. Mishto, M. *et al.* Immunoproteasome LMP2 60HH Variant Alters MBP Epitope Generation and Reduces the Risk to Develop Multiple Sclerosis in Italian Female Population. *PLoS One* **5**, (2010).
51. Diaz-Hernandez, M. *et al.* Neuronal induction of the immunoproteasome in Huntington's disease. *J. Neurosci.* **23**, 11653–11661 (2003).
52. Basler, M., Beck, U., Kirk, C. J. & Groettrup, M. The antiviral immune response in mice devoid of immunoproteasome activity. *J. Immunol.* **187**, 5548–57 (2011).
53. Seliger, B. Novel insights into the molecular mechanisms of HLA class I abnormalities. *Cancer Immunol. Immunother.* **61**, 249–54 (2012).
54. Schwartz, A. L. & Ciechanover, A. The ubiquitin-proteasome pathway and pathogenesis of human diseases. *Annu. Rev. Med.* **50**, 57–74 (1999).
55. Molineaux, S. M. Molecular Pathways: Targeting Proteasomal Protein Degradation in Cancer. *Clin. CANCER Res.* **18**, 15–20 (2012).
56. Frankland-Searby, S. & Bhaumik, S. R. The 26S proteasome complex: an attractive target for cancer therapy. *Biochim. Biophys. Acta* **1825**, 64–76 (2012).
57. Navon, A. & Ciechanover, A. The 26 S Proteasome: From Basic Mechanisms to Drug Targeting. *J. Biol. Chem.* **284**, 33713–33718 (2009).
58. Adams, J. The proteasome: A suitable antineoplastic target. *Nat. Rev. CANCER* **4**, 349–360 (2004).
59. Orłowski, R. Z. & Kuhn, D. J. Proteasome inhibitors in cancer therapy: Lessons from the first decade. *Clin. CANCER Res.* **14**, 1649–1657 (2008).
60. Altun, M. *et al.* Effects of PS-341 on the activity and composition of proteasomes in multiple myeloma cells. *Cancer Res.* **65**, 7896–7901 (2005).
61. Kuhn, D. J. *et al.* Targeted inhibition of the immunoproteasome is a potent strategy against models of multiple myeloma that overcomes resistance to conventional drugs and nonspecific proteasome inhibitors. *Blood* **113**, 4667–4676 (2009).
62. Vigneron, N. & den Eynde, B. J. Insights into the processing of MHC class I ligands gained from the study of human tumor epitopes. *Cell. Mol. LIFE Sci.* **68**, 1503–1520 (2011).
63. Singh, A. V *et al.* PR-924, a selective inhibitor of the immunoproteasome subunit LMP-7, blocks multiple myeloma cell growth both in vitro and in vivo. *Br. J. Haematol.* **152**, 155–63 (2011).
64. Lee, W. & Kim, K. B. The Immunoproteasome: An Emerging Therapeutic Target. *Curr. Top. Med. Chem.* **11**, 2923–2930 (2011).

65. Ho, Y. K. (Abby), Bargagna-Mohan, P., Wehenkel, M., Mohan, R. & Kim, K.-B. LMP2-specific inhibitors: Chemical genetic tools for proteasome biology. *Chem. Biol.* **14**, 419–430 (2007).
66. Palumbo, A. & Anderson, K. MEDICAL PROGRESS Multiple Myeloma. *N. Engl. J. Med.* **364**, 1046–1060 (2011).
67. Morabito, F. *et al.* Therapeutic approaches for newly diagnosed multiple myeloma patients in the era of novel drugs. *Eur. J. Haematol.* **85**, 181–191 (2010).
68. Bonafe, M., Storci, G. & Franceschi, C. Inflamm-aging of the stem cell niche: Breast cancer as a paradigmatic example. *BIOESSAYS* **34**, 40–49 (2012).
69. Hoves, S. *et al.* In situ analysis of the antigen-processing machinery in acute myeloid leukaemic blasts by tissue microarray. *Leukemia* **23**, 877–885 (2009).
70. Matsui, M., Machida, S., Itani-Yohda, T. & Akatsuka, T. Downregulation of the proteasome subunits, transporter, and antigen presentation in hepatocellular carcinoma, and their restoration by interferon-gamma. *J. Gastroenterol. Hepatol.* **17**, 897–907 (2002).
71. Dissemond, J. *et al.* Immunoproteasome subunits LMP2 and LMP7 downregulation in primary malignant melanoma lesions: association with lack of spontaneous regression. *Melanoma Res.* **13**, 371–377 (2003).
72. Hayashi, T. *et al.* Mice-lacking LMP2, immuno-proteasome subunit, as an animal model of spontaneous uterine leiomyosarcoma. *Protein Cell* **1**, 711–717 (2010).
73. Speiser, D. E. & Romero, P. Molecularly defined vaccines for cancer immunotherapy, and protective T cell immunity. *Semin. Immunol.* **22**, 144–154 (2010).
74. Cascio, P., Hilton, C., Kisselev, A. F., Rock, K. L. & Goldberg, A. L. 26S proteasomes and immunoproteasomes produce mainly N-extended versions of an antigenic peptide. *EMBO J.* **20**, 2357–2366 (2001).
75. Van den Eynde, B. J. & Morel, S. Differential processing of class-I-restricted epitopes by the standard proteasome and the immunoproteasome. *Curr. Opin. Immunol.* **13**, 147–53 (2001).
76. Morel, S. *et al.* Processing of some antigens by the standard proteasome but not by the immunoproteasome results in poor presentation by dendritic cells. *Immunity* **12**, 107–117 (2000).
77. Chapiro, J. *et al.* Destructive cleavage of antigenic peptides either by the immunoproteasome or by the standard proteasome results in differential antigen presentation. *J. Immunol.* **176**, 1053–1061 (2006).
78. Dalet, A., Stroobant, V., Vigneron, N. & van den Eynde, B. J. Differences in the production of spliced antigenic peptides by the standard proteasome and the immunoproteasome. *Eur. J. Immunol.* **41**, 39–46 (2011).
79. Wang, X., Zhao, Z., Luo, Y., Chen, G. & Li, Z. Gel-based proteomics analysis of the heterogeneity of 20S proteasomes from four human pancreatic cancer cell lines. *PROTEOMICS Clin. Appl.* **5**, 484–492 (2011).
80. Guillaume, B. *et al.* Two abundant proteasome subtypes that uniquely process some antigens presented by HLA class I molecules. *Proc. Natl. Acad. Sci. U. S. A.* **107**, 18599–18604 (2010).
81. Mishto, M. *et al.* Modeling the in vitro 20S proteasome activity: The effect of PA28-alpha beta and of the sequence and length of polypeptides on the degradation kinetics. *J. Mol. Biol.* **377**, 1607–1617 (2008).
82. Tai, H.-C. & Schuman, E. M. Ubiquitin, the proteasome and protein degradation in neuronal function and dysfunction. *Nat. Rev. Neurosci.* **9**, 826–838 (2008).
83. Lee, Y. K., Menezes, J. S., Umesaki, Y. & Mazmanian, S. K. Proinflammatory T-cell responses to gut microbiota promote experimental autoimmune encephalomyelitis. *Proc. Natl. Acad. Sci. U. S. A.* **108**, 4615–4622 (2011).

84. Ochoa-Reparaz, J., Mielcarz, D. W., Begum-Haque, S. & Kasper, L. H. Gut, Bugs, and Brain: Role of Commensal Bacteria in the Control of Central Nervous System Disease. *Ann. Neurol.* **69**, 240–247 (2011).
85. Ochoa-Repáraz, J., Mielcarz, D. W., Haque-Begum, S. & Kasper, L. H. Induction of a regulatory B cell population in experimental allergic encephalomyelitis by alteration of the gut commensal microflora. *Gut Microbes* **1**, 103–108 (2010).
86. SELKOE, D. J. THE MOLECULAR PATHOLOGY OF ALZHEIMERS-DISEASE. *Neuron* **6**, 487–498 (1991).
87. Keck, S., Nitsch, R., Grune, T. & Ullrich, O. Proteasome inhibition by paired helical filament-tau in brains of patients with Alzheimer's disease. *J. Neurochem.* **85**, 115–122 (2003).
88. Checler, F. *et al.* Role of the proteasome in Alzheimer's disease. *Biochim. Biophys. ACTA-MOLECULAR BASIS Dis.* **1502**, 133–138 (2000).
89. Keller, J. N., Hanni, K. B. & Markesbery, W. R. Impaired proteasome function in Alzheimer's disease. *J. Neurochem.* **75**, 436–439 (2000).
90. Gillardon, F. *et al.* The 20S proteasome isolated from Alzheimer's disease brain shows post-translational modifications but unchanged proteolytic activity. *J. Neurochem.* **101**, 1483–1490 (2007).
91. Mishto, M. *et al.* Immunoproteasomes and immunosenescence. *Ageing Res. Rev.* **2**, 419–432 (2003).
92. Cardozo, C. & Michaud, C. Proteasome-mediated degradation of tau proteins occurs independently of the chymotrypsin-like activity by a nonprocessive pathway. *Arch. Biochem. Biophys.* **408**, 103–110 (2002).
93. Friese, M. A. & Fugger, L. Autoreactive CD8(+) T cells in multiple sclerosis: a new target for therapy? *BRAIN* **128**, 1747–1763 (2005).
94. Giovannoni, G. & Ebers, G. Multiple sclerosis: the environment and causation. *Curr. Opin. Neurol.* **20**, 261–268 (2007).
95. Fugger, L., Friese, M. A. & Bell, J. I. From genes to function: the next challenge to understanding multiple sclerosis. *Nat. Rev. Immunol.* **9**, 408–17 (2009).
96. Friese, M. A. *et al.* Opposing effects of HLA class I molecules in tuning autoreactive CD8(+) T cells in multiple sclerosis. *Nat. Med.* **14**, 1227–1235 (2008).
97. Zheng, J. & Bizzozero, O. A. Decreased activity of the 20S proteasome in the brain white matter and gray matter of patients with multiple sclerosis. *J. Neurochem.* **117**, 143–153 (2011).
98. Zang, Y. C. Q. *et al.* Increased CD8(+) cytotoxic T cell responses to myelin basic protein in multiple sclerosis. *J. Immunol.* **172**, 5120–5127 (2004).
99. TSUCHIDA, T. *et al.* AUTOREACTIVE CD8(+) T-CELL RESPONSES TO HUMAN MYELIN PROTEIN-DERIVED PEPTIDES. *Proc. Natl. Acad. Sci. U. S. A.* **91**, 10859–10863 (1994).
100. Jurewicz, A., Biddison, W. E. & Antel, J. P. MHC class I-restricted lysis of human oligodendrocytes by myelin basic protein peptide-specific CD8 T lymphocytes. *J. Immunol.* **160**, 3056–3059 (1998).
101. Perucca, E., French, C. & Bialer, M. Development of new antiepileptic drugs: challenges, incentives, and recent advances. *Lancet Neurol.* **6**, 793–804 (2007).
102. Ravizza, T. *et al.* Interleukin Converting Enzyme inhibition impairs kindling epileptogenesis in rats by blocking astrocytic IL-1 beta production. *Neurobiol. Dis.* **31**, 327–333 (2008).
103. Maroso, M. *et al.* Toll-like receptor 4 and high-mobility group box-1 are involved in icogenesis and can be targeted to reduce seizures. *Nat. Med.* **16**, 413–U91 (2010).

104. Parlati, F. *et al.* Carfilzomib can induce tumor cell death through selective inhibition of the chymotrypsin-like activity of the proteasome. *Blood* **114**, 3439–3447 (2009).
105. Zhou, H.-J. *et al.* Design and Synthesis of an Orally Bioavailable and Selective Peptide Epoxyketone Proteasome Inhibitor (PR-047). *J. Med. Chem.* **52**, 3028–3038 (2009).
106. Kuhn, D. J., Orłowski, R. Z. & Bjorklund, C. C. Second Generation Proteasome Inhibitors: Carfilzomib and Immunoproteasome-Specific Inhibitors (IPSIs). *Curr. Cancer Drug Targets* **11**, 285–295 (2011).
107. Adams, J. L. *et al.* Pyrimidinylimidazole inhibitors of CSBP/P37 kinase demonstrating decreased inhibition of hepatic cytochrome P450 enzymes. *Bioorg. Med. Chem. Lett.* **8**, 3111–3116 (1998).
108. Van der Linden, W. A. *et al.* Discovery of a potent and highly beta 1 specific proteasome inhibitor from a focused library of urea-containing peptide vinyl sulfones and peptide epoxyketones. *Org. Biomol. Chem.* **10**, 181–194 (2012).
109. Gräwert, M. A. & Groll, M. Exploiting nature's rich source of proteasome inhibitors as starting points in drug development. *Chem. Commun. (Camb)*. **48**, 1364–78 (2012).
110. Groll, M. & Potts, B. C. Proteasome Structure, Function, and Lessons Learned from Beta-Lactone Inhibitors. *Curr. Top. Med. Chem.* **11**, 2850–2878 (2011).
111. Moore, B. S., Eustaquio, A. S. & McGlinchey, R. P. Advances in and applications of proteasome inhibitors. *Curr. Opin. Chem. Biol.* **12**, 434–440 (2008).
112. Gulder, T. A. M. & Moore, B. S. Salinosporamide Natural Products: Potent 20 S Proteasome Inhibitors as Promising Cancer Chemotherapeutics. *Angew. CHEMIE-INTERNATIONAL Ed.* **49**, 9346–9367 (2010).
113. Qian, K. *et al.* New betulinic acid derivatives as potent proteasome inhibitors. *Bioorg. Med. Chem. Lett.* **21**, 5944–5947 (2011).
114. Nickeleit, I. *et al.* Argyrin A reveals a critical role for the tumor suppressor protein p27(kip1) in mediating antitumor activities in response to proteasome inhibition. *Cancer Cell* **14**, 23–35 (2008).
115. Gallastegui, N. *et al.* Hydroxyureas as noncovalent proteasome inhibitors. *Angew. Chem. Int. Ed. Engl.* **51**, 247–9 (2012).
116. Huang, L. & Chen, C. H. Proteasome Regulators: Activators and Inhibitors. *Curr. Med. Chem.* **16**, 931–939 (2009).
117. Katsiki, M., Chondrogianni, N., Chinou, I., Rivett, A. J. & Gonos, E. S. The olive constituent oleuropein exhibits proteasome stimulatory properties in vitro and confers life span extension of human embryonic fibroblasts. *Rejuvenation Res.* **10**, 157–172 (2007).
118. Bulteau, A. L., Moreau, M., Saunois, A., Nizard, C. & Friguet, B. Algae extract-mediated stimulation and protection of proteasome activity within human keratinocytes exposed to UVA and UVB irradiation. *Antioxid. Redox Signal.* **8**, 136–143 (2006).
119. Huang, L., Ho, P. & Chen, C.-H. Activation and inhibition of the proteasome by betulinic acid and its derivatives. *FEBS Lett.* **581**, 4955–4959 (2007).
120. Chondrogianni, N. *et al.* Anti-ageing and rejuvenating effects of quercetin. *Exp. Gerontol.* **45**, 763–771 (2010).
121. Bedford, L., Lowe, J., Dick, L. R., Mayer, R. J. & Brownell, J. E. Ubiquitin-like protein conjugation and the ubiquitin-proteasome system as drug targets. *Nat. Rev. DRUG Discov.* **10**, 29–46 (2011).
122. Lee, B.-H. *et al.* Enhancement of proteasome activity by a small-molecule inhibitor of USP14. *Nature* **467**, 179–U63 (2010).
123. D'Arcy, P. *et al.* Inhibition of proteasome deubiquitinating activity as a new cancer therapy. *Nat. Med.* **17**, 1636–U150 (2011).

124. Bordoli, L. *et al.* Protein structure homology modeling using SWISS-MODEL workspace. *Nat. Protoc.* **4**, 1–13 (2009).
125. Huber, E. M. *et al.* Immuno- and Constitutive Proteasome Crystal Structures Reveal Differences in Substrate and Inhibitor Specificity. *Cell* **148**, 727–738 (2012).
126. Subramaniam, S., Mehrotra, M. & Gupta, D. Support Vector Machine Based Prediction of *P. falciparum* Proteasome Inhibitors and Development of Focused Library by Molecular Docking. *Comb. Chem. High Throughput Screen.* **14**, 898–907 (2011).
127. Basse, N. *et al.* Novel Organic Proteasome Inhibitors Identified by Virtual and in Vitro Screening. *J. Med. Chem.* **53**, 509–513 (2010).
128. Lei, B. *et al.* Molecular Basis of the Selectivity of the Immunoproteasome Catalytic Subunit LMP2-Specific Inhibitor Revealed by Molecular Modeling and Dynamics Simulations. *J. Phys. Chem. B* **114**, 12333–12339 (2010).
129. Genin, E., Reboud-Ravaux, M. & Vidal, J. Proteasome Inhibitors: Recent Advances and New Perspectives In Medicinal Chemistry. *Curr. Top. Med. Chem.* **10**, 232–256 (2010).
130. Caporuscio, F., Rastelli, G., Imbriano, C. & Del Rio, A. Structure-Based Design of Potent Aromatase Inhibitors by High-Throughput Docking. *J. Med. Chem.* **54**, 4006–4017 (2011).
131. Del Rio, A., Barbosa, A. J. M., Caporuscio, F. & Mangiatordi, G. F. CoCoCo: a free suite of multiconformational chemical databases for high-throughput virtual screening purposes. *Mol. Biosyst.* **6**, 2122–2128 (2010).
132. Del Rio, A., Barbosa, A. J. M., Caporuscio, F. & Mangiatordi, G. F. CoCoCo: a free suite of multiconformational chemical databases for high-throughput virtual screening purposes. *Mol. Biosyst.* **6**, 2122–8 (2010).
133. Moura Barbosa, A. J. & Del Rio, A. Freely accessible databases of commercial compounds for high-throughput virtual screenings. *Curr. Top. Med. Chem.* **12**, 866–77 (2012).
134. Maestro, version 9.3, Schrödinger, LLC, New York, NY, 2012.
135. Glide, version 5.8, Schrödinger, LLC, New York, NY, 2012.
136. Mishto, M. *et al.* Driving forces of proteasome-catalyzed peptide splicing in yeast and humans. *Mol. Cell. Proteomics* **11**, 1008–23 (2012).
137. Dahlmann, B., Ruppert, T., Kuehn, L., Merforth, S. & Kloetzel, P. M. Different proteasome subtypes in a single tissue exhibit different enzymatic properties. *J. Mol. Biol.* **303**, 643–53 (2000).
138. Tanny, J. C., Dowd, G. J., Huang, J., Hilz, H. & Moazed, D. An enzymatic activity in the yeast Sir2 protein that is essential for gene silencing. *Cell* **99**, 735–745 (1999).
139. Imai, S., Armstrong, C. M., Kaeberlein, M. & Guarente, L. Transcriptional silencing and longevity protein Sir2 is an NAD-dependent histone deacetylase. *Nature* **403**, 795–800 (2000).
140. Finkel, T., Deng, C.-X. & Mostoslavsky, R. Recent progress in the biology and physiology of sirtuins. *Nature* **460**, 587–591 (2009).
141. Frye, R. A. Characterization of five human cDNAs with homology to the yeast SIR2 gene: Sir2-like proteins (sirtuins) metabolize NAD and may have protein ADP-ribosyltransferase activity. *Biochem. Biophys. Res. Commun.* **260**, 273–279 (1999).
142. Dani, N., Barbosa, A. J. M., Del Rio, A. & Di Girolamo, M. ADP-Ribosylated Proteins as Old and New Drug Targets for Anticancer Therapy: The Example of ARF6. *Curr. Pharm. Des.* **19**, 624–633 (2013).
143. Libert, S. *et al.* SIRT1 activates MAO-A in the brain to mediate anxiety and exploratory drive. *Cell* **147**, 1459–72 (2011).
144. Wang, R.-H. *et al.* Impaired DNA damage response, genome instability, and tumorigenesis in SIRT1 mutant mice. *Cancer Cell* **14**, 312–323 (2008).

145. Kim, H.-S. *et al.* SIRT3 Is a Mitochondria-Localized Tumor Suppressor Required for Maintenance of Mitochondrial Integrity and Metabolism during Stress. *Cancer Cell* **17**, 41–52 (2010).
146. Kim, H.-S. *et al.* SIRT2 Maintains Genome Integrity and Suppresses Tumorigenesis through Regulating APC/C Activity. *Cancer Cell* **20**, 487–499 (2011).
147. Finley, L. W. S. *et al.* SIRT3 Opposes Reprogramming of Cancer Cell Metabolism through HIF1 alpha Destabilization. *Cancer Cell* **19**, 416–428 (2011).
148. Yeung, F. *et al.* Modulation of NF-kappa B-dependent transcription and cell survival by the SIRT1 deacetylase. *EMBO J.* **23**, 2369–2380 (2004).
149. Firestein, R. *et al.* The SIRT1 Deacetylase Suppresses Intestinal Tumorigenesis and Colon Cancer Growth. *PLoS One* **3**, (2008).
150. North, B. J., Marshall, B. L., Borra, M. T., Denu, J. M. & Verdin, E. The human Sir2 ortholog, SIRT2, is an NAD(+)-dependent tubulin deacetylase. *Mol. Cell* **11**, 437–444 (2003).
151. Van Meter, M., Mao, Z., Gorbunova, V. & Seluanov, A. SIRT6 overexpression induces massive apoptosis in cancer cells but not in normal cells. *CELL CYCLE* **10**, 3153–3158 (2011).
152. Kawahara, T. L. A. *et al.* SIRT6 links histone H3 lysine 9 deacetylation to NF-kappaB-dependent gene expression and organismal life span. *Cell* **136**, 62–74 (2009).
153. Zhong, L. *et al.* The Histone Deacetylase Sirt6 Regulates Glucose Homeostasis via Hif1 alpha. *Cell* **140**, 280–293 (2010).
154. Luo, J. Y. *et al.* Negative control of p53 by Sir2 alpha promotes cell survival under stress. *Cell* **107**, 137–148 (2001).
155. Vaziri, H. *et al.* hSIR2(SIRT1) functions as an NAD-dependent p53 deacetylase. *Cell* **107**, 149–159 (2001).
156. Brunet, A. *et al.* Stress-dependent regulation of FOXO transcription factors by the SIRT1 deacetylase. *Science (80-.)*. **303**, 2011–2015 (2004).
157. Cohen, H. Y. *et al.* Calorie restriction promotes mammalian cell survival by inducing the SIRT1 deacetylase. *Science (80-.)*. **305**, 390–392 (2004).
158. Langley, E. *et al.* Human SIR2 deacetylates p53 and antagonizes PML/p53-induced cellular senescence. *EMBO J.* **21**, 2383–2396 (2002).
159. Menssen, A. *et al.* The c-MYC oncoprotein, the NAMPT enzyme, the SIRT1-inhibitor DBC1, and the SIRT1 deacetylase form a positive feedback loop. *Proc. Natl. Acad. Sci. U. S. A.* **109**, E187–E196 (2012).
160. Heltweg, B. *et al.* Antitumor activity of a small-molecule inhibitor of human silent information regulator 2 enzymes. *Cancer Res.* **66**, 4368–4377 (2006).
161. Lain, S. *et al.* Discovery, in vivo activity, and mechanism of action of a small-molecule p53 activator. *Cancer Cell* **13**, 454–463 (2008).
162. Cea, M. *et al.* Synergistic Interactions between HDAC and Sirtuin Inhibitors in Human Leukemia Cells. *PLoS One* **6**, (2011).
163. Wang, B. *et al.* NAMPT overexpression in prostate cancer and its contribution to tumor cell survival and stress response. *Oncogene* **30**, 907–921 (2011).
164. Audrito, V. *et al.* Nicotinamide Blocks Proliferation and Induces Apoptosis of Chronic Lymphocytic Leukemia Cells through Activation of the p53/miR-34a/SIRT1 Tumor Suppressor Network. *Cancer Res.* **71**, 4473–4483 (2011).
165. Yuan, H. *et al.* Activation of stress response gene SIRT1 by BCR-ABL promotes leukemogenesis. *Blood* **119**, 1904–1914 (2012).
166. Li, L. *et al.* Activation of p53 by SIRT1 Inhibition Enhances Elimination of CML Leukemia Stem Cells in Combination with Imatinib. *Cancer Cell* **21**, 266–281 (2012).

167. Peck, B. *et al.* SIRT Inhibitors Induce Cell Death and p53 Acetylation through Targeting Both SIRT1 and SIRT2. *Mol. Cancer Ther.* **9**, 844–855 (2010).
168. Li, Y. *et al.* SIRT2 down-regulation in HeLa can induce p53 accumulation via p38 MAPK activation-dependent p300 decrease, eventually leading to apoptosis. *GENES TO CELLS* **16**, 34–45 (2011).
169. Zhang, Y. *et al.* Identification of a small molecule SIRT2 inhibitor with selective tumor cytotoxicity. *Biochem. Biophys. Res. Commun.* **386**, 729–733 (2009).
170. Dan, L. *et al.* The role of sirtuin 2 activation by nicotinamide phosphoribosyltransferase in the aberrant proliferation and survival of myeloid leukemia cells. *Haematologica* **97**, 551–9 (2012).
171. Inoue, T. *et al.* SIRT2 downregulation confers resistance to microtubule inhibitors by prolonging chronic mitotic arrest. *CELL CYCLE* **8**, 1279–1291 (2009).
172. Alhazzazi, T. Y. *et al.* Sirtuin-3 (SIRT3), a Novel Potential Therapeutic Target for Oral Cancer. *Cancer* **117**, 1670–1678 (2011).
173. Mostoslavsky, R. *et al.* Genomic instability and aging-like phenotype in the absence of mammalian SIRT6. *Cell* **124**, 315–329 (2006).
174. Jia, G., Su, L., Singhal, S. & Liu, X. Emerging roles of SIRT6 on telomere maintenance, DNA repair, metabolism and mammalian aging. *Mol. Cell. Biochem.* 345–350 (2012). doi:10.1007/s11010-012-1236-8
175. McCord, R. A. *et al.* SIRT6 stabilizes DNA-dependent protein kinase at chromatin for DNA double-strand break repair. *AGING-US* **1**, 109–121 (2009).
176. Van Gool, F. *et al.* Intracellular NAD levels regulate tumor necrosis factor protein synthesis in a sirtuin-dependent manner. *Nat. Med.* **15**, 206–210 (2009).
177. Truyers, C. *et al.* The use of human tissue in epidemiological research; ethical and legal considerations in two biobanks in Belgium. *Med. Heal. CARE Philos.* **13**, 169–175 (2010).
178. Allavena, P., Germano, G., Marchesi, F. & Mantovani, A. Chemokines in cancer related inflammation. *Exp. Cell Res.* **317**, 664–673 (2011).
179. Barber, M. F. *et al.* SIRT7 links H3K18 deacetylation to maintenance of oncogenic transformation. *Nature* **487**, 114+ (2012).
180. Tervo, A. J. *et al.* An in silico approach to discovering novel inhibitors of human sirtuin type 2. *J. Med. Chem.* **47**, 6292–6298 (2004).
181. Jung-Hynes, B., Nihal, M., Zhong, W. & Ahmad, N. Role of Sirtuin Histone Deacetylase SIRT1 in Prostate Cancer A TARGET FOR PROSTATE CANCER MANAGEMENT VIA ITS INHIBITION? *J. Biol. Chem.* **284**, 3823–3832 (2009).
182. Jackson, M. D., Schmidt, M. T., Oppenheimer, N. J. & Denu, J. M. Mechanism of nicotinamide inhibition and transglycosidation by Sir2 histone/protein deacetylases. *J. Biol. Chem.* **278**, 50985–50998 (2003).
183. Schmidt, M. T., Smith, B. C., Jackson, M. D. & Denu, J. M. Coenzyme specificity of Sir2 protein deacetylases - Implications for physiological regulation. *J. Biol. Chem.* **279**, 40122–40129 (2004).
184. Fatkins, D. G., Monnot, A. D. & Zheng, W. N-epsilon-thioacetyl-lysine: A multi-facet functional probe for enzymatic protein lysine N-epsilon-deacetylation. *Bioorg. Med. Chem. Lett.* **16**, 3651–3656 (2006).
185. Jamonnak, N., Fatkins, D. G., Wei, L. & Zheng, W. N-epsilon-methanesulfonyl-lysine as a non-hydrolyzable functional surrogate for N-epsilon-acetyl-lysine. *Org. Biomol. Chem.* **5**, 892–896 (2007).
186. Jamonnak, N., Hirsch, B. M., Pang, Y. & Zheng, W. Substrate specificity of SIRT1-catalyzed lysine N-epsilon-deacetylation reaction probed with the side chain modified N-epsilon-acetyl-lysine analogs. *Bioorg. Chem.* **38**, 17–25 (2010).

187. Smith, B. C. & Denu, J. M. Acetyl-lysine analog peptides as mechanistic probes of protein deacetylases. *J. Biol. Chem.* **282**, 37256–37265 (2007).
188. Smith, B. C., Settles, B., Hallows, W. C., Craven, M. W. & Denu, J. M. SIRT3 Substrate Specificity Determined by Peptide Arrays and Machine Learning. *ACS Chem. Biol.* **6**, 146–157 (2011).
189. Kiviranta, P. H. *et al.* N-epsilon-Thioacetyl-Lysine-Containing Tri-, Tetra-, and Pentapeptides as SIRT1 and SIRT2 Inhibitors. *J. Med. Chem.* **52**, 2153–2156 (2009).
190. Huhtiniemi, T. *et al.* N-epsilon-Modified lysine containing inhibitors for SIRT1 and SIRT2. *Bioorg. Med. Chem.* **18**, 5616–5625 (2010).
191. Suzuki, T. *et al.* Identification of a cell-active non-peptide sirtuin inhibitor containing N-thioacetyl lysine. *Bioorg. Med. Chem. Lett.* **19**, 5670–5672 (2009).
192. He, B., Du, J. & Lin, H. Thiosuccinyl Peptides as Sirt5-Specific Inhibitors. *J. Am. Chem. Soc.* **134**, 1922–1925 (2012).
193. Grozinger, C. M., Chao, E. D., Blackwell, H. E., Moazed, D. & Schreiber, S. L. Identification of a class of small molecule inhibitors of the sirtuin family of NAD-dependent deacetylases by phenotypic screening. *J. Biol. Chem.* **276**, 38837–38843 (2001).
194. Ota, H. *et al.* Sirt1 inhibitor, Sirtinol, induces senescence-like growth arrest with attenuated Ras-MAPK signaling in human cancer cells. *Oncogene* **25**, 176–185 (2006).
195. Lara, E. *et al.* Salermide, a Sirtuin inhibitor with a strong cancer-specific proapoptotic effect. *Oncogene* **28**, 781–791 (2009).
196. Bedalov, A., Gatabonton, T., Irvine, W. P., Gottschling, D. E. & Simon, J. A. Identification of a small molecule inhibitor of Sir2p. *Proc. Natl. Acad. Sci. U. S. A.* **98**, 15113–15118 (2001).
197. Neugebauer, R. C. *et al.* Structure-activity studies on splitomicin derivatives as sirtuin inhibitors and computational prediction of binding mode. *J. Med. Chem.* **51**, 1203–1213 (2008).
198. Marshall, G. M. *et al.* SIRT1 Promotes N-Myc Oncogenesis through a Positive Feedback Loop Involving the Effects of MKP3 and ERK on N-Myc Protein Stability. *PLoS Genet.* **7**, (2011).
199. Uciechowska, U. *et al.* Thiobarbiturates as Sirtuin Inhibitors: Virtual Screening, Free-Energy Calculations, and Biological Testing. *ChemMedChem* **3**, 1965–1976 (2008).
200. Napper, A. D. *et al.* Discovery of indoles as potent and selective inhibitors of the deacetylase SIRT1. *J. Med. Chem.* **48**, 8045–8054 (2005).
201. Trapp, J. *et al.* Adenosine mimetics as inhibitors of NAD(+)-dependent histone deacetylases, from kinase to sirtuin inhibition. *J. Med. Chem.* **49**, 7307–7316 (2006).
202. Howitz, K. T. *et al.* Small molecule activators of sirtuins extend *Saccharomyces cerevisiae* lifespan. *Nature* **425**, 191–196 (2003).
203. McGeary, R. P., Bennett, A. J., Tran, Q. B., Cosgrove, K. L. & Ross, B. P. Suramin: Clinical Uses and Structure-Activity Relationships. *MINI-REVIEWS Med. Chem.* **8**, 1384–1394 (2008).
204. Gill, J. S. & Windebank, A. J. Suramin induced ceramide accumulation leads to apoptotic cell death in dorsal root ganglion neurons. *Cell Death Differ.* **5**, 876–883 (1998).
205. Trapp, J. *et al.* Structure-activity studies on suramin analogues as inhibitors of NAD(+)-dependent histone deacetylases (Sirtuins). *ChemMedChem* **2**, 1419–1431 (2007).
206. Schuetz, A. *et al.* Structural basis of inhibition of the human NAD(+)-dependent deacetylase SIRT5 by suramin. *STRUCTURE* **15**, 377–389 (2007).
207. Outeiro, T. F. *et al.* Sirtuin 2 inhibitors rescue alpha-synuclein-mediated toxicity in models of Parkinson's disease. *Science (80-)*. **317**, 516–519 (2007).
208. Mai, A. *et al.* Study of 1,4-Dihydropyridine Structural Scaffold: Discovery of Novel Sirtuin Activators and Inhibitors. *J. Med. Chem.* **52**, 5496–5504 (2009).

209. Tavares, J. *et al.* Bisnaphthalimidopropyl Derivatives as Inhibitors of Leishmania SIR2 Related Protein 1. *ChemMedChem* **5**, 140–147 (2010).
210. Gey, C. *et al.* Phloroglucinol derivatives guttiferone G, aristoforin, and hyperforin: Inhibitors of human sirtuins SIRT1 and SIRT2. *Angew. CHEMIE-INTERNATIONAL Ed.* **46**, 5219–5222 (2007).
211. Oh, W. K. *et al.* Amurensin G, a Potent Natural SIRT1 Inhibitor, Rescues Doxorubicin Responsiveness via Down-Regulation of Multidrug Resistance 1. *Mol. Pharmacol.* **78**, 855–864 (2010).
212. Kahyo, T., Ichikawa, S., Hatanaka, T., Yamada, M. K. & Setou, M. A Novel Chalcone Polyphenol Inhibits the Deacetylase Activity of SIRT1 and Cell Growth in HEK293T Cells. *J. Pharmacol. Sci.* **108**, 364–371 (2008).
213. Gutierrez, M. *et al.* Structural and Synthetic Investigations of Tanikolide Dimer, a SIRT2 Selective Inhibitor, and Tanikolide seco-Acid from the Madagascar Marine Cyanobacterium *Lyngbya majuscula*. *J. Org. Chem.* **74**, 5267–5275 (2009).
214. Mak, L. *et al.* Anti-cancer Drug Development: Computational Strategies to Identify and Target Proteins Involved in Cancer Metabolism. *Curr. Pharm. Des.* **19**, 532–577 (2013).
215. Milne, J. C. *et al.* Small molecule activators of SIRT1 as therapeutics for the treatment of type 2 diabetes. *Nature* **450**, 712–716 (2007).
216. Dai, H. *et al.* SIRT1 Activation by Small Molecules KINETIC AND BIOPHYSICAL EVIDENCE FOR DIRECT INTERACTION OF ENZYME AND ACTIVATOR. *J. Biol. Chem.* **285**, 32695–32703 (2010).
217. Gupta, S. C., Kim, J. H., Prasad, S. & Aggarwal, B. B. Regulation of survival, proliferation, invasion, angiogenesis, and metastasis of tumor cells through modulation of inflammatory pathways by nutraceuticals. *CANCER METASTASIS Rev.* **29**, 405–434 (2010).
218. Chauhan, D. *et al.* Preclinical evaluation of a novel SIRT1 modulator SRT1720 in multiple myeloma cells. *Br. J. Haematol.* **155**, 588–598 (2011).
219. Huhtiniemi, T. *et al.* Structure-Based Design of Pseudopeptidic Inhibitors for SIRT1 and SIRT-2. *J. Med. Chem.* **54**, 6456–6468 (2011).
220. Huber, J. L., McBurney, M. W., DiStefano, P. S. & McDonagh, T. SIRT1-independent mechanisms of the putative sirtuin enzyme activators SRT1720 and SRT2183. *Future Med. Chem.* **2**, 1751–1759 (2010).
221. Borra, M. T., Smith, B. C. & Denu, J. M. Mechanism of human SIRT1 activation by resveratrol. *J. Biol. Chem.* **280**, 17187–17195 (2005).
222. Kaeberlein, M. *et al.* Substrate-specific activation of sirtuins by resveratrol. *J. Biol. Chem.* **280**, 17038–17045 (2005).
223. Pacholec, M. *et al.* SRT1720, SRT2183, SRT1460, and Resveratrol Are Not Direct Activators of SIRT1. *J. Biol. Chem.* **285**, 8340–8351 (2010).
224. Beher, D. *et al.* Resveratrol is Not a Direct Activator of SIRT1 Enzyme Activity. *Chem. Biol. Drug Des.* **74**, 619–624 (2009).
225. Park, S.-J. *et al.* Resveratrol Ameliorates Aging-Related Metabolic Phenotypes by Inhibiting cAMP Phosphodiesterases. *Cell* **148**, 421–433 (2012).
226. Price, N. L. *et al.* SIRT1 Is Required for AMPK Activation and the Beneficial Effects of Resveratrol on Mitochondrial Function. *Cell Metab.* **15**, 675–690 (2012).
227. Denu, J. M. Fortifying the Link between SIRT1, Resveratrol, and Mitochondrial Function. *Cell Metab.* **15**, 566–567 (2012).
228. Sanders, B. D., Jackson, B. & Marmorstein, R. Structural basis for sirtuin function: what we know and what we don't. *Biochim. Biophys. Acta* **1804**, 1604–16 (2010).

229. Andreoli, F., Barbosa, A. J. M., Parenti, M. D. & Del Rio, A. Modulation of epigenetic targets for anticancer therapy: clinicopathological relevance, structural data and drug discovery perspectives. *Curr. Pharm. Des.* **19**, 578–613 (2013).
230. Bruzzone, S. *et al.* Rejuvenating sirtuins: the rise of a new family of cancer drug targets. *Curr. Pharm. Des.* **19**, 614–23 (2013).
231. Zhao, X. *et al.* The 2.5 Å crystal structure of the SIRT1 catalytic domain bound to nicotinamide adenine dinucleotide (NAD⁺) and an indole (EX527 analog) reveals a novel mechanism of histone deacetylase inhibition. *J. Med. Chem.* (2013). doi:10.1021/jm301431y
232. Gertz, M. *et al.* Ex-527 inhibits Sirtuins by exploiting their unique NAD⁺-dependent deacetylation mechanism. *Proc. Natl. Acad. Sci. U. S. A.* **110**, E2772–81 (2013).
233. Disch, J. S. *et al.* Discovery of thieno[3,2-d]pyrimidine-6-carboxamides as potent inhibitors of SIRT1, SIRT2, and SIRT3. *J. Med. Chem.* **56**, 3666–79 (2013).
234. Nguyen, G. T. T., Schaefer, S., Gertz, M., Weyand, M. & Steegborn, C. Structures of human sirtuin 3 complexes with ADP-ribose and with carba-NAD⁺ and SRT1720: binding details and inhibition mechanism. *Acta Crystallogr. D. Biol. Crystallogr.* **69**, 1423–32 (2013).
235. Nguyen, G. T. T., Gertz, M. & Steegborn, C. Crystal structures of sirt3 complexes with 4'-bromo-resveratrol reveal binding sites and inhibition mechanism. *Chem. Biol.* **20**, 1375–85 (2013).
236. Schuetz, A. *et al.* Structural basis of inhibition of the human NAD⁺-dependent deacetylase SIRT5 by suramin. *Structure* **15**, 377–89 (2007).
237. Yamagata, K. *et al.* Structural basis for potent inhibition of SIRT2 deacetylase by a macrocyclic peptide inducing dynamic structural change. *Structure* **22**, 345–52 (2014).
238. Milne, J. C. *et al.* Small molecule activators of SIRT1 as therapeutics for the treatment of type 2 diabetes. *Nature* **450**, 712–6 (2007).
239. Gertz, M. *et al.* A molecular mechanism for direct sirtuin activation by resveratrol. *PLoS One* **7**, e49761 (2012).
240. Schlicker, C., Boanca, G., Lakshminarasimhan, M. & Steegborn, C. Structure-based development of novel sirtuin inhibitors. *Aging (Albany, NY)*. **3**, 852–72 (2011).
241. Bellamacina, C. R. The nicotinamide dinucleotide binding motif: a comparison of nucleotide binding proteins. *FASEB J.* **10**, 1257–69 (1996).
242. Prasad, G. S., Sridhar, V., Yamaguchi, M., Hatefi, Y. & Stout, C. D. Crystal structure of transhydrogenase domain III at 1.2 Å resolution. *Nat. Struct. Biol.* **6**, 1126–31 (1999).
243. Min, J., Landry, J., Sternglanz, R. & Xu, R. M. Crystal structure of a SIR2 homolog-NAD complex. *Cell* **105**, 269–79 (2001).
244. Avalos, J. L., Boeke, J. D. & Wolberger, C. Structural Basis for the Mechanism and Regulation of Sir2 Enzymes. *Mol. Cell* **13**, 639–648 (2004).
245. Pan, P. W. *et al.* Structure and biochemical functions of SIRT6. *J. Biol. Chem.* **286**, 14575–87 (2011).
246. Yuan, H. & Marmorstein, R. Structural basis for sirtuin activity and inhibition. *J. Biol. Chem.* **287**, 42428–35 (2012).
247. Cosgrove, M. S. *et al.* The structural basis of sirtuin substrate affinity. *Biochemistry* **45**, 7511–21 (2006).
248. Arnold, K., Bordoli, L., Kopp, J. & Schwede, T. The SWISS-MODEL workspace: a web-based environment for protein structure homology modelling. *Bioinformatics* **22**, 195–201 (2006).
249. Biasini, M. *et al.* SWISS-MODEL: modelling protein tertiary and quaternary structure using evolutionary information. *Nucleic Acids Res.* **42**, W252–8 (2014).

250. Guex, N., Peitsch, M. C. & Schwede, T. Automated comparative protein structure modeling with SWISS-MODEL and Swiss-PdbViewer: a historical perspective. *Electrophoresis* **30 Suppl 1**, S162–73 (2009).
251. Kiefer, F., Arnold, K., Künzli, M., Bordoli, L. & Schwede, T. The SWISS-MODEL Repository and associated resources. *Nucleic Acids Res.* **37**, D387–92 (2009).
252. Di Fruscia, P. *et al.* The Discovery of Novel 10,11-Dihydro-5H-dibenz[b,f]azepine SIRT2 Inhibitors. *Medchemcomm* (2012). doi:10.1039/C2MD00290F
253. Fridén-Saxin, M. *et al.* Synthesis and evaluation of substituted chroman-4-one and chromone derivatives as sirtuin 2-selective inhibitors. *J. Med. Chem.* **55**, 7104–13 (2012).
254. Khanfar, M. A. *et al.* Development and characterization of 3-(benzylsulfonamido)benzamides as potent and selective SIRT2 inhibitors. *Eur. J. Med. Chem.* **76**, 414–26 (2014).
255. Mahajan, S. S. *et al.* Development of pyrazolone and isoxazol-5-one cambinol analogues as sirtuin inhibitors. *J. Med. Chem.* **57**, 3283–94 (2014).
256. Medda, F. *et al.* Novel cambinol analogs as sirtuin inhibitors: synthesis, biological evaluation, and rationalization of activity. *J. Med. Chem.* **52**, 2673–82 (2009).
257. Rotili, D. *et al.* Simplification of the tetracyclic SIRT1-selective inhibitor MC2141: coumarin- and pyrimidine-based SIRT1/2 inhibitors with different selectivity profile. *Bioorg. Med. Chem.* **19**, 3659–68 (2011).
258. Suzuki, T. *et al.* Design, synthesis, and biological activity of a novel series of human sirtuin-2-selective inhibitors. *J. Med. Chem.* **55**, 5760–73 (2012).
259. Parenti, M. D. *et al.* Discovery of Novel and Selective SIRT6 Inhibitors. *J. Med. Chem.* **57**, 4796–804 (2014).
260. Notredame, C., Higgins, D. G. & Heringa, J. T-Coffee: A novel method for fast and accurate multiple sequence alignment. *J. Mol. Biol.* **302**, 205–17 (2000).
261. Waterhouse, A. M., Procter, J. B., Martin, D. M. A., Clamp, M. & Barton, G. J. Jalview Version 2--a multiple sequence alignment editor and analysis workbench. *Bioinformatics* **25**, 1189–91 (2009).
262. Giralt, A. & Villarroya, F. SIRT3, a pivotal actor in mitochondrial functions: metabolism, cell death and aging. *Biochem. J.* **444**, 1–10 (2012).
263. Lombard, D. B. *et al.* Mammalian Sir2 homolog SIRT3 regulates global mitochondrial lysine acetylation. *Mol. Cell. Biol.* **27**, 8807–14 (2007).
264. Ahn, B.-H. *et al.* A role for the mitochondrial deacetylase Sirt3 in regulating energy homeostasis. *Proc. Natl. Acad. Sci. U. S. A.* **105**, 14447–52 (2008).
265. Haigis, M. C., Deng, C.-X., Finley, L. W. S., Kim, H.-S. & Gius, D. SIRT3 Is a Mitochondrial Tumor Suppressor: A Scientific Tale That Connects Aberrant Cellular ROS, the Warburg Effect, and Carcinogenesis. *Cancer Res.* **72**, 2468–2472 (2012).
266. Etchegaray, J.-P., Zhong, L. & Mostoslavsky, R. The Histone Deacetylase SIRT6: At the Crossroads Between Epigenetics, Metabolism and Disease. *Curr. Top. Med. Chem.* **13**, 2991–3000 (2013).
267. Zhong, L. *et al.* The histone deacetylase Sirt6 regulates glucose homeostasis via Hif1alpha. *Cell* **140**, 280–93 (2010).
268. Sebastián, C. *et al.* The histone deacetylase SIRT6 is a tumor suppressor that controls cancer metabolism. *Cell* **151**, 1185–99 (2012).
269. Bauer, I. *et al.* The NAD⁺-dependent histone deacetylase SIRT6 promotes cytokine production and migration in pancreatic cancer cells by regulating Ca²⁺ responses. *J. Biol. Chem.* **287**, 40924–37 (2012).
270. Mao, Z. *et al.* SIRT6 promotes DNA repair under stress by activating PARP1. *Science* **332**, 1443–6 (2011).

271. Jiang, H. *et al.* SIRT6 regulates TNF- α secretion through hydrolysis of long-chain fatty acyl lysine. *Nature* **496**, 110–3 (2013).
272. Mostoslavsky, R. *et al.* Genomic instability and aging-like phenotype in the absence of mammalian SIRT6. *Cell* **124**, 315–29 (2006).
273. Van Gool, F. *et al.* Intracellular NAD levels regulate tumor necrosis factor protein synthesis in a sirtuin-dependent manner. *Nat. Med.* **15**, 206–10 (2009).
274. Bruzzone, S. *et al.* Catastrophic NAD⁺ depletion in activated T lymphocytes through Nampt inhibition reduces demyelination and disability in EAE. *PLoS One* **4**, e7897 (2009).
275. Lipinski, C. A., Lombardo, F., Dominy, B. W. & Feeney, P. J. Experimental and computational approaches to estimate solubility and permeability in drug discovery and development settings. *Adv. Drug Deliv. Rev.* **46**, 3–26 (2001).
276. Baell, J. B. & Holloway, G. A. New substructure filters for removal of pan assay interference compounds (PAINS) from screening libraries and for their exclusion in bioassays. *J. Med. Chem.* **53**, 2719–40 (2010).
277. Avalos, J. L., Bever, K. M. & Wolberger, C. Mechanism of sirtuin inhibition by nicotinamide: altering the NAD(+) cosubstrate specificity of a Sir2 enzyme. *Mol. Cell* **17**, 855–68 (2005).
278. Szczepankiewicz, B. G. *et al.* Synthesis of carba-NAD and the structures of its ternary complexes with SIRT3 and SIRT5. *J. Org. Chem.* **77**, 7319–29 (2012).
279. Michishita, E. *et al.* SIRT6 is a histone H3 lysine 9 deacetylase that modulates telomeric chromatin. *Nature* **452**, 492–6 (2008).
280. Yasuda, M., Wilson, D. R., Fugmann, S. D. & Moaddel, R. Synthesis and characterization of SIRT6 protein coated magnetic beads: identification of a novel inhibitor of SIRT6 deacetylase from medicinal plant extracts. *Anal. Chem.* **83**, 7400–7 (2011).
281. Kokkonen, P. *et al.* Peptides and Pseudopeptides as SIRT6 Deacetylation Inhibitors. *ACS Med. Chem. Lett.* **3**, 969–974 (2012).
282. Zhu, T. *et al.* Hit identification and optimization in virtual screening: practical recommendations based on a critical literature analysis. *J. Med. Chem.* **56**, 6560–72 (2013).
283. Xiao, C. *et al.* SIRT6 deficiency results in severe hypoglycemia by enhancing both basal and insulin-stimulated glucose uptake in mice. *J. Biol. Chem.* **285**, 36776–84 (2010).
284. Elsas, L. J. & Longo, N. Glucose transporters. *Annu. Rev. Med.* **43**, 377–93 (1992).
285. Lagorce, D., Sperandio, O., Galons, H., Miteva, M. A. & Villoutreix, B. O. FAF-Drugs2: free ADME/tox filtering tool to assist drug discovery and chemical biology projects. *BMC Bioinformatics* **9**, 396 (2008).
286. Lagorce, D. *et al.* The FAF-Drugs2 server: a multistep engine to prepare electronic chemical compound collections. *Bioinformatics* **27**, 2018–20 (2011).
287. McCord, R. A. *et al.* SIRT6 stabilizes DNA-dependent protein kinase at chromatin for DNA double-strand break repair. *Aging (Albany, NY)*. **1**, 109–21 (2009).
288. Khongkow, M. *et al.* SIRT6 modulates paclitaxel and epirubicin resistance and survival in breast cancer. *Carcinogenesis* **34**, 1476–86 (2013).
289. Wu, J. *et al.* Discovery and Mechanism Study of SIRT1 Activators that Promote the Deacetylation of Fluorophore-Labeled Substrate. *J. Med. Chem.* (2013). doi:10.1021/jm301032j
290. Lord, C. J., Tutt, A. N. J. & Ashworth, A. Synthetic Lethality and Cancer Therapy: Lessons Learned from the Development of PARP Inhibitors. *Annu. Rev. Med.* **66**, 455–70 (2014).
291. Liu, Y. *et al.* Inhibition of SIRT6 in prostate cancer reduces cell viability and increases sensitivity to chemotherapeutics. *Protein Cell* (2013). doi:10.1007/s13238-013-3054-5
292. Lefort, K. *et al.* A miR-34a-SIRT6 axis in the squamous cell differentiation network. *EMBO J.* **32**, 2248–63 (2013).

293. Ming, M. *et al.* SIRT6 promotes COX-2 expression and acts as an oncogene in skin cancer. *Cancer Res.* **74**, 5925–33 (2014).
294. Heinrich, P. C., Castell, J. V & Andus, T. Interleukin-6 and the acute phase response. *Biochem. J.* **265**, 621–36 (1990).
295. Tanaka, T. & Kishimoto, T. The biology and medical implications of interleukin-6. *Cancer Immunol. Res.* **2**, 288–94 (2014).
296. Rose-John, S., Scheller, J., Elson, G. & Jones, S. A. Interleukin-6 biology is coordinated by membrane-bound and soluble receptors: role in inflammation and cancer. *J. Leukoc. Biol.* **80**, 227–36 (2006).
297. Boulanger, M. J., Chow, D., Brevnova, E. E. & Garcia, K. C. Hexameric structure and assembly of the interleukin-6/IL-6 alpha-receptor/gp130 complex. *Science* **300**, 2101–4 (2003).
298. Hong, D. S., Angelo, L. S. & Kurzrock, R. Interleukin-6 and its receptor in cancer: implications for translational therapeutics. *Cancer* **110**, 1911–28 (2007).
299. Franceschi, C. *et al.* Inflamm-aging. An evolutionary perspective on immunosenescence. *Ann. N. Y. Acad. Sci.* **908**, 244–54 (2000).
300. Ershler, W. B. Interleukin-6: a cytokine for gerontologists. *J. Am. Geriatr. Soc.* **41**, 176–81 (1993).
301. Harris, T. B. *et al.* Associations of elevated interleukin-6 and C-reactive protein levels with mortality in the elderly. *Am. J. Med.* **106**, 506–12 (1999).
302. Ferrucci, L. *et al.* Serum IL-6 level and the development of disability in older persons. *J. Am. Geriatr. Soc.* **47**, 639–46 (1999).
303. Huang, H., Patel, D. D. & Manton, K. G. The immune system in aging: roles of cytokines, T cells and NK cells. *Front. Biosci.* **10**, 192–215 (2005).
304. Guo, Y., Xu, F., Lu, T., Duan, Z. & Zhang, Z. Interleukin-6 signaling pathway in targeted therapy for cancer. *Cancer Treat. Rev.* **38**, 904–10 (2012).
305. Yao, X. *et al.* Targeting interleukin-6 in inflammatory autoimmune diseases and cancers. *Pharmacol. Ther.* **141**, 125–39 (2014).
306. Ekins, S., Williams, A. J., Krasowski, M. D. & Freundlich, J. S. In silico repositioning of approved drugs for rare and neglected diseases. *Drug Discov. Today* **16**, 298–310 (2011).
307. Kalai, M. *et al.* Analysis of the human interleukin-6/human interleukin-6 receptor binding interface at the amino acid level: proposed mechanism of interaction. *Blood* **89**, 1319–33 (1997).
308. Bravo, J., Staunton, D., Heath, J. K. & Jones, E. Y. Crystal structure of a cytokine-binding region of gp130. *EMBO J.* **17**, 1665–74 (1998).
309. Kurth, I. *et al.* Importance of the membrane-proximal extracellular domains for activation of the signal transducer glycoprotein 130. *J. Immunol.* **164**, 273–82 (2000).
310. Paonessa, G. *et al.* Two distinct and independent sites on IL-6 trigger gp 130 dimer formation and signalling. *EMBO J.* **14**, 1942–51 (1995).
311. Barton, V. A., Hudson, K. R. & Heath, J. K. Identification of three distinct receptor binding sites of murine interleukin-11. *J. Biol. Chem.* **274**, 5755–61 (1999).
312. PDBePISA service. at <http://www.ebi.ac.uk/msd-srv/prot_int/pistart.html>
313. Loving, K., Salam, N. K. & Sherman, W. Energetic analysis of fragment docking and application to structure-based pharmacophore hypothesis generation. *J. Comput. Aided. Mol. Des.* **23**, 541–54 (2009).